Thermal cycling of saturated Ghibli granite and Rotokawa andesite using distilled water and geothermal brine.

A thesis submitted in partial fulfilment of the requirements for the degree of

Master of Science in Engineering Geology

at the

University of Canterbury

by

Michael James Eatson

2016

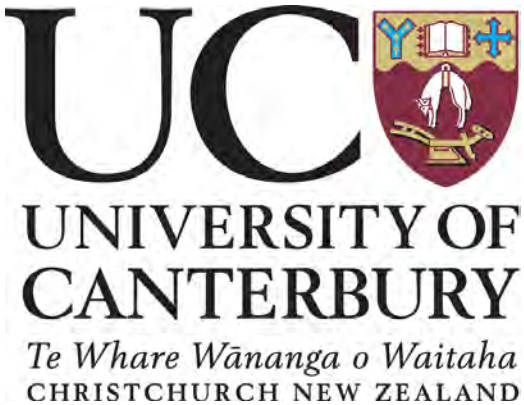

Abstract

Thermal stimulation is a technique commonly employed by geothermal operators to enhance permeability of both production and reinjection reservoirs. Through the cyclic injection of cold fluid, induced thermal stresses lead to significant development of micro-fractures, porosity and permeability. How thermal-cycling affects the physical and mechanical properties of a rock-mass is not well understood. Previous experiments by Siratovich et al. (2013, 2015a) consider thermal-cycling using only distilled water. In this study thermal-cycling methodology has been developed to also consider the effects of thermal-cycling using saline low-pressure brine retrieved from Nga Awa Purua (NAP) geothermal power station.

Results obtained in this project clearly indicate that the chemistry of H_2O and NAP brine play significant roles in the alteration of Ghibli granite. Methods were then translated to samples of Rotokawa andesite, the main reservoir lithology at the Rotokawa geothermal field, with differences in how the two lithologies responde to the thermal-cycling being observed. Variability in the physical disturbance and chemical alteration of samples was observed in thin-section and by the measurement of porosity, permeability, density, ultrasonic-wave velocity and limited XRD and SEM. In geologically short periods of time, saturated thermal-cycling using both H_2O and NAP brine has resulted in measurable amounts of mineral alteration to samples, with alteration products observable in thin-section.

Ghibli granite samples that were thermally-cycled in H_2O developed more permeability than those cycled in NAP brine, despite developing less porosity. This is associated with the alteration of biotite to chlorite, which was more prevalent in H_2O treated experiments. It is suggested that the new chlorite assemblage has allowed for the linking of flow-paths, reducing tortuosity and enhancing permeability. Samples thermally-cycled in NAP brine were observed through XRD to have greater amounts of albitization than those cycled in H_2O. Albitization and associated reordering process are thought to be responsible for the measured differences in porosity development, with NAP brine treated samples on average developing more porosity than H_2O treated samples. When these experiments were applied to the Rotokawa andesite, both porosity and permeability were observed to initially decline and then recover, although not to their initial level. The specific mechanisms responsible for these changes could not be identified.

To comprehensively understand reservoir processes during thermal-cycling, and to better understand reservoir operational management, more experimentation and numerical modelling is required. In the Further Research section, key areas have been indicated where additional studies could be advantageous.

Acknowledments

The following people are acknowledged for their contribution to this thesis:

Supervisors: Marléne Villeneuve, Ben Kennedy and Paul Siratovich.
Funding: Mighty River Power, Source to Surface, Callaghan Innovation and Freemasons Trust.
Technical staff: Cathy Higgins, Sarah Pope, Rob Spiers, Matt Cockcroft and Chris Grimshaw.
Kerry Walton, Mike Heap and Stephen Browne for SEM and XRD analysis.
Kevin Brown for spectrophotometric analysis and geochemical modelling.
Jim Cole for always being open to discussion and for untold edits.
Anne Smith and Doug Sheppard for proof-reading.

Most importantly, I thank my extended family. Your support and endless encouragement to pursue my dreams has taken me places I would have never thought possible.

“He tina ki runga, he tãmore ki raro - In order to flourish above, one must be firmly rooted below.”

Contents

List of Figures

List of Tables

Chapter 1

Introduction

1.1 Project Background

Porosity and permeability are critical for geothermal systems and the reinjection of geothermal brines. Understanding the relationships between porosity and permeability is necessary in the estimation, utilisation and optimisation of a geothermal reserve. As a geothermal operator, the maintenance of field permeability is very important. Fouling of the system and loss of well productivity or injectivity can cause persistent problems. To ensure good return for investment, geothermal operators are continually seeking techniques to improve field efficiency, and prolong well life. Heterogeneity and anisotropy of the rock mass, combined with secondary chemical and physical alteration processes, make the evaluation of porosity and permeability of a geothermal reservoir difficult and often misleading (Siratovich et al. 2014).

A common issue for geothermal field operators is the deterioration of reinjection well performance with time. This is especially true for binary type geothermal plants. The cost of working over a reinjection well is time consuming, and costly. Often the drilling of new wells is required to make up losses. To improve station efficiency, preserve reservoir conditions, prolong well life, and ensure good return to investors, significant interest has been focused around the thermo-mechanical and chemical processes associated with the reinjection and management of mineral-rich geothermal brines. The reduction, or even elimination, of silica scaling by appropriate handling of the geothermal waste water creates an opportunity for increased efficiency in the use of high-temperature geothermal resources.

1.2 Thesis Scope

At Rotokawa geothermal field the reinjection of brines from both Rotokawa, and Nga Awa Purua stations is a requirement of the field's resource consent. Mineral rich brines must be returned back into the reservoir. Reinjection also provides critical pressure support to the field. Loss of reservoir pressure can lead to the permanent destruction of permeability. The reinjected brines are highly saturated in amorphous silica and at a significantly lower temperature than the ground-mass they are being returned to. Temperature contrast between the reinjected fluids, and the groundmass, induce thermal stresses which can be shown to lead to cause the development of micro-fractures of crystals within the groundmass, enhancing permeability (Grant and Bixley 2011, Siratovich et al. 2014).

To minimise amorphous silica polymerization, acidification (H_2SO_4) is utilised before the flashing of intermediate pressure steam. This is effective in significantly reducing silica precipitation on surfaces within the plant and downstream piping. However, upon reinjection to the reservoir, brine is buffered back to reservoir pH. This allows for the polymerization and precipitation of amorphous silica to begin. The precipitation of amorphous silica on near well surfaces such as pore space within the groundmass is shown to reduce near well permeability (Addison et al. 2015). Wells that display significant loss in flow rates, may be recovered by imparting high thermal stresses through the injection of cold river water. This is not always successful, with a new well being required to make up for the losses in fluid circulation.

This thesis uses laboratory based experiments to explore the chemical and physical processes occurring during saturated thermal cycling of crustal rocks. Samples are saturated in distilled water, or low-pressure geothermal brine retrieved from Mighty River Power's (MRP) Nga Awa Purua (NAP) plant. Thermal gradients used are similar to those induced during well stimulation and the re-injection of spent fluid back into the geothermal reservoir.

The importance of this study is in the further development of modelling relationships occurring between injectate chemistry and reservoir permeability as a result of thermal cycling. Thermal stressing of a geothermal reservoir, and the resulting increased permeability may be beneficial to the operation of the reservoir. There is however, a potential risk to well-bore stability. Understanding reservoir thresholds is important and beneficial to resource utilisation. Furthermore, if continued thermal cycling is shown to result in decreases to overall groundmass permeability, through secondary mineral precipitation, project feasibility may diminish with alternative methods for field management being required.

For this thesis, initial thermal-cycling experiments have been conducted on the assumed isotropic and homogeneous Ghibli granite. Granites are not commonly host to high-enthalpy geothermal systems, however, the thermal cycling of granites has been previously well explored

1.3 Research Questions

- Does thermal-cycling induced alteration of the Ghibli granite vary when H_2O is substituted with Nga Awa Purua (NAP) geothermal brine?
- Does thermal-cycling induced alteration from either H_2O or NAP brine vary when Ghibli granite is substituted with Rotokawa andesite, the main reservoir lithology at Rotokawa geothermal field?
- Are the key processes responsible for the observed changes to the Ghibli granite and Rotokawa andesite rock-masses able to be identified and constrained?
- Does amorphous silica have a significant role in the thermal-cycling process when either H_2O or NAP brine is used?

1.4 Application to Geothermal Industry

The purpose of conducting this research is to provide the geothermal operators at Rotokawa further insight of the thermo-mechanical, and chemical processes occurring to reservoir groundmass during the reinjection of geothermal fluids. Establishing relationships such as; the ideal fluid and rock temperature contrast, the fluids being used and the number of thermal cycles that are effective in generating permeability are likely to provide invaluable information to the field operator. Prolongation of field life and preservation of this natural resource is beneficial to the Mighty River Power company but also to those who consume electricity within New Zealand. The cost of drilling a make up well for one that has deteriorated through the scaling of silica is high. If information such as ideal thermal contrast between reservoir and reinjection temp can be identified, this may provide a cost effective solution.

1.5 Geothermal Systems

Geothermal systems are an important and often under-utilised resource for developed and developing nations. The uses of geothermal energy are vast (Figure 1.1) but perhaps most importantly, high-temperature systems allow for the renewable generation of electricity. A correctly operated geothermal field can provide a stable generation platform suitable for base load electricity, with little sensitivity to climatic variation (unlike wind, solar and hydro energy). New Zealand and many other countries around the world are moving away from conventional fossil fuels and toward renewable sources of energy. The optimisation and utilisation of geothermal resources has become an important consideration.

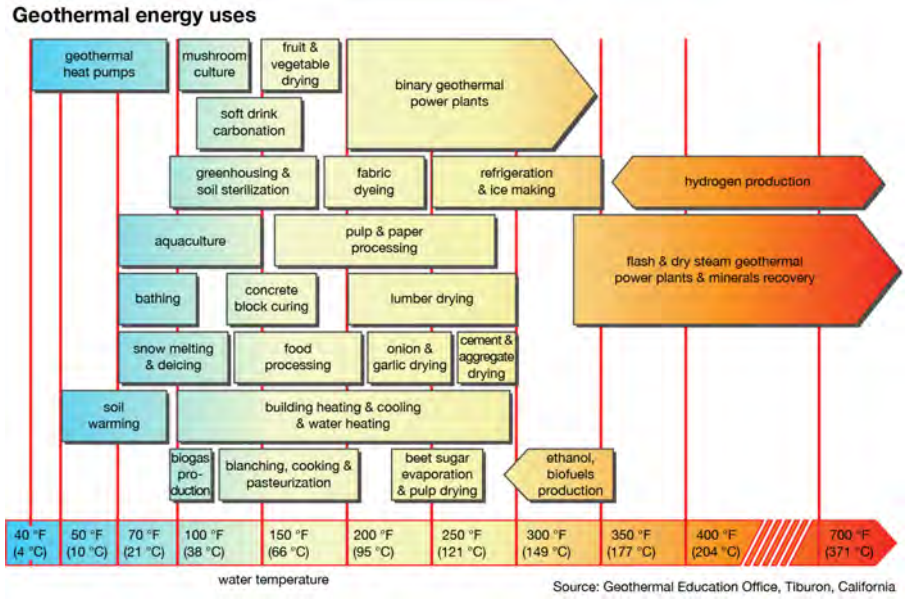

Figure 1.1: Diagram of various geothermal energy uses displayed according to the water temperature of the geothermal resource (Britannica 2015).

The New Zealand Geothermal Association (NZGA 2013) states that the production of geothermal energy currently meets about 13% of the total New Zealand electricity demand; an installed generation capacity of about 754 MWe spread over 14 power plants. Thirteen of these plants utilise high-temperature fields within the Taupo Volcanic Zone (TVZ), a further 25MW is produced at the stand alone Ngawha power station in Northland. A further 600MW of developed generation capacity has been forecast by 2025. However, falling electricity demand through the introduction of energy efficient appliances raises an uncertainty in this forecast. The increased availability and affordability of electric cars may see this demand begin to increase (M.E.D 2011).

Large-scale geothermal developments, such as Nga Awa Purua station, extract fluid at a greater rate than the natural recharge to the system. In cases where reservoir pressures have been significantly reduced by exploitation, the rate of geothermal fluid replenishment from depth has increased to match discharge rates. This, combined with the ability to recycle fluids through reinjection, creates difficulty in defining what is meant by renewable and sustainable operation of a geothermal resource. Geothermal resources such as Ohaaki have been over-exploited, resulting in reduced generation capacity. To date however, no geothermal fields have been exhausted. Wairakei geothermal field has been operating for over 50 years, and has resource consent for a further 25 years at the same generation capacity. Reservoir modelling indicates that the resource will remain viable for at least another 25 years beyond that demonstrating the longevity of a correctly managed geothermal resource (NZGA 2013).

High-temperature geothermal systems are commonly hosted in active volcanic environments and on continental plate boundaries, where high thermal gradients are found at shallow depths. Economic geothermal systems require three main elements: a subsurface heat source, permeable ground mass, and fluid to transport heat from the heating source to the reservoir. These conditions are often met through natural processes. Figure 1.2 provides a good representation of a simplified intrusive volcanic-related geothermal system.

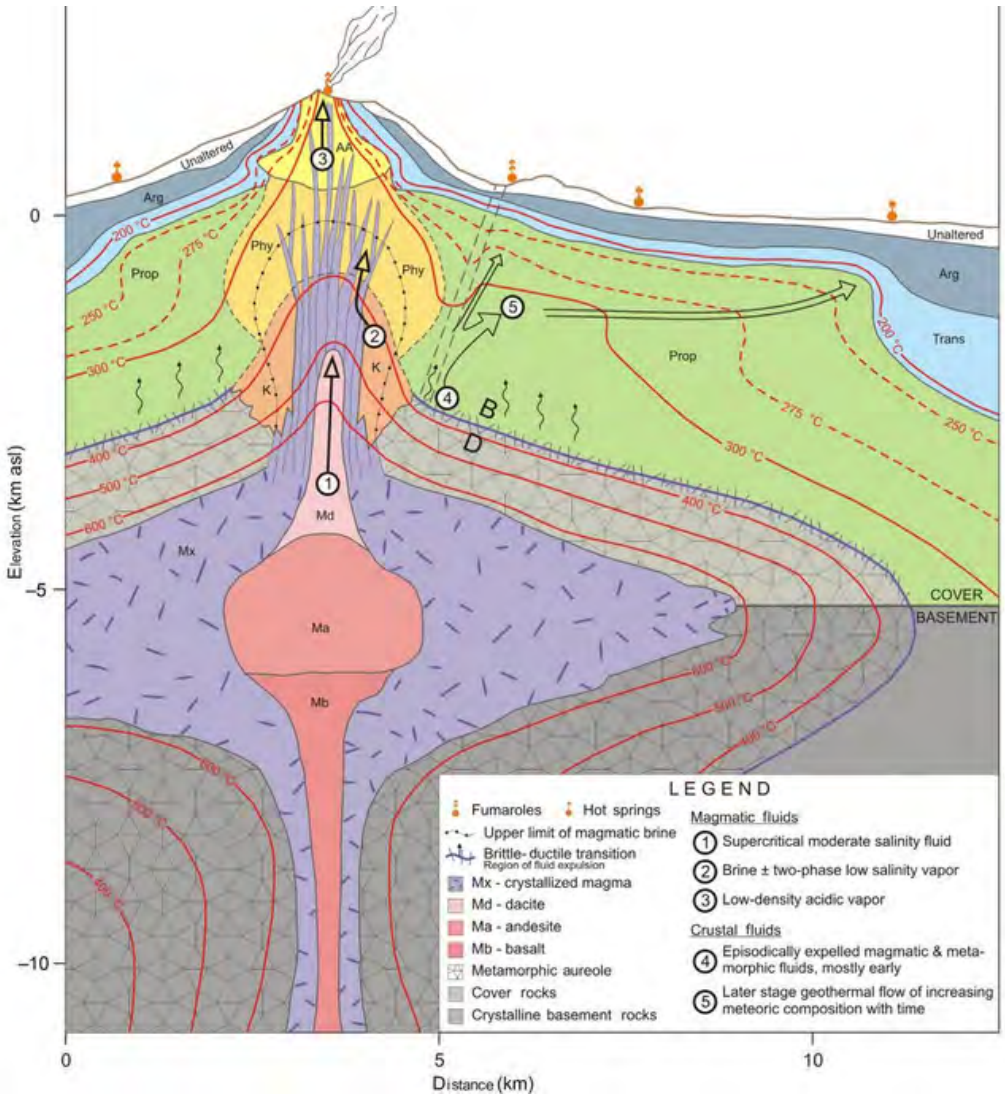

Figure 1.2: Schematic cross-section through a typical arc volcanic-intrusive system. Shown are main alteration zones, isotherms, and sources of deep fluids, inluding their ascent paths (arrows; meteoric fluid descent paths not shown). Propylitic (Prop), transition (Trans), and argillic (Arg) alteration formed by long-term circulation of heated meteoric waters affect virtually all the cover rocks above brittle-ductile transitionn (B-D) with greatest intensity close to intrusion. Metamorphism affects both cover rocks and basement rocks in the ductile regime proximal to the intrusion. Expulsion of metamorphic fluid contributes to brittle fracture during the early stages of the larger pluton but wanes with time as meteroric circulation progressively invades the created fracture network. Potassic (K), phyllic (PHY), and advanced argillic (AA) alteration are more directly related to the flux of magmatic volatiles and circulation of magmatic-hydrothermal fluids that form an envelope around the volcano conduit system. Argillic Alteration may also form more broadly by absorption of H_2S-rich steam by oxygenated meteoric waters. From Sigurdsson et al. (2015).

By comparison, geothermal fields that are influenced by tectonic processes and rifting are highly complicated; for example the Rotokawa geothermal field (Figure 1.3) in the TVZ. In the TVZ fields typically lie on the boundary of calderas where normal faulting and formation interfaces provide conduits for both vertical and horizontal infiltration of meteoric water, and for the return flow of hot fluids from depth. If the ascending hot water is trapped beneath an impermeable formation, it fills the pore-spaces of the surrounding rock forming a geothermal reservoir. In liquid-dominated reservoirs high fluid temperatures can be achieved due to increasing hydrostatic pressure with depth thus allowing for elevated fluid temperatures without boiling. High-enthalpy fluid provides a favourable resource for geothermal operators.

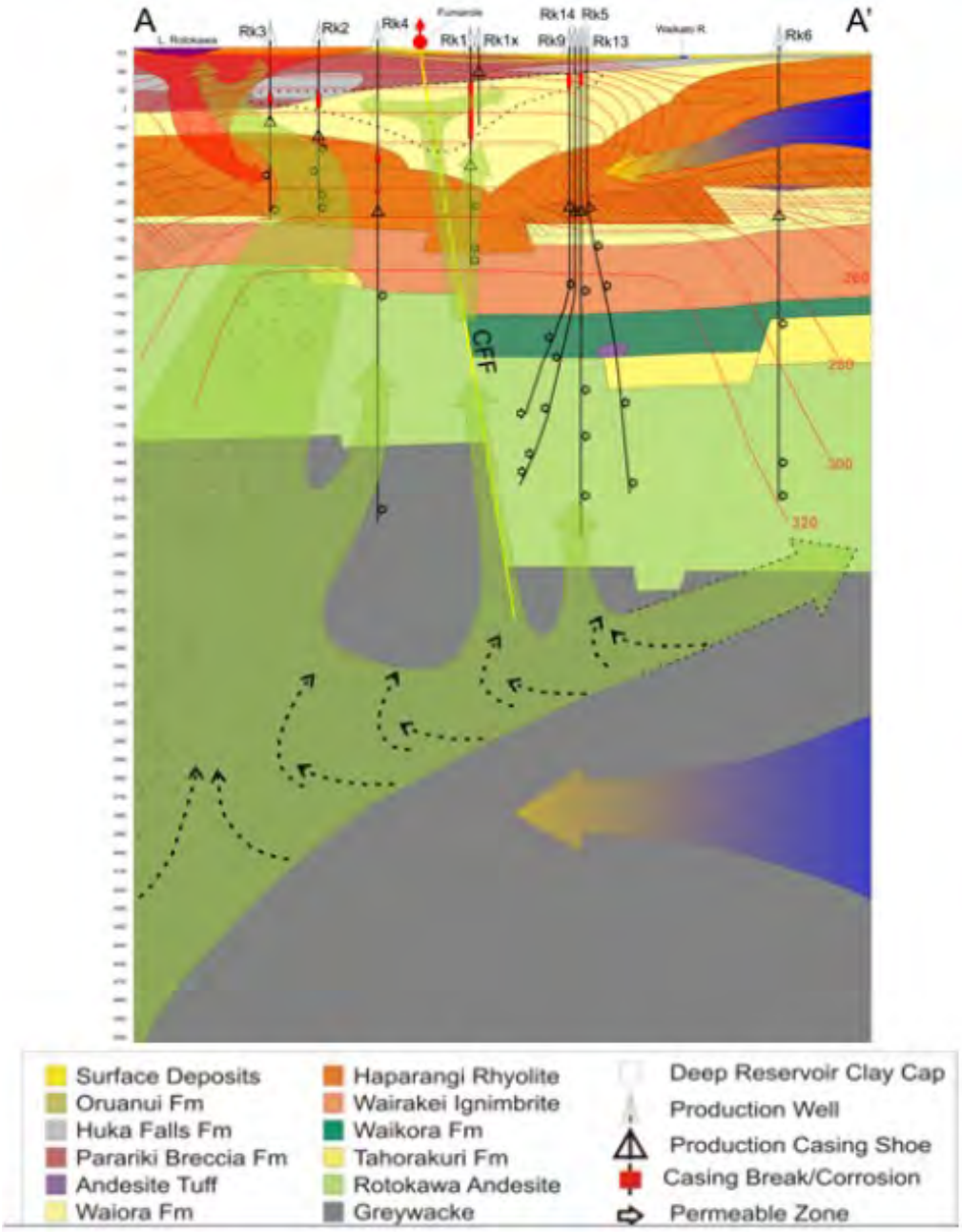

Figure 1.3: Cross-section and geochemical model of the Rotokawa Geothermal Field, showing geologic lithologies, structural features (CFF), thermal isobars, surface features, assumed fluid-flow and the production and reinjection wells. From Winick et al. (2009).

1.6 Properties of Geothermal Reservoirs

1.6.1 Porosity

Porosity is the volumetric measure of the void (or pore) space within the rock mass. No indication is given to the shape, size, distribution or degree of connectivity of the pores. Pores that display connectivity (referred to as the effective porosity) typically impart a primary permeability and allow for the transmission of geothermal fluids and steam. The pore-volume of high-enthalpy geothermal systems, such as the Rotokawa field, play an important role in the storage capacity and permeability of the reservoir (Krupp and Seward 1987).

The primary porosity of volcanic rocks (common hosts of geothermal systems) is determined by the geologic method of emplacement. Variations in porosity are influenced by cooling time (Snelling and Woodmorappe 1998), gas content (Gilluly 1937), mode of deposition (Barton et al. 1995), and weathering (Olalla et al. 2010). The formation process of intrusive igneous rocks results in a holocrystalline matrix with porosity typically of 1-2%. For extrusive volcanic formations such as those found in the TVZ, the primary porosity can be highly variable. Eruptive TVZ deposits are typically characterised by the presence of vesicles, but in the case of pyroclastic rocks, grain size distribution, sorting and density of the clasts will define the primary porosity. Lavas may contain vesicles and miarolitic or diktytaxitic cavities (Williams et al. 1982) but typically only develop a connected porosity if they are brecciated during emplacement.

Numerous processes may influence primary porosity that to the development of a secondary porosity. These processes include: the abundance and aperture size of pores (Heap et al. 2014), the dilation or contraction of pores (Gowd and Rummel 1980), thermal stressing leading to evolution of micro-fracture densities (Fredrich and Wong 1986, Siratovich et al. 2015b, Faoro et al. 2013), tectonic stresses, secondary mineralization and the dissolution of minerals.

The geometry and connectivity of pore-space plays an important role in rock-mass strength and permeability. For a pressure-dependant permeability the geometry of pores plays a critical role. Guéguen and Palciauskas (1994) observed that fractures are easily closed with changes to effective stress (i.e. reduction in pore-fluid pressure), whereas isotropic pores are not easily closed. Increased pore pressure or thermal cooling may result in the dilation of pore space. The dilation of pore-space may also occur under low confining stress, but at greater confining stresses, compaction will dominate dilation processes and, lead to the destruction of porosity (Gowd and Rummel 1980). Variations in hydrological conditions within the field, such as the change in pore pressure, can lead to the destruction of permeability. This is important when considering the effects of removing steam from a reservoir.

Rhyolite, and andesite common within the TVZ and Rotokawa geothermal field display porosities of 10%. However, the porosity of shallow and deep reservoirs are often as high as 25% (Rae 2007). Siratovich et al. (2012) reports that the matrix-porosity of core taken from three production-wells within the Rotokawa andesite (RKA) varied from 5.82% to 13.49% respectively. Cant (2015) concluded that the pore structure type (i.e. vesicles or micro-fractures) plays a significant role in rock mass permeability. Samples with micro-fractured pore structures displayed relatively low porosity values ($< 8\%$), whereas samples displaying vesicular pore structure tended to have higher porosities ($> 10\%$). If the rock-mass is subject to alteration through the circulation of hydrothermal fluids, and tectonic processes, a secondary porosity and permeability can develop (Wyering et al. 2014).

1.6.2 Permeability

Permeability is a measure of fluid flow through the void spaces within a rock mass. Reservoir permeability is a critical and often deciding factor as to whether a geothermal reserve is economic. The rate at which steam can be extracted from the system, the rate of reservoir recharge, fluid enthalpy and fluid chemistry ultimately defines the electricity generation potential. The bulk permeability of a geothermal reservoir and immediate surroundings is a function of both primary (formation) and secondary (fracture and/or chemical) processes (Barton et al. 1995). The distribution of primary permeability zones relate to the groundmass texture and method of emplacement for the geological unit. A secondary permeability may be enhanced through mechanical, thermal and chemical processes. Mechanical processes include: brittle fracturing and faulting of the rock mass through the distribution of thermal stress and/or regional strain. Chemical processes include the dissolution and precipitation of minerals. This process is often enhanced by the boiling of geothermal fluids. The relationship between primary and secondary processes create permeable zones with networked flow-paths (Massiot et al. 2015) and dynamic relationships between these processes will determine the overall reservoir permeability.

In any geothermal environment high fluid-flow conditions can develop. However, bulk permeability of a rock-mass is continually modified by fracturing and brecciation as well as by cementation from hydrothermal precipitation (Barton et al. 1995). Chemical processes such as prolonged hydrothermal alteration, dissolution of glass minerals, or mineral deposition also play an important role in the circulation of geothermal fluids (Rae 2007). Mineral deposition limits high-flow periods to short-time intervals. Intermittent cycles of fracture opening via tectonism, dike intrusion, and/or volcanic eruption, followed by mineral sealing is a key attribute of epithermal systems (Rowland and Simmons 2012). The development of a reservoir leads to changes in pressure, temperature, and the chemistry of circulating fluids, affecting system equilibrium and increasing the potential for permeability enhancement or destruction (Winick et al. 2015).

1.6.3 Fractures

Fracture permeability is often the dominant mode of fluid transport in geothermal systems, with fractures and fracture networks occurring at all scales in crustal rocks (Fredrich and Wong 1986). Fracturing of the groundmass has numerous origins, which include: tectonic movement and proximity to faults, differential compaction causing stress fractures, cooling contractions, thermal spallation, and eruptive/emplacement brecciation. Successful targeting of permeable fractures in geothermal fields is aided by understanding the spatial and geometric characteristics of fracture populations (Massiot et al. 2015). The nature of fractures in the reservoir's immediate surroundings are also important considerations in field operation. In geothermal reservoir engineering, increased fracturing of the groundmass is often desired, as it results in increased porosity, permeability, surface area, and reductions in brittle strength (Ashby and Sammis 1990) and acoustic velocity (Wyering et al. 2012).

Thermal stresses develop fracture networks through thermal expansion and contraction of minerals. Thermal cracking in quartz-bearing rocks is commonly attributed to the high volumetric thermal expansion of quartz (Simmons and Cooper 1977). Numerical simulation of fracturing by Dobroskok

et al. (2005) shows that propagation of fractures is influenced by thermal and liquid stresses. Thermo-chemical reactions can also have affect on mineralogy, these include: fluid inclusions, dehydration and decarbonation processes and mineral phase change. Previous studies (Heard and Page 1982, Bourbie and Zinszner 1985, Rust and Cashman 2004, Stimac et al. 2004, Heap et al. 2014) show that porosity and matrix permeability are closely related but not mutually exclusive. High porosity values typically correlate to high permeability, however permeability is predominantly controlled by pore microstructure and morphology (Sammis and Ashby 1986). Large scale fractures or faults may act as impermeable barriers to cross-fault flow or as high permeability conduits, although their permeability relative to the host rock is likely time dependent, varying with displacement, host lithology and hydrothermal cementation (Rowland and Simmons 2012, Sewell et al. 2015).

1.7 Management of Geothermal Fields

1.7.1 Reinjection

The reinjection of processed geothermal fluids (referred to as brine) is critical to the sustainable operation of some production fields. Reinjection provides pressure support, reduces subsidence, and is an environmentally sustainable method for disposing mineral-rich waste fluids. Lack of reinjection may result in rapid pressure decline of the geothermal reservoir, resulting in a decline of production wells output, and also providing opportunity for the incursion of peripheral fluids which cool the geothermal reservoir. Reinjection at rates that are too high or in poor locations can result in thermal breakthrough. Thermal breakthrough impacts fluid enthalpy, reducing system efficiency (Kaya et al. 2011).

Reinjection methods can be simplified to either infield or outfield injection, dictated by the physical characteristics of the geothermal system and plant operation methods. For infield reinjection, brines are returned to the deep reservoir close to production wells and within the fields resistivity boundary (marked by the abundance of clay mineral) and hot zone. Outfield reinjection refers to the injection wells further away from the production wells and outside the field's resistivity boundary or hot zone. The temperature, chemistry and physical volumes of fluids reinjected can differ greatly from the produced deep fluids and are dependant on field conditions, plant design (flash or binary), and operator methods (Buscarlet et al. 2014). In high enthalpy, two-phase geothermal systems, such as the Rotokawa Geothermal Field, integrated management of re-injection directly above reservoirs is required to maintain field pressure and productivity. The re-injection of cool brine and steam condensate back into the reservoir is shown to increase local porosity and permeability through thermal stresses (Grant and Bixley 2011, Siratovich et al. 2014, Plummer et al. 2015). Reductions in down-well pressures indicate the opening of new flow channels as a result of thermal stresses created between the rock and fluid. Typically reinjection rates are observed to increase throughout the wells life until a point at which mineral precipitation is thought to surpass new fracture formation. At this point well-permeability declines and the well requires a stimulation programme or needs to be replaced. The precipitation of minerals from the saturated brines onto pore-space within the rock mass as a result of reinjection is not comprehensively understood.

1.7.2 Thermal Stimulation

Thermal stresses that are induced through the rapid cooling and heating of the groundmass are shown to increase near-well permeability of geothermal fields around the world (ie: Japan, Iceland, New Zealand) (Kitao et al. 1990, Axelsson and Thorhallsson 2009, Siratovich et al. 2011). This process is commonly refereed to as thermal stimulation. Thermal stimulation has become an important tool of geothermal operators to enhance reservoir permeability. Thermal gradients derived through the injection of cold water into a high-temperature reservoir results in the dilation of existing fractures and pore-space, and the creation of new micro-fractures (David et al. 1999), leading to the degradation of strength (Heap et al. 2013), and an increase in permeability (Faoro et al. 2013, Siratovich et al. 2011). Increases to permeability, as result of thermal stressing can be as much as two orders of magnitude (Axelsson and Thorhallsson 2009, Siratovich et al. 2015b). Thermal stimulation of a geothermal reservoir results in an increase to fracture network connectivity and opens further hydrological connections to permeable zones not intersected by wells (Grant and Bixley 2011).

The most common method of stimulation employed is high-pressure water injection, or through the intermittent injection of relatively cold water (or brine) to thermally stress the near-well formations. Stimulation also occurs during the drilling of wells through temperature contrast between the cold drilling fluid and hot reservoir rock. Upon completion of drilling, the well is further stimulated by pumping cold water down the well at high rates. This process thermally stresses the ground-mass, flushes loose particulate from the well and enhances near-well permeability. If a well behaves poorly over time, noted by high well-head pressures and low injection rates, recovery stimulation by thermal cycling of the well may be necessary. This process involves the intermittent injection of cold water, with cycling typically lasting from several days to several months. A successful stimulation program will be observed as a reduction in well-head pressure combined with increases rates of fluid flow. The process of stimulation cannot continue indefinitely, and is highly dependant on the existence of a temperature contrast between reservoir and brine; but it has been observed to continue for a few years (Grant and Bixley 2011).

The formation of new fractures can be attributed to the anisotropic expansion of minerals resulting in fracture formation along grain boundaries and through the mineral grains. Simmons and Cooper (1977) concluded that thermal expansion and contraction that induces fracturing is most effective in rocks that are not already fractured, theorising that existing fractures provide space for expansion to occur without subsequent fracturing. Fortin et al. (2011) shows that mechanically-induced cracks have lesser influence on permeability change than pre-existing thermal cracks. Axelsson and Thorhallsson (2009) showed that permeability of hot fractured rock increases strongly with decreases in temperature by a factor of 2-3. Clearwater et al. (2015) derived a simple analytic model based on the recognition that injection wells tend to follow a power law improvement over time with an exponent between 0.2 and 0.7.

Siratovich et al. (2014, 2015b) conducted laboratory-scale thermal cycling experiment of crustal rocks using distilled water. Significant increases in both porosity and permeability were observed, particularly in granite and basalt lithologies. Granites increased permeability from $1.27e^{-20}$ to $4.87e^{-17}$ m^2; basalts increase from $7.37e^{-20}$ to $1.08e^{-17}$ m^2; and rhyolites show less increase from $6.08e^{-18}$ to $2.08e^{-17}$ m^2. Increases in permeability were attributable to increased micro-fracture densities and

dilatency of existing fractures. Reductions in rock-mass density (through dissolution of glass, mechanical fracturing and potential sediment loss were also observed. Rhyolite samples tested showed increases in porosity, but significantly lower changes in permeability were observed, suggesting that groundmass-rich rhyolites behave in a more ductile manner during thermal stimulation, with some dissolution of glass occurring.

1.7.3 Fluid Dispersion

Where infield reinjection is essential to maintain reservoir pressure, such as the Rotokawa field, the location and the rate of injection are critical considerations in field operation. Reductions in pressure support can result in the closure of pores resulting in permanent destruction of porosity and permeability (Heap et al. 2014). Therefore targeted reinjection of spent brines is highly important to the geothermal system. At the injection point, fluids are not dispersed uniformly. Heterogeneity of rock mass, hydraulic pressure gradients (between the reinjection and the production point), fracture permeability and hydrodynamic instabilities such as viscous fingering (McDowell et al. 2015) drive and control convection of the reservoir. The rate at which fluids can return to the production reservoir is determined by fracture permeability connecting the area of production and reinjection, which have a differential hydraulic pressure gradient. As the reinjected fluid moves from the injection area towards the production area, heat is extracted from the rock matrix cooling the reservoir. The injection of relatively cool fluids into a hot geothermal reservoir is the driving process of thermal stressing and stimulation of the groundmass. In two-phase production zones, if cool brine reaches production reservoir too early and without sufficient reheating, thermal breakdown may result. Thermal breakthrough can lead to a number of operational problems. This includes the lowering of boiling temperatures of the fluids which reduces production enthalpy and results in the power plant running below design capacity. To make up for enthalpy losses, make-up wells and modifications to field operations may be necessary (Shook 2001).

1.7.4 Micro-Earthquakes

Micro-earthquakes (MEQs) are shown to be most frequent around zones of injection (Figures 1.4 and 1.5) (Sewell et al. 2013, 2015). This is due to the micro-fracture weakening of the rock mass, reducing stiffness and elasticity which results in the redistributing of stresses leading to micro-earthquakes developing as the system returns towards equilibrium. Fluctuations in pore-pressure are likely to play an important role in the distribution of forces that are acting upon pre-existing fractures.

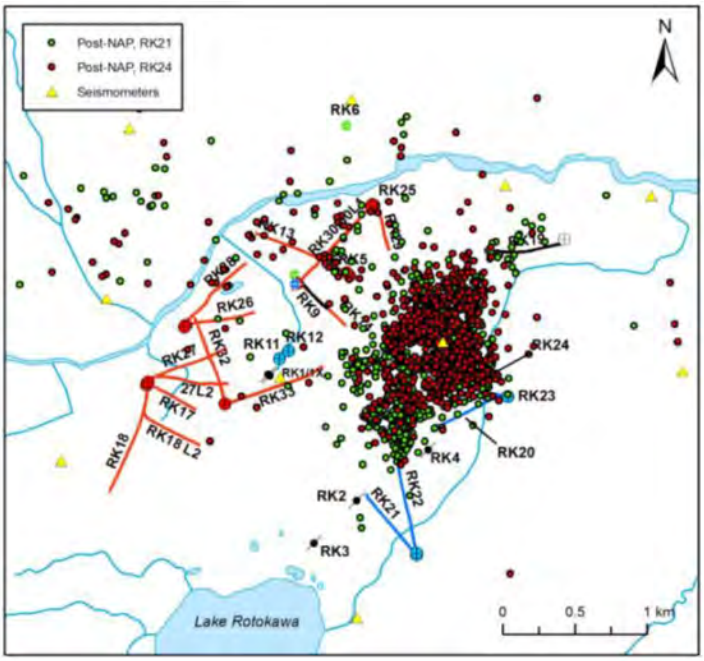

Figure 1.4: Map of MEQ locations from February 2010 to December 2012. A shift in the location of MEQ activity to the northwest is coincident with a large shift of injection from RK21 into RK24 (Sewell et al. 2013).

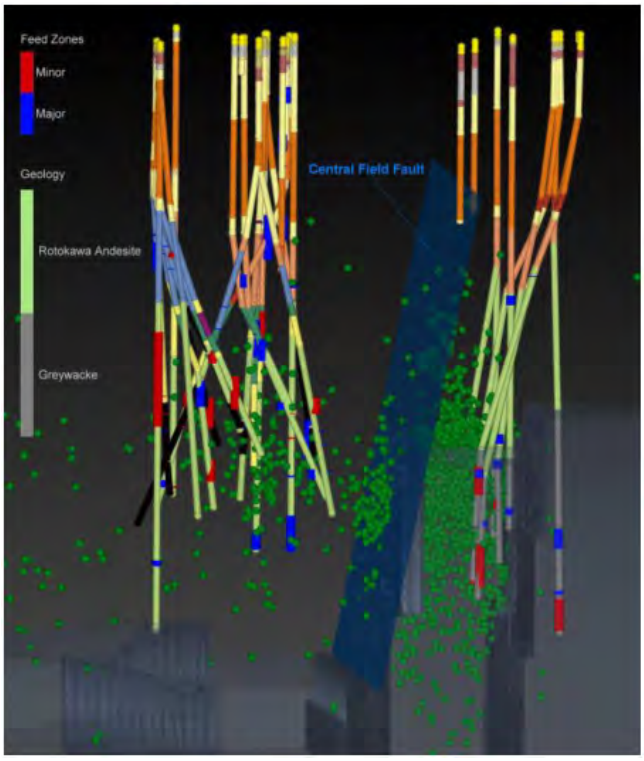

Figure 1.5: Three dimensional model of MEQ's from July 2008 to December 2012 at Rotokawa Field. Reinjection wells (right of CFF) and production wells (left of CFF). Reinjection is thought responsible for the MEQ's with the CFF providing an impermeable flow barrier restricting injectate from entering the production reservoir. From (Sewell et al. 2013).

1.8 Brine Chemistry

Optimisation of a geothermal system typically aims to extract as much work from produced fluids as is technically and economically feasible; this requires a sound understanding of the fluid chemistry. An understanding of pressure and temperatures gradients and permeable structures within the reservoir are also required for brine chemistry optimisation. Variations in chemical and isotopic composition of fluids, fluid temperature and enthalpy, as well as reservoir heterogeneity often prevent one method of optimisation being applied across the board (Giggenbach 1995).

The chemistry of geothermal fluids is affected by numerous processes including: the chemistry and gas content of reservoir fluid, pressure and temperature of the reservoir, gas solubility in the liquid phase, proportionate mass of steam produced, the stage at which steam separation occurs and reactions occurring during the steam phase. When steam is separated (flashed) from superheated geothermal fluids, either during ascension at the wellhead or at the plant, the separated liquid-phase becomes enriched in minerals and is referred to as brine. During flashing, more soluble minerals such as chloride, silica, and sodium remain in the fluid phase, resulting in the brine having increased salinity, and potentially becoming saturated or super-saturated with respect to dissolved minerals. Conversely, the steam-phase and subsequent steam condensates are typically under-saturated with respect to the dissolved mineral content. The temperature and pressure at which flashing occurs plays an important role in the relative concentrations of minerals left behind in the brine.

1.8.1 Silica

Silica is the second most common mineral in geothermal fluids and processed brines, sodium chloride salt (NaCl) being the first most common. The management of amorphous silica is of particular concern to geothermal operators and in many geothermal areas the optimisation of work taken from high-temperature (>200°C) fluid is significantly limited by silica scale that forms as the fluid cools (Zarrouk et al. 2014). The Silica Saturation Index (SSI) is typically used to characterise the relative concentrations of amorphous silica in geothermal fluids. For fluids over-saturated with silica (ie SSI>1), as defined by fluid temperature, pH, and dissolved mineral content two processes can occur. The process that occurs is dependant on the fluid environment. The first process is the deposition of monomeric silica onto available surfaces. This process is more common in turbulent flow conditions. The second process is the polymerization of monomeric silica to form silica polymers. This process is more common in low-turbulence environments (Gunnarsson et al. 2010). Amorphous silica can exist in many crystalline forms, with crystal structure and density determined by solution pressure and reactions with available cations (e.g. Al, Fe, Mg, Ca, Zn, etc.) forming co-precipitated silicate deposits (Guerra et al. 2012). Crystalline form plays a significant role on solubility, with the solubility of amorphous silica being 34 times higher than that of quartz.

Extensive work on the solubility of silica in pure water (White et al. 1956, Fournier 1977, Fournier and Potter 1982, Henley et al. 1984, Rimstidt 1997, Verma 1997) has lead to the development and subsequent refinement of the silica geothermometer. Mahon (1966) showed that the concentration of silica in wet-steam discharged from wells at Wairakei, New Zealand is in agreement with the solubility of quartz after corrections are made for adiabatic steam loss. This is in agreement with the silica content

of geothermal fluids being controlled by the solubility of quartz at depth, rather than the solubility of amorphous silica at and near the ground surface (White et al. 1956). The silica content of fluids at the surface provide an indication of the temperature at which the fluid was last in equilibrium with quartz at depth. However, when a single geothermometer is applied to all wells in a geothermal field, a wide variation in predicted reservoir temperature results. Reasons justifying these discrepancies include: the gain or loss of steam-phase fluid in the reservoir, mixing of different types of fluids or fluids from different sources, re-equilibration with ground-mass during ascension to the surface, and precipitation-dissolution processes (Truesdell and Fournier 1977). However, the silica geothermometer continues to be an integral part of almost all geochemical investigations of geothermal systems around the world. Verma and Electricas (2000) presented an equation (see 1.8.3) for the solubility of quartz along the water-vapour saturation curve for temperatures ranging from 0 to 374°C. This equation makes the basic assumption that the reservoir fluid is or was in equilibrium with quartz at depth. Limitations arise from the need to know the vapour fraction of two-phase fluids; to determine the vapour fraction, knowledge of the reservoir temperature is required.

1.8.2 Solubility

The transport of mineral components in geologic systems is a disequilibrium process which can be quantified through the understanding of dissolution and precipitation kinetics. Alkali cations strongly affect the dissolution kinetics of quartz (Dove and Crerar 1990). Rate constants that do not account for the accelerating effect of solutes may overestimate the temperature required to release a known amount of silica or the amount of reacting fluid required to pass through the system. However, the solubility of quartz is thought to control silica concentrations in active hydrothermal systems at temperatures greater than 180°C (Fournier and Rowe 1977a, Fournier and Potter 1982).

Amorphous silica begins to dissolve in H_2O at 0°C, solubility increases with temperature, peaking at approximately 340°C. For geothermal reservoirs of 200°C - 350°C amorphous silica or silicon dioxide (SiO_2) concentrations typically range from 300 - 700mg/l (Fournier and Rowe 1966). Two-phase fluid at NAP has silica concentrations of 950mg/l (GNS, May 2015). High concentrations are due to operator methods. The abundance of sodium chloride in the fluid, changes fluid pH, density and increases amorphous silica solubility. In the natural-state reservoir amorphous silica is in equilibrium with quartz.

1.8.3 Solubility Equations

$$\mathrm{SiO_{2(Quartz)}} \rightleftharpoons \mathrm{SiO_{2(aq)}} \tag{1.1}$$

Quartz Solubility $\mathrm{SiO_{2(aq)}}$

$$\mathrm{T(^{\circ}C)} = -42.196 + 0.28831\mathrm{C} - 0.00036685 * \mathrm{C}^2 + -0.00000031665 * \mathrm{C}^3 + 77.034 * \mathrm{Log(C)} \tag{1.2}$$

from (Fournier and Potter 1982)

Amorphous Silica Solubility $\mathrm{SiO_{2(s)}}$

$$\mathrm{Log(C)} = -\frac{731}{\mathrm{T(^{\circ}C + 273.15)}} + 4.52 \tag{1.3}$$

from (Fournier and Rowe 1977b)
Where:
C = $\mathrm{SiO_2}$ mg/kg or ppm
T = Temperature (°C)

Saturation of amorphous silica occurs in boiling zones and after an induction-time monomeric silica begins to polymerise resulting in the precipitation of silica in veins and void spaces. This leads to the destruction of local permeability, and the migration of fluid flow paths. Tectonic events may see the development of fractures and a return of geothermal fluids to the system. Studies into the silica induction period and polymerization rate are helpful in developing methods to controlling silica precipitation from geothermal brines. Modelling and experimentation by Björke et al. (2012) indicated that the solubility of silica is dependent on both pH and $\mathrm{Al(OH)_4}$ concentrations. Calculations showed that amorphous aluminous silica can precipitate from geothermal brine at temperatures as much as 25°C higher than that of pure amorphous silica. Alkali cations also markedly increase the dissolution rate of quartz and amorphous silica. (Dove and Crerar 1990) for example: a sodium-bearing solution at 200°C can mobilise silica at the same rate as pure water at 300°C.

The temperature of fluids flashed at the wellhead depend on the wellhead pressure. Temperatures typically range between 160°C and 250°C. Cooling occurs by conduction at the surface, particularly if the fluids are passed through a heat exchanger. The amorphous silica saturation point is reached during the cooling of processed brines. This typically occurs at temperatures between 100°C and 200°C, but is also highly dependant on the fluid pH. If the fluid cools below the saturation point, relatively rapid precipitation of amorphous silica can occur. Depending on the plant operation methods, amorphous silica scaling may form in production wells, surface facilities, and downstream injection wells (Angcoy and Arnórsson 2010). Silica scaling causes serious reductions in fluid flow to production wells, flash vessels, binary units and the injection system. In addition to causing flow reduction, silica scaling seriously affects heat transfer in a binary unit plant (Burton et al. 2003). To avoid amorphous silica scaling, it is common to dispose of (or re-inject) the brines at temperatures above the amorphous silica saturation point. This method of disposal results in a relatively inefficient use of the heat energy brought to the surface (Gunnarsson and Arnórsson 2005).

1.8.4 Silica Saturation Index

The level of energy extraction from produced geothermal fluids is generally controlled by silica rather than other chemical components. Until relatively recently almost all geothermal power developments that reinjected fluid operated by keeping the amorphous silica under-saturated (SSI < 1.0) or at low levels of silica saturation (SSI < 1.2). However, to optimise generation capacity by maximising the work that the 2-phase geothermal fluid does, the SSI is often raised to values significantly higher than saturation level. For example, the Nga Awa Purua station operates reinjection at at a SSI of between 1.9 and 2.3 (Addison et al. 2015). To operate with fluids at these high SSI values, the pH of brine requires modification to prevent silica precipitation.

Many methods exist for the control of silica precipitation (Guerra et al. 2012). Further opportunities exist to develop standard technological tools and methods to both monitor silica management and reduce silica deposition risk within the plant, the wells and in the near well-bore reservoir (Addison et al. 2015). Recent developments in New Zealand (Addison et al. 2015) have utilised pH modification to inhibit silica polymerization. Acidification (or pH modification) of single phase geothermal brine by the addition of sulfuric acid or hydrochloric acid is shown to have a kinetic effect, delaying the initiation of silica polymerisation; with minor changes to silica solubility also observed (Iler 1979). The acidification of brines has become an important tool to field operators, allowing fluids to do more work and be returned to the reservoir deep reservoir at lower temperatures, while still minimising or preventing scaling. The addition of low-pH steam condensate is often used in binary plants or flash plants where shell and tube condensers are utilised. The reduction in pH in brines that are reduced to low temperatures, can lead to the possibility of other species depositing such as antimony sulfide or arsenic sulfide. As the pH is reduced, the risk of corrosion for carbon steel increases.

Monitoring well injection rates and well pressures can provide early warning of silica scaling, with affected injection wells potentially requiring a mechanical work-over, acidizing the well or drilling of a new replacement well. A common injection strategy is the periodic switching between separated brine and condensate across injection wells in order to manage their decline and recovery cycles. This method temporarily enhances injection wells performance, and delays the immediate need of a make-up well (Kaya et al. 2011).

1.9 Taupo Volcanic Zone (TVZ)

The low-pressure geothermal brines used in this thesis have been recovered downstream from the triple-flash Nga Awa Purua station. Nga Awa Purua is one of two geothermal power plants on the high-enthalpy Rotokawa geothermal field. Samples of Rotokawa andesite were retrieved from the Rotokawa field during the drilling of production well RK30. The Rotokawa field is one of 23 high-temperature geothermal systems identified within the Taupo Volcanic Zone (TVZ), New Zealand. Temperatures of these systems range from 265°C (Wairakei) to 326°C (Mokai) (Kissling and Weir 2005). It is estimated that the natural heat flux of TVZ is 4200±500 MW (Bibby et al. 1995). The heat flux is channeled through geothermal systems that predominantly exist along the east and western margins of the TVZ.

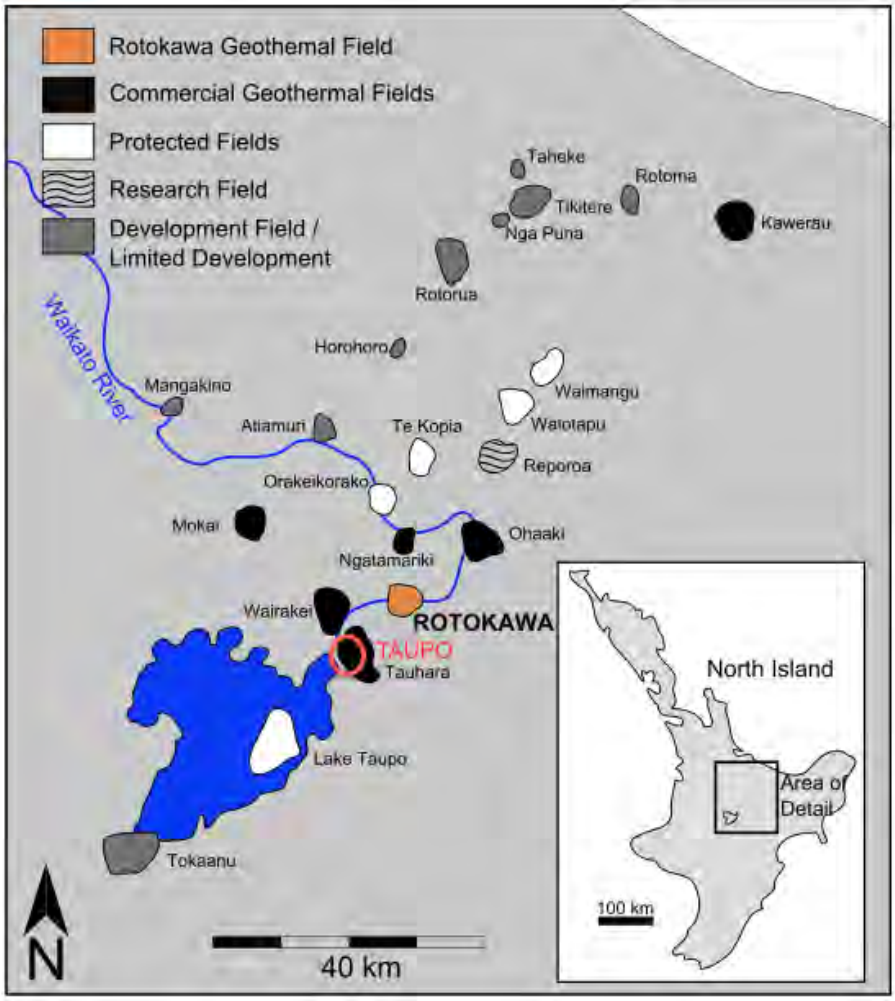

Figure 1.6: Geothermal fields of the Taupo Volcanic Zone (TVZ), North Island, New Zealand. Core and brines used in this study were sourced from wells drilled in the Rotokawa Geothermal Field (Figure adapted from Sewell et al. (2012)).

1.9.1 Geologic Setting

The Taupo Volcanic Zone (TVZ) is a 350km long by 100km wide region dominated by volcanic and tectonic processes. The TVZ arc-basin has formed to accommodate rigid flexure of the continental crust. Central sections of the TVZ reach elevations of 300m to 600m above sea-level. Regional extension and crustal thinning of the TVZ is associated with subduction of the oceanic Pacific Plate beneath the continental Australian Plate (Figure 1.7). Subduction rates range from 38mm/year in the south to 45mm/year in the north (DeMets et al. 1994). Subduction processes drive partial-melting and magmatic processes. As a result, silica-rich volcanism is thought to have dominated the landscape for the last 2 Ma (Wilson et al. 1995), with widespread ignimbrite eruptions occurring from the TVZ area for the past 0.6 Ma (Cole 1990).

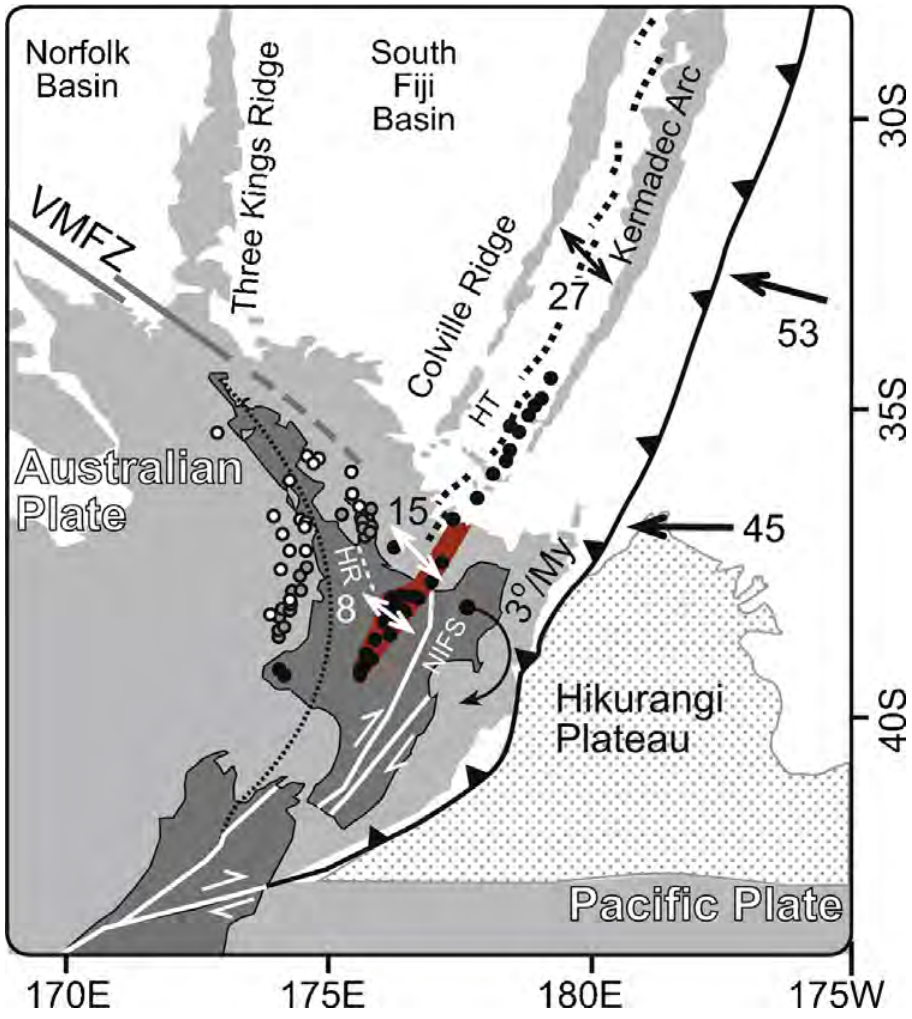

Figure 1.7: Current tectonic setting of northern New Zealand, annotated with loci of volcanism for three different time periods ±0.5Ma (Circles: black = 0Ma, grey = 8Ma,white = 16Ma) from Seebeck et al. (2013), geodetic vectors of extension (doublearrows: (Parson and Wright 1996, Wallace et al. 2004)) and relative plate motion(single arrows: DeMets et al. (1994)) in mm/year. Terrane suture in basement rocks as inferred from magnetic anomaly = dotted line. Rotation of eastern North Island shown for the period 3Ma to present (Wallace et al. 2004). HR = Hauraki Rift; HT = Havre trough; NIFS = North Island Fault System; VMFZ = Vening Meinesz Fracture Zone. From Wilson and Rowland (2015).

The central region of the TVZ is characterised by active rifting and normal faulting. The actively rifting arc, referred to as the Taupo - Rotorua Fault Belt, is widening at a rate of 7mm/year in the south and 15 mm/year at the Bay of Plenty coastline (Wilson and Rowland 2015). Stretching and

normal faulting have resulted in continental crust thinning to 15-16 km in thickness (Spinks et al. 2005, Bibby et al. 1995). The depth to basement greywacke varies between 500m to 1000 m below sea-level. However, the basement is found at greater depths beneath calderas within the region (Healy, 1982). Surface expressions of rhyolite, ignimbrite, dacite, andesite and high-Al basalts along with lacustrine and volcanic-derived sediments are found within the TVZ (Grindley 1960). The northern and southern ends of the TVZ are marked by andesitic stratovolcanoes, the central region is marked predominantly by rhyolitic caldera volcanoes (Graham et al. 1995). Rhyolitic magmatism and large caldera-styled eruptions have been dominant within the TVZ landscape, with 8 calderas active within the last 1.6 Ma, the most recent of which was the Taupo caldera eruption in 186AD (Wilson et al. 1995, Manville et al. 2009). Geothermal systems of the TVZ commonly occur on caldera margins where there is enhanced deep permeability.

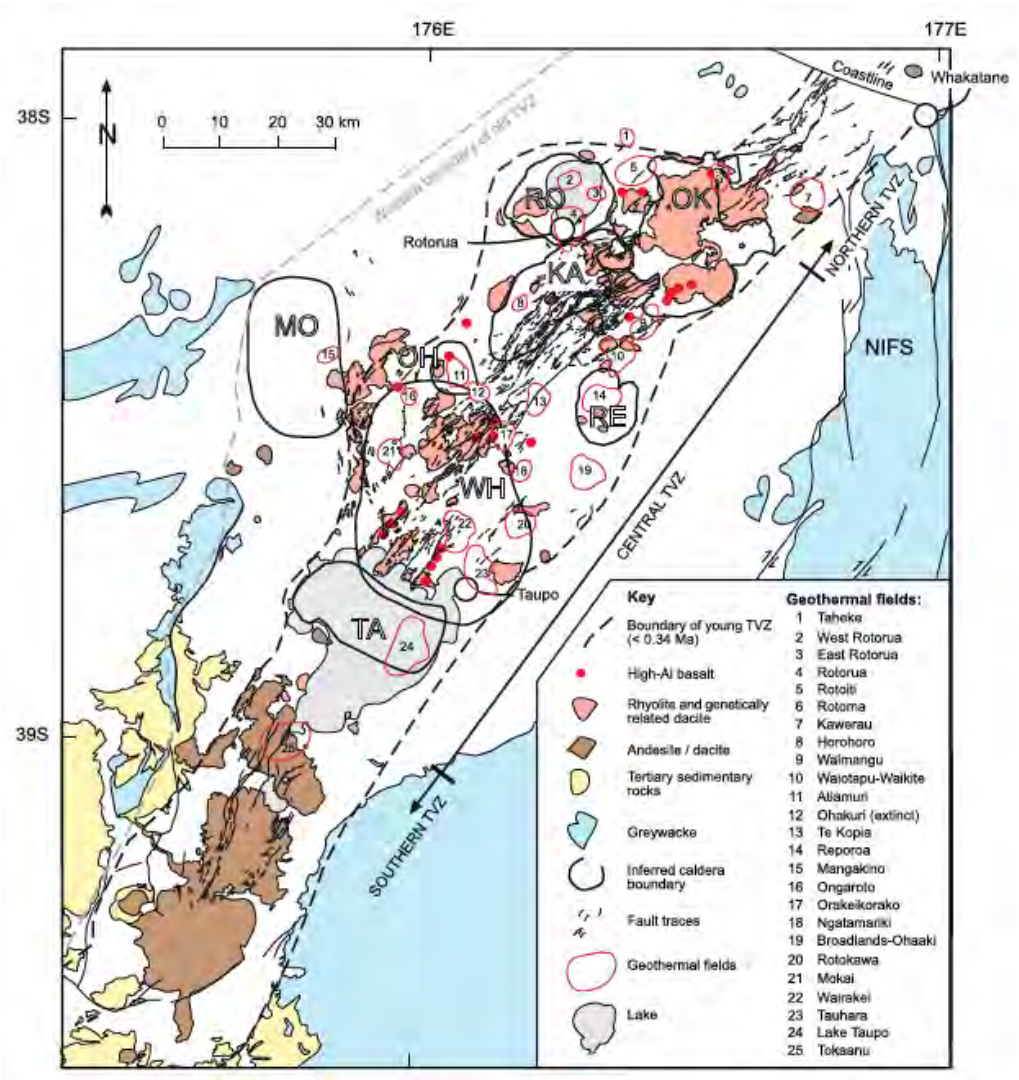

Figure 1.8: Geology of the TVZ showing major lithological units (after (Grindley 1960); Healy et al. (1964); Leonard et al. (2010)). White regions represent rock types other than those indicated (i.e., volcaniclastic rocks, lake sediments, reworked materials). Caldera boundaries are after Nairn et al. (1994), Gravley et al. (2007): KA - Kapenga, MO - Mangakino, OH - Ohakuri, OK - Okataina, RE - Reporoa, RO - Rotorua, TA - Taupo, WH - Whakamaru. Boundaries of the TVZ are modified after Wilson et al. (1995) and Villamor and Berryman (2001, 2006). The young TVZ boundary is a composite of that defined on volcanic grounds (Wilson et al. 1995) and that defined on structural grounds (Villamor and Berryman 2001, 2006). NIFS = North Island Fault System. Low-resistivity zones were used to delimit the geothermal fields (Bibby et al. 1995). Major towns labelled. From Wilson and Rowland (2015)

The Rotokawa geothermal field lies on the eastern margin of the Whakamaru Caldera (Figure 1.8). The Whakamaru group represents the most intense period of voluminous eruptions from the TVZ (approximately 0.34-0.36 Ma), where 200m thick ignimbrite have been deposited. Rhyolite and genetically related dacite can be found directly to the north of the Rotokawa field. Isotopic signatures provide geological evidence for a genetic link between sub-caldera magma chambers, and geothermal systems (Bégué et al. 2014).

1.9.2 Rotokawa Geothermal System

The Rotokawa geothermal field (Figure 1.6) is located towards the south-eastern margin of the Taupo Volcanic Zone (TVZ) about 10km to the north-east of Taupo township. The field's extent was initially discovered through deep drilling by the New Zealand Ministry of Works and the Department of Science and Industrial Research (DSIR) in the 1980s. Resistivity studies were also conducted (Bibby 1988, Bibby and Hohmann 1993, Heise et al. 2008) on numerous occasions. The field resistivity boundary indicates that the field covers an area of up to 28km^2, comparable in size to other successful geothermal fields in New Zealand.

The Rotokawa field is host to two power plants, and in 2015 generated close to 180 MW. Generation at the 24MW Rotokawa 1 (RGEN) combined-cycle binary-plant began in 1997 and a number of minor expansions within the next decade brought production up to 35 MW. The Nga Awa Purua (NAP) 140 MW triple-flash conventional evaporative-cooling plant was commissioned in early 2010. Twelve production wells (2000-2500m deep) along a SW-NE axis in the central field, south of the Waikato River supply two-phase high-enthalpy (1,560kJ/kg) fluid to both RGEN and NAP plants. Injection of flashed brines and condensate from both RGEN and NAP is through 5 ($\sim$3000m deep) injectors drilled south of the Central Field Fault (CFF)(Figure 1.10) along the southeastern margin of the reservoir. A limited amount of spent water is also injected into a shallow (450m) thermal aquifer to mitigate acid carbonate corrosion to production well casings (Bowyer et al. 2008, Horie 2008, Powell 2011).

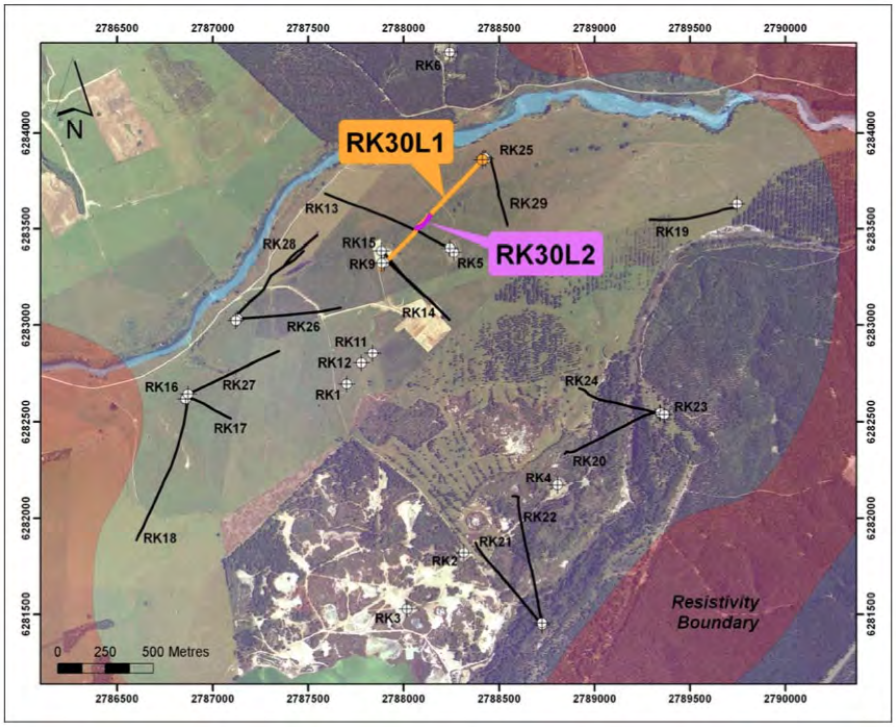

Figure 1.9: Map of the Rotokawa geothermal field showing location of forked production well RK30. Leg (RK30L1) is shown in orange. Leg 2 (RK30L2) has a similar azimuth direction to RK30L1 but with a steeper inclination is shown in purple. The red shaded area represents the inferred resistivity boundary for the Rotokawa Geothermal Field (Risk 2000). Image from (Rae et al. 2010).

Surface thermal activity at the Rotokawa field (Figure 1.10) comprises of steaming ground, fumaroles, and springs, and is concentrated to an area ($\sim$1.2km^2) that extends northeast from the margin of Lake Rotokawa. Breccia deposits from at least eight hydrothermal eruptions (dating back to 22,000 years) have been identified in the southern part of the field, a result of some of the largest hydrothermal eruptions known globally for geothermal environments (Collar 1985, Collar and Browne 1985, Browne and Lawless 2001). The largest eruption, $\sim$6,000 years ago, sourced from Lake Rotokawa, produced deposits that cover an area of about 15km^2 with the youngest known eruption occurring ca.3,700 years ago. The location of hydrothermal eruption vents, deduced from deposit thickness and the distribution of large clasts, align on a northeasterly trend. These surface expressions extend >1km along strike and are the likely trace of a fault and a zone of elevated fluid flow (Collar 1985). Comparison of extrusive ejecta breccia clasts with stratigraphic units taken from drill cores suggest that focal points for eruptions exceed 450m in depth (Collar 1985, Collar and Browne 1985).

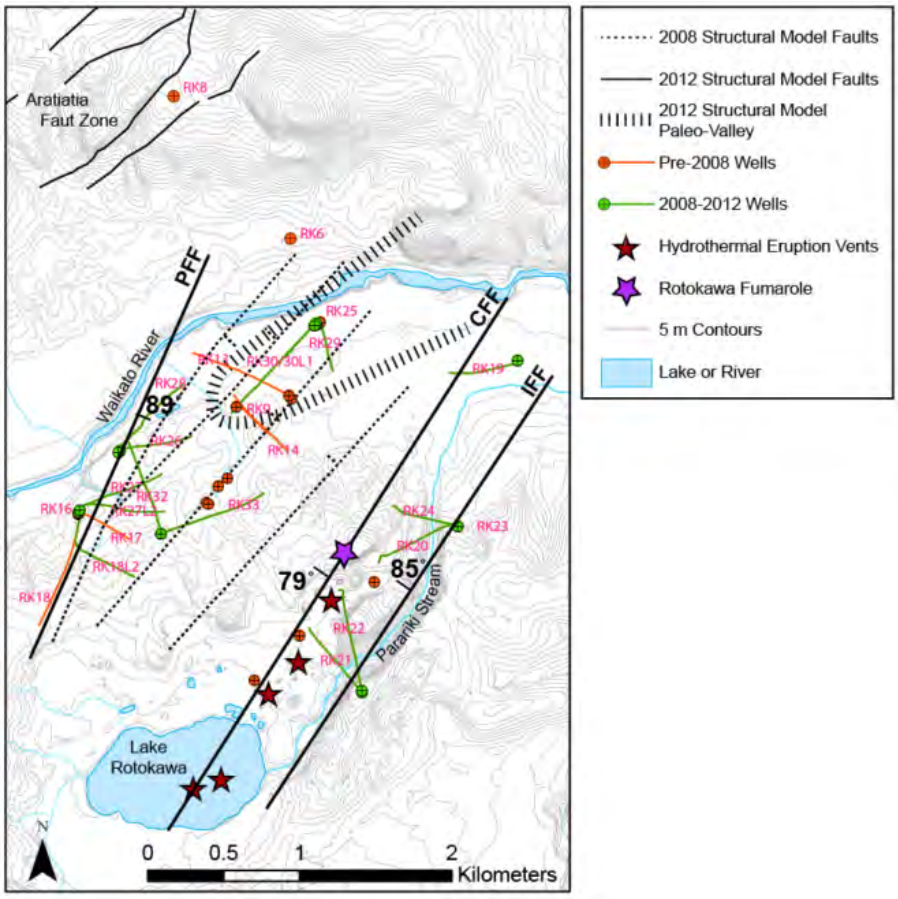

Figure 1.10: Map of the Rotokawa geothermal field showing the Bowyer et al. (2008) structural fault model (dotted lines) and the Wallis et al. (2013) structural fault model (solid lines). PFF - Production Field Fault, CFF - Central Field Fault, IFF - Injection Field Fault. Image from Wallis et al. (2013)

Deep basement structure of the Rotokawa Geothermal Field is dominated by regional extension, with north-east trending normal fault systems providing the major conduits for fluid flow within the deep reservoir. Basement block-faulted greywacke is overlain by primary reservoir lithology, the Rotokawa Andesite (RKA), a porous, flow banded, mottled pale green and reddish purple, pyroxene-bearing, porphyritic andesite lava (Siratovich et al. 2012). The RKA ranges in thickness from 865m to 2190 m (Rae 2007). The rank and style of hydrothermal alteration occurring in both pores and fractures of the RKA is indicative of high-temperature and high-permeability conditions. High permeability is likely due to large fault structures in the deep reservoir acting as major conduits for up-flow through the basement greywacke into overlying RKA. The primary formation-permeability of the RKA also allows for vertical and horizontal flow of fluids along lava interfaces, breccias and cooling joints. The RKA reservoir is capped by the relatively impermeable, intra-caldera, Wairakei Ignimbrite, a member of the Whakamaru Group. Faulting allows fluid to pass through this formation, and is responsible for surface activity, such as those marking the trace of the CFF. At shallow depths, a low vertical primary-permeability persists in the rhyolite and breccias. However, the interface between formations provides horizontal permeability for cold meteoric water inflow (Rae 2007, Winick et al. 2009).

Formation Name	Thickness Range	Lithology
SUPERFICIAL (incl. Oruanui Formation)	10 to 30 m	Unaltered and thermally oxidised pumice tuff, rhyolite lava lithic clasts and unaltered quartz and feldspar crystals
HUKA FALLS FORMATION	15 to 150 m	Fine sandstone and siltstone with some pumice-rich subunits.
PARARIKI BRECCIA	20 to 220 m	Strongly altered, quartz-feldspar rich tuffaceous breccia with a silty-clay matrix
WAIORA FORMATION	90 to 550 m	Crystal-rich, hornblende bearing vitric tuff
RHYOLITE LAVA AND BRECCIA	110 to 660 m	Crystal-poor, rhyolite lava and breccia
WAIRAKEI IGNIMBRITE	200 to 390 m	White, crystal-rich, non to densely welded ignimbrite. Large quartz crystals are often heavily embayed
WAIKORA FORMATION	10 to 250 m	Rounded to sub-rounded greywacke and argillite gravels.
TAHORAKURI FORMATION	20 to 250 m	White, crystal-vitric-lithic tuff
ROTOKAWA ANDESITE	865 to 2190 m	Mottled, pale green and reddish purple, pyroxene-bearing andesite lava.
GREYWACKE BASEMENT	-	Dark to pale grey, weakly metamorphosed argillite and fine silty sandstone

Figure 1.11: Generalised stratigraphy of the Rotokawa geothermal field from (Rae 2007)

Resistivity studies by Bibby (1988), Bibby and Hohmann (1993), Heise et al. (2008) reveal a low resistivity layer (1-3Ωm) at shallow depths (250-400 m below surface) representing a porous aquifer on top of the geothermal system characterised with intense hydrothermal clay alteration ($< 200°$C). Beneath the shallow aquifer, resistivity of $\sim$20Ωm represents a transition to higher temperature ($> 200°$C) alteration clays such as illite and chlorite. The resistivity increases at deeper levels ($>$ 1.2km) to $\sim$35Ωm, as porosity reduces and the intensity of alteration in the andesite decreases (Rae 2007). Knowledge about the deep, high-temperature part of the geothermal system is interpreted from core that has been recovered from drill holes and fluid chemistry, as geophysical exploration techniques are not able to clearly resolve structures below $\sim$1500m (Heise et al. 2008).

The clearly defined Central Field Fault (CFF), identified as a normal fault in production well RK17, indicates that the Rotokawa andesite has been downthrown to the south-southeast by more than 690 meters (Rosenberg et al. 2005). The CFF is part of a larger graben structure that has since been infilled by reservoir capping Reporoa Group sediments and the Wairakei Ignimbrite. The CFF is assumed to act as an impermeable barrier across its strike, preventing injectate from flowing between injection and production reservoirs. This is evident in the modelling of micro-earthquake swarms (Figures 1.4 and 1.5) which clearly cluster around injection points but reduce drastically at inferred fault location (Sewell et al. 2013, 2015, Winick et al. 2015).

Long term subsidence at the Rotokawa geothermal field is associated with metasomatic rock mass removal due to propylitic hydrothermal alteration and the dissolution of plagioclase feldspar phenocrysts in the andesite rock-matrix (Pochee 2010). When compared to unaltered samples, highly altered samples show a porosity of up to 18% and silica (SiO_2) loss of as much as 15%. Surface and subsurface discharge of hydrothermal fluids to outside of the system is likely to account for a majority of net losses but not all dissolved silica leaves system. Deposition in fractures and zones of matrix silicification are likely to account for some of the migrating SiO_2 mass, local decreases in porosity, and a net mass gain. Lithostatic loading has lead to the gradual collapse of the alteration-developed porosity, resulting in the long-term compaction and subsidence of the Rotokawa reservoir. Fracturing, associated with this long-term subsidence plays an important roll in reservoir permeability.

Rock-matrix that displays significant alteration to chlorite-mica is substantially weaker than the matrix of unaltered andesite lava. Evidence suggests that hard or brittle rock features would be most susceptible to fracturing due to alteration-induced compaction (Powell 2011). High temperatures would likely favour ductile failure in softer material surrounding any isolated patches of harder rock rather than brittle fracturing of hard patches of rock. Brittle features need to exist as interconnected networks within the compacting rock rather than as isolated bodies. The most likely zones to be fractured by alteration induced compaction would be pre-existing networks of hard rock, such as quartz veins and zones of silicification, and perhaps layers of very hard primary rock, such as welded ignimbrite. In this way, progressive hydrothermal alteration may enhance local permeability by repeatedly fracturing a surrounding network of hard vein material, leading to a positive feedback between alteration and permeability development, as greater local permeability promotes further alteration (Pochee 2010, Powell 2011).

1.9.3 Rotokawa Geochemistry

Interactions between magmatic, tectonic and hydrothermal processes in the Taupo Volcanic Zone have produced inherent variability in the nature and evolution of hydrothermal flow paths, hydrothermal alteration, and the potential sites of epithermal mineralisation making fluid-flow paths complex and difficult to predict (Rowland and Simmons 2012). Despite significant efforts to identify a single geochemical source for fluids of the Rotokawa geothermal system, ambiguity to the exact origin of deep-reservoir fluids remains. A conceptual model (Figure 1.3) by Winick et al. (2009) accommodates both single and multiple-parent geochemical fluid sources, as well as the potential for steady-state and transient reservoir conditions. Factors such as boiling and reservoir dilution are accounted for in modelling and while a single geochemical parent could be likely, multiple fluid sources can not be ruled out (Winick et al. 2009).

Hot, deep two-phase up-flow, flows from the system toward the north. Progressive dilution along the outflow from marginal fluids is largely responsible for geochemical gradients. The large structural feature of the CFF provides a zone of enhanced permeability, allowing deep reservoir fluids to ascend and boil within an intermediate reservoir. The intermediate aquifer is a complex mixture of deep fluids, steam condensate, fluids from nearby reservoirs and ground water (Winick et al. 2009). Drill cuttings from the Rotokawa field indicate that acid sulphate and bicarbonate fluids are present in the cooler, shallow, groundwater aquifer (<500mRSL). The presence of these fluids is attributed to hot (>250°C) deep reservoir fluids, leaking through the otherwise impermeable Wairakei Ignimbrite reservoir cap rock, boiling and then condensing CO_2 and H_2S into the groundwater aquifer.

The Nga Awa Purua station handles 45,000t of two-phase fluid per day, with around 75% of that fluid being reinjected back into the deep reservoir. Limited injection of brine into the shallow reservoir aims to saturate the zone and neutralise corrosive fluids, slowing the rate of well-casing corrosion (Bowyer et al. 2008). Injectate is pure steam-condensate, or separated-brine mixed with low-ph dilute steam condensate. The Silica Saturation Index (SSI) of reinjected brine ranges from 1.9 to 2.3 (Addison et al. 2015). Due to super-saturation in respect of amorphous silica, brine acidification and dilution with steam condensate is required to inhibit amorphous silica polymerisation. The dosing of brines with

sulphuric acid (H_2SO_4) lowers brine pH, significantly suppressing the polymerisation of colloidal silica, and delaying scaling across pipes and injection well surfaces. Once the brine reaches the reservoir, pH is buffered immediately through the mixing of fluids. At this point precipitation of silica will occur if the reservoir temperature in the injection area is below the brine saturation point. Amorphous silica is deposited in pore spaces resulting in a reduction in new-well formation permeability and injection well flow-capacity (Buscarlet et al. 2014).

Thermal gradients between injectate and reservoir temperature is high. Injectate temperature ranges from 90°C to 130°C with the injection reservoirs measured natural-state temperature ranging between 320°C - 340°C (Sewell et al. 2012). The thermal contrasts between reservoir and injectate drives thermals stresses resulting in anisotropic thermal contraction and fracturing of minerals. This results in the reduction of groundmass stiffness and elasticity. With time, the effect of injectivity decreases at which point mineral precipitation is thought to take over (Grant and Bixley 2011). The threshold between cyclic stimulation and effectiveness for Rotokawa andesite is not well known (Addison et al. 2015).

1.9.4 Nga Awa Purua

Nga Awa Purua (NAP) or Rotokawa II (commissioned April 2010) is New Zealand's second largest geothermal power station, with a generation capacity of 140MW and an annual generation of 1100 GWh. The power station is a joint venture between Mighty River Power (MRP) and the Tauhara North No.2 Trust. See Appendix A for an overview of the Nga Awa Purua power station and operating procedures including steam separation system and full geochemical analysis of Nga Awa Purua low-pressure brine.

Figure 1.12: Photograph of the Nga Awa Purua power generation facility. From (Horie and Muto 2010).

Modelling of silica polymerisation indicated that without treatment, colloidal silica formation would likely occur at the IP stage of separation. To prevent polymerisation and deposition of silica in the Intermediate Pressure (IP) and Low Pressure (LP) brine systems, sulfuric acid is dosed into High Pressure (HP) brine. The rate of acid injection is adjusted to maintain a pH of 5.0 in the LP brine reinjection system. However, the acid dosing rate is highly dependant on brine composition which is observed to change when production-well flows are adjusted. Steam purity monitors give on line readings of steam pH, Chloride (Cl^-) Silica (SiO_2) and non-condensable gas (NCG) concentrations (Horie and Muto 2010).

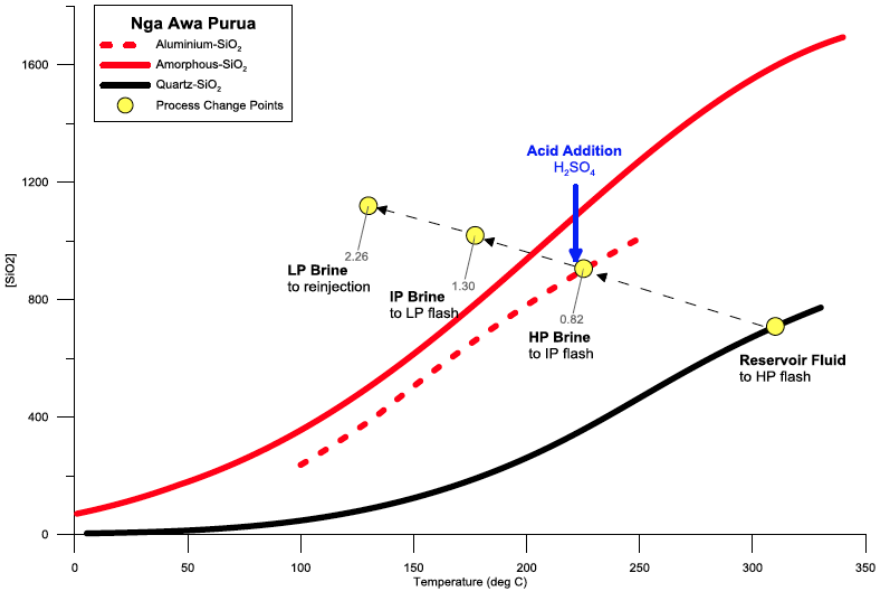

Figure 1.13: Overview of the Nga Awa Purua brine managment showing addition of H_2SO_4 to lower pH and delay silica polmerisation. (Addison et al. 2015)

Chapter 2

Materials and Methodology

The Rotokawa geothermal reservoir is heterogenous, anisotropic and highly altered (Rae 2007, McNamara et al. 2015). Because of this, experimentation with the Rotokawa andesite can be complicated with results difficult to interpret (Siratovich et al. 2014). To simplify alteration mechanisms occurring during thermal-cycling experimentation, initial testing used a isotropic, homogenous and unaltered Ghibli granite.

By minimising the effects of rock heterogeneity, and pre-existing chemical alteration, the focus of this study could be directed towards developing robust methods to explore physical changes occurring as a result of thermal stresses through repeated thermal cycling. Once the methodology was developed for distilled water and Ghibli granite, geothermal brines and Rotokawa andesite were used in experiments.

2.1 Materials

The effects of thermal cycling of granites have already well explored (Fredrich and Wong 1986, Darot et al. 1992, David et al. 1998, Chaki et al. 2008, Siratovich et al. 2014). The initial thermal cycling experiments on Ghibli granite provided a benchmark for comparison to subsequent thermal cycling experiments to cores of Rotokawa andesite. Physical changes to rock properties as a result of thermal cycling of the two lithologies has been reported in Results.

There are significant differences between the two lithologies tested in this thesis (refer to Petrographic section in Results). Ghibli granite was chosen for its physical properties; medium grained, holocrystalline, homogenous, non-weathered, minimal secondary fracturing and alteration and ease of availibility. Rotokawa andesite in comparison, is highly variable, heterogenous, of significantly higher porosity than granite, and often displays high hydrothermal alteration. Initial properties of the RKA samples used in this thesis (density, porosity and permeability) was obtained from Jones (2016).
Previous experimentation by Siratovich et al. (2014) looked at the thermal cycling of granite and Rotokawa andesite using distilled water. Experimental simulation of fluid-mineral interaction was conducted by Mountain and Sonney (2011) using continuous flow-through hydrothermal apparatus capable of high temperature, high pressure and low flow conditions. New Zealand greywacke was reacted with distilled water and re-injection brines (from Wairakei station) to study the effects on brine chemistry and secondary mineral formation. Experiments using unaltered greywacke, reacted with distilled water and re-injection brine, showed the formation of clay minerals and possible zeolite

phases. Those conducted at re-injection temperatures using re-injection brines showed the formation of amorphous silica deposits whose textural characteristics were affected by the amount of silica polymerisation.

The depositional characteristics of cold separated geothermal water (SGW) were determined at the Wairakei geothermal field by Mroczek et al. (2013). Aged and cooled SGW was passed through a bed packed with dacite chips in a month long trial. No silica was deposited in the packed bed but iron and silica rich scale was deposited at the inlet screen. It is likely that the colloidal silica was flocculated by the iron corrosion product. Based on these positive results Contact Energy implemented an injection trial, with 200 t/hr of cold SGW injected into a cooler outfield sector west of the field, which successfully ran for 10 months.

2.2 Sample Preparation

2.2.1 Core Samples

The preparation of core samples was undertaken at the University of Canterbury. Core was drilled from 120 x 120 x 30 mm blocks of Ghibli granite using a Wendt 20mm internal-diameter diamond-tip coring bit mounted to a drill press. Drill speed was maintained at 740rpm with tap water used as a drilling fluid to both lubricate and cool the drill bit. Orientation of the core was maintained approximately perpendicular to an observed weak biotite-mica fabric. Drilled samples were cut and diamond polished to 40mm in length and within 0.02mm of square. Ulusay and Hudson (2007) recommends using a 2:1 (1:1.8 1:2.2) length to diameter ratio. Samples that did not meet these conditions were used in point load testing and subsequently discarded. After grinding samples were rinsed with distilled deionized water and submerged in an ultrasonic bath for no less than 5 minutes to remove loose particulate that has been derived through the preparation of samples. Axial and diametral lengths were measured using calibrated digital callipers (accurate to $\pm$0.01mm) ensuring measurements were taken parallel to the axis being measured. Rotokawa Andesite samples were prepared by Tim Jones (Jones 2016) in other thesis work.

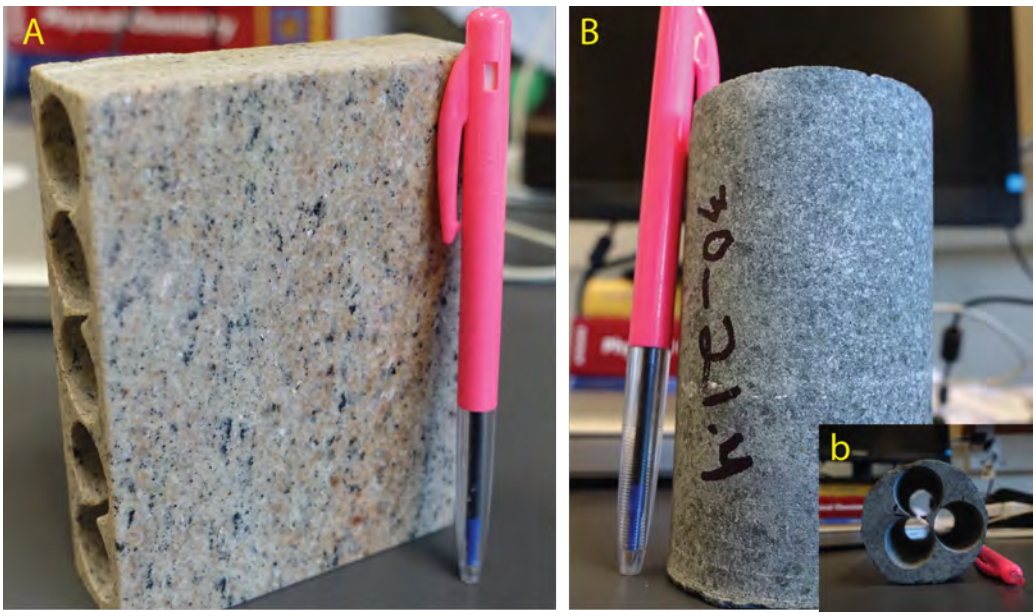

Figure 2.1: Photograph of Ghibli granite (A) and Rotokawa andesite core (B) (RK30-21.4). For A note the core-sample orientation being approximately perpindicular to biotite-mica fabric. For the RKA, note the close proximity of samples (b) with physical properties giving indication of high heterogeneity.

2.2.2 Thin Sections

The preparation of thin sections was undertaken with help from Rob Spiers, Senior Lab Technician in the department of Geological Sciences at the University of Canterbury. Thin sections were made from off-cuts of Ghibli Granite and Rotokawa Andesite. Thin sections were cut to 30μm in thickness, polished with colloidal silica and mounted on a glass slide for petrographic observation, both before and after thermal cycling.

2.2.3 Scanning Electron Microscopy

Mounted thin-sections of Ghibli granite were imaged using EDS in the Scanning Electron Microscopy (SEM) to determine infilled fracture composition. Carbon coating to enhance conductivity was applied under supervision of Dr. Kerry Swanson. Mike Flaws from the Mechanical Engineering Department helped with operating the scanning electron microscope.

2.3 Porosity and Density Measurements

Bulk volume, pore volume, porosity and the dry density of samples used in this thesis were determined using the triple weight method as suggested by Ulusay and Hudson (2007). This method requires the measurement of the saturated, submerged and dry weight of each sample. All weights were measured using the same digital scales (accurate to 0.001g) which were levelled prior to use. For saturation, samples were submerged in a bath of de-ionised, distilled water (H_2O). A vacuum pressure of -100kPa was applied for a period of no less than 24 hours to overcome capillary pressure. The sample was then suspended beneath the scales in a bath of H_2O. Submerged weight was recorded once the sample became motionless. The sample was removed from bath, surfaces were dried with paper towels and then the saturated weight was recorded. Speed between these two tests was important as the sample

began to dry (decrease in mass) immediately after leaving the bath, introducing experimental error. Samples were placed in an oven at 105°C and dried for a minimum period of 24 hours, until a constant dry-weight was recorded. Using the following equations (Ulusay and Hudson 2007), sample bulk volume, pore volume, porosity and dry density were calculated.

$$\text{Bulk Volume (V)} = \frac{M_{sat} - M_{sub}}{\rho_w} \tag{2.1}$$

$$\text{Pore Volume } (V_v) = \frac{M_{sat} - M_s}{\rho_w} \tag{2.2}$$

$$\text{Porosity } (\eta) = \frac{100V_v}{V}\% \tag{2.3}$$

$$\text{Dry Density } (\rho_d) = \frac{M_s}{V} \tag{2.4}$$

Where:
M_{sat} = Saturated weight
M_{sub} = Submerged weight
M_s = Dry weight
ρ_w = Density of pore fluid

The triple-weight method was repeated after thermal-cycling experiments, with changes to sample bulk volume, pore volume, porosity and dry density reported.

2.4 Point Load Test

Point load strength index testing is a quick, simple test that gives good estimation of tensile rock strength. Fracturing and failure induced by point load testing occurs under tension, similar to failure induced by thermal stressing. By conducting this test, anisotropic mechanical strength across two axis which may influence the direction for propagation for thermally induced stress fractures may be identified.

Point load strength index testing of the Ghibli granite core was undertaken in the Soil Mechanics laboratory at the University of Canterbury using an Enerpac Saf-Y-Lite point load tester. Ghibli granite core ($\sim$ 19.9mm$\oslash$) was subject to diametral loading every $\sim$ 20mm along the length of the core. Load was applied slowly and uniformly ensuring the loading points were centred and perpendicular to the diametral axial plane. Peak-load (kN) at fracturing was recorded to an accuracy of 0.01kN. Tests that did not fracture in accordance with ISRM methods were subsequently discarded. Fractured segments were then used for axial point loading, with the axial length and peak-load also recorded at testing.

2.5 Ultrasonic Wave Velocity

The velocity of ultrasonic waves are closely related to both mineralogical and structural properties of the rock mass. The presence of micro-fractures and void spaces have a significant impact on the overall velocities. Wyering et al. (2012) reported that increases in porosity through the development of void spaces and/or micro-fractures attenuate ultrasonic wave velocity, whereas a reduction in porosity typically results in an increase to ultrasonic wave velocities. The measurement of P (pressure) and S (shear) wave velocities also enable the determination of dynamic sample stiffness (Young's modulus) and deformational behaviour (Poisson's ratio).

The measurement of P and S waves in this thesis was conducted using a Geotechnical Consulting and Testing Systems Computer Aided Ultrasonic Velocity Testing System (CATS ULT-100). Piezoelectric transmitters emit and receive ultrasonic waves with the time taken for waves to propagate through the samples appropriately recorded. To ensure solid contact between piezoelectric transducers and the sample, a 30kg static load (0.94 MPa of stress) was applied to the samples. The application of a constant stress reduces acoustic noise allowing for more consistent waveforms to be produced. Sixty-four waveforms for both P and S waves were collected from each sample. Arrival times were picked manually and corresponding velocities recorded accordingly. Initial poor wave-forms and results were thought to be a result of poor conductivity between platen and sample. To improve conductivity, a thin film of premium New Zealand honey was applied to both ends of the sample. The application of honey resulted in clean wave-forms with little to no noise.

Ultrasonic wave velocities were measured on samples in both dry and saturated conditions. Saturated samples were submerged in a bath of H_2O. A -100kPa vacuum was applied for no less than 24 hours. Ultrasonic wave velocities were collected from samples pre and post thermal cycling experiments, changes to wave velocities, poison's ratio and young's modulus were reported accordingly.

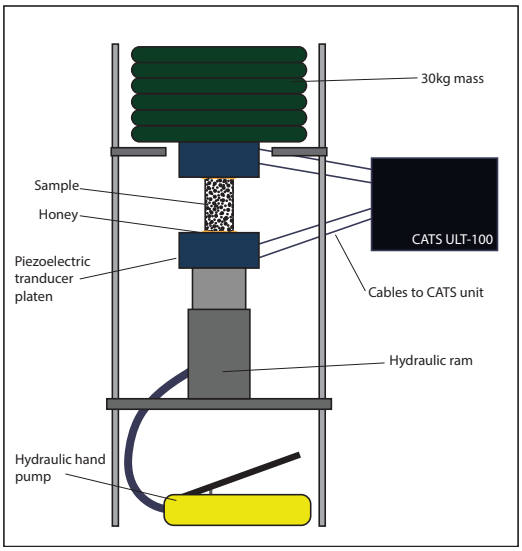

Figure 2.2: Diagram of apparatus used for testing ultrasonic wave velocity (Jones 2016).

From ultrasonic velocity results, dynamic rock properties that include Poisson's ratio and Young's modulus could be calculated using the following formula (Guéguen and Palciauskas 1994):

$$\nu = \frac{Vp^2 - 2Vs^2}{2(Vp^2 - Vs^2)} \tag{2.5}$$

$$E = \frac{\rho Vs^2(3Vp^2 - 4Vs^2}{Vp^2 - Vs^2} \tag{2.6}$$

Where:
ν = Poisson's ratio
E = Young's modulus (Pa)
Vp = P (compressional) wave velocity (m/s)
Vs = S (shear) wave velocity (m/s)
ρ = Density (kg/m^3)

2.6 Measuring Permeability

Permeability is a measure of open pore spaces in a cross section that is perpendicular to the direction of flow. The International System of Units (SI), quotes permeability as an area in m^2, with typical permeabilities for all rock types extending over 13 orders of magnitude, from 10^{-20} m^2 to 10^{-7}m^2 (Brace 1980). Another commonly used unit of permeability is the Darcy, which is equivalent to about 10^{-12}m^2.

The permeability of samples in this study have been determined using the pressure-decay method. The pressure-decay method is particularly good for measuring low-permeability samples. This is because a steady-state flow through samples of this nature takes a very long time to achieve (Nolan-Hoeksema 2014). In the pressure-decay method, equal pore-pressure is applied to reservoirs both up and down-stream of a sample and monitored. Pressure is reduced down-stream and the time taken for the system to return to equilibrium is monitored, enabling for the calculation of sample gas permeability.

Permeability was measured using a Core Laboratories Pulse Decay Permeameter (PDP-200), which applies the pressure-decay method using nitrogen gas pore fluid (Figure 2.3). Samples were inserted into an impermeable viton sleeve which is housed inside a stainless steel oil-filled pressure vessel. Confining pressure was applied to the viton sleeve via a hand-operated hydraulic pump. The confining pressure ensures that pore-fluid passes through the sample and not along the viton sleeve inner walls, and can therefore also be used to recreate confining pressure (and temperature) conditions found at depth. For this thesis respective confining pressures of 3MPa for the Ghibli granite and 5MPa for the Rotokawa Andesite were used. Ideally confining pressure would be zero, the same conditions that thermal cycling was conducted under. However, the permeameter requires a minimum of 3MPa to minimise or eliminate gas leakage around the sample. Initial testing of the Rotokawa andesite permeability was conducted by (Jones 2016) used 5MPa confining pressure. Permeability measurement

after thermal-cycling also used 5MPa for confining pressure.

The permeameter is housed within a perspex box, where an element and two fans regulate ambient temperature to 30°C. Nitrogen pore fluid is supplied via stainless steel tubing. Platens at either end of the sample and within the viton sleeve distribute pore-fluid across the sample. Equal pore-pressure was applied to gas reservoirs on both up and downstream sides of the sample via electronic controllers. The sample was then left in this state for no less than 2 hours to allow gas to soak pores and for thermal equilibrium to be reached. Once equilibrium has been reached, a pressure difference of 12psi was applied across the sample by bleeding pressure from the downstream reservoir. The rate at which the upstream reservoir returns to equilibria with the downstream reservoir is measured in the amount of time for each 0.1psi of pressure drop in the upstream reservoir. Once the pressure differential reached approximately 5psi or the calculated permeability had flat lined for a significant period of time, the test was concluded. A new pore-pressure could then be applied and the next test was started.

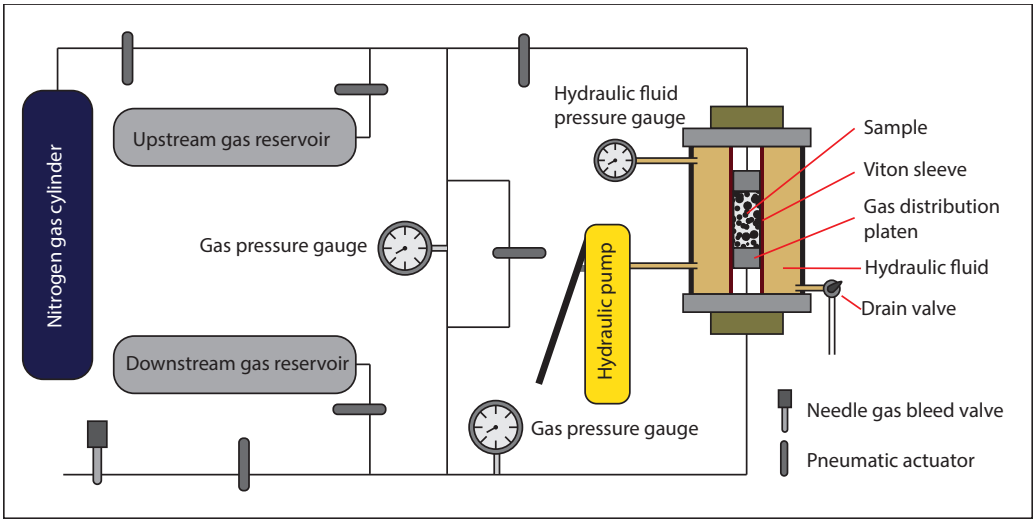

Figure 2.3: Apparatus used for permability testing. Core Laboratories Pulse Decay Permeameter (PDP-200). Figure retreived from Jones (2016)

2.6.1 Gas Permeability

Pore Fluid

The pore fluid used for permeability measurements is nitrogen (see BOC laboratory report in Appendix). The viscosity of the pore-fluid at 30°C, is 1.793x10^{-}5kg/m^{-s}. Gas viscosity is typically thought of as being independent of gas pressure, however fluctuations in temperature are likely to affect gas viscosity. The temperature of the permeameter is regulated and therefore we can assume that pore-fluid viscosity had remained constant.

Pressure-Decay Method

The pressure-decay method assumes Darcy's Law as the scientific basis of fluid permeability and is commonly used to describe fluid flow through a porous medium (Darcy 1856). The gas (or apparent) permeability of samples in this thesis is calculated using the pressure-decay method. The pressure-decay method makes a fundamental assumption that pore-fluid flow is non-turbulent (Darcian) in nature. Gas permeability is calculated using the following relationship.

$$K_{gas} = \frac{2\mu L}{A} \frac{V_{up}}{P_{up}^2 - P_{down}^2} \frac{\Delta P_{up}}{\Delta t} \tag{2.7}$$

Where:
K_{gas} = apparent gas permeability
μ = viscosity
A = sample cross-sectional area (m^2)
V_{up} = upstream pore volume
P_{up} = upstream pore-pressure
P_{down} = downstream pore-pressure
t = time

Gas Slippage

Darcy flow (a fundamental assumption of the pressure decay method) assumes that fluid velocity at pore walls is zero. Gas slippage occurs due to gas having viscosity lower than that of fluids. Low flow resistance results in a finite velocity at pore walls (Figure 2.4).

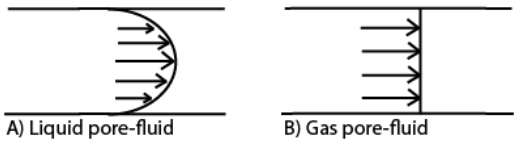

Figure 2.4: Example A, shows idealised fluid flow in which fluid viscosity is high and therefore turbulence at pore walls results in a velocity of zero. Examble B shows low-viscosity gas pore-fluid. Low turbulence results in gas slippage and a finite velocity at the pore walls.

2.6.2 True Permeability

Klinkenberg Correction

To account for gas slippage the Klinkenberg correction (Klinkenberg 1941) has been applied to gas permeability measurements. The Klinkenberg correction is an extrapolation to infinite gas pressure, at which point gas is assumed to behave like a liquid and slippage does not occur (Nolan-Hoeksema 2014). To correct for gas slippage, permeability is measured at 4 different pore-fluid pressures. When permeability is plotted against the reciprocal of pore pressure, a straight line relationship exists.

$$K_{true} = K_{gas} \times (1 + \frac{\beta}{P_{mean}}) \tag{2.8}$$

Where:

K_{true} = Klinkenberg corrected permeability

K_{gas} = apparent gas permeability

P_{mean} = mean pore-pressure

β = constant

To apply the Klinkenberg correction slopes similar to Figure 2.5 were produced.

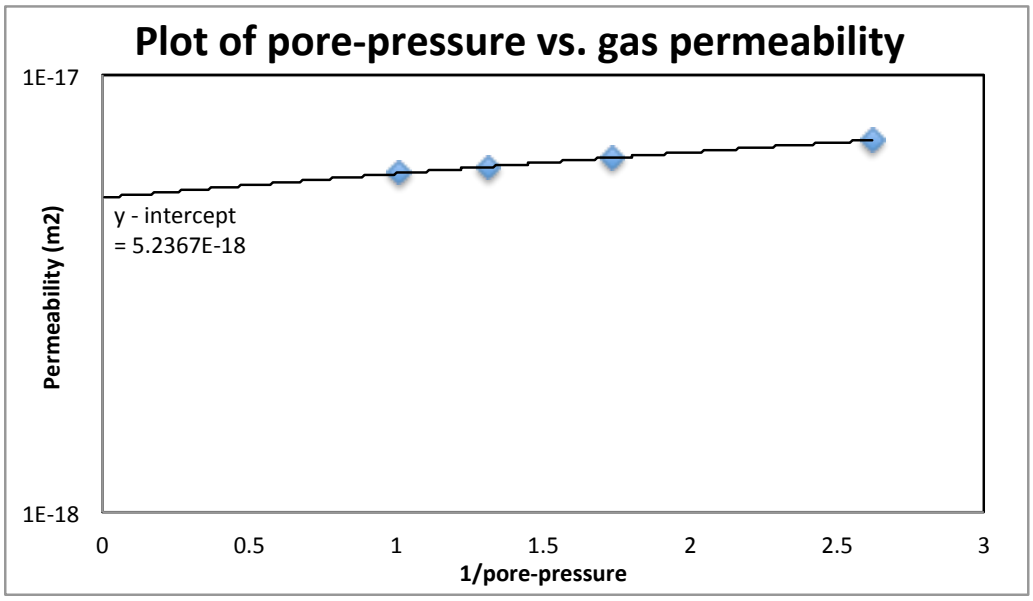

Figure 2.5: Plot of Kmd (permeameter output in millidarcys) converted to m^2 (1 md = 9.87x10⁻16m^2). Pore pressure is converted from PSI to MPa (1Psi = 0.0069 MPa) with the inverse of pore pressure being plotted along the x axis. As pore pressure approaches infinite the inverse approaches zero. At infinite pore pressure gas is assumed to behave as a liquid and the effect of gas slippage removed.

Pmean	Kmd	1/Pmean (x)	K (y)
55.3	0.0071922	2.62274	7.098E-18
83.7	0.0065458	1.73283	6.460E-18
110.7	0.0062394	1.31018	6.158E-18
143.6	0.0060394	1.01001	5.960E-18

Table 2.1: Table of values used to account for gas slippage and caluclate sample true permeability. Pmean is mean pore pressure for the test. Kmd is the corresponding gas permeability in milidarcys. 1/Pmean is the reciprocal of Pmean and is plotted on the x-axis. K (y) is the Kmd values converted to m^2 and plotted on the y-axis

2.7 Thermal-Cycling Apparatus and Methodology

2.7.1 Design Parameters

Thermal cycling experiments were conducted in a high pressure/temperature autoclave (Fig 2.6). The autoclave was assembled, and initial methodology developed by Siratovich et al. (2013) to investigate thermal cycling of crustal rocks in saturated conditions using distilled deionized water. The autoclave is simple in design, yet allows for the thermal cycling of geothermal core using single-phase geothermal brines. Reservoir temperatures of 325°C with 20MPa of confining pressure are easily obtained. The reservoir is built of 316 stainless steel and has a capacity of 1 litre. Heating is via an external ceramic heater, with the heating rate restricted to 2.0 °C/min by a Eurotherm controller. Cooling of the reservoir is controlled by the injection of 20°C fluid at a rate of 8.6 L/hr. This rapid quenching provided conditions analogous to those occurring in geothermal reservoirs during the reinjection of geothermal brines.

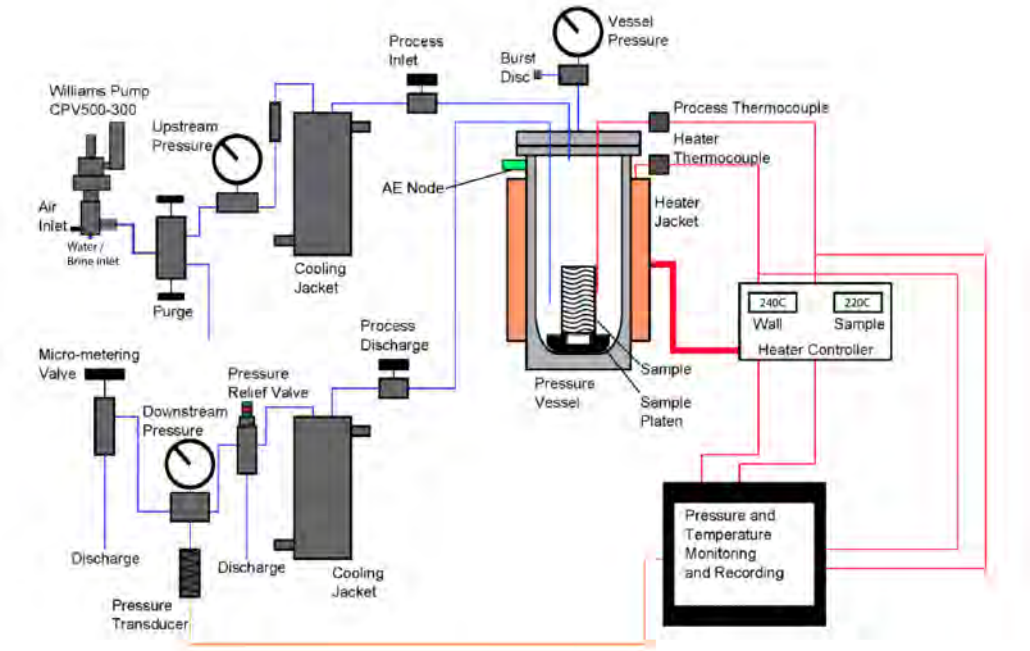

Figure 2.6: Schematic diagram (not to scale) of the system used in quenching experiments. The fluid (distilled water or brine) and pressure are provided to the system by the Williams pump, passing through a cooling jacket before injection into the pressure vessel. The sample sits at the bottom of the pressure vessel on a notched platen (316 SS) allowing for the circulation of fluid below the sample. Fluids can be flushed through the system at a rate of 8.6L/hour through the pressure relief valve. Vessel pressure is monitored downstream of the relief valve. Temperature inside the vessel is recorded by a k-type thermocouple next to the sample with a signal sent to a National Instruments Data DAQ. Modified from Siratovich et al. (2015b)

.

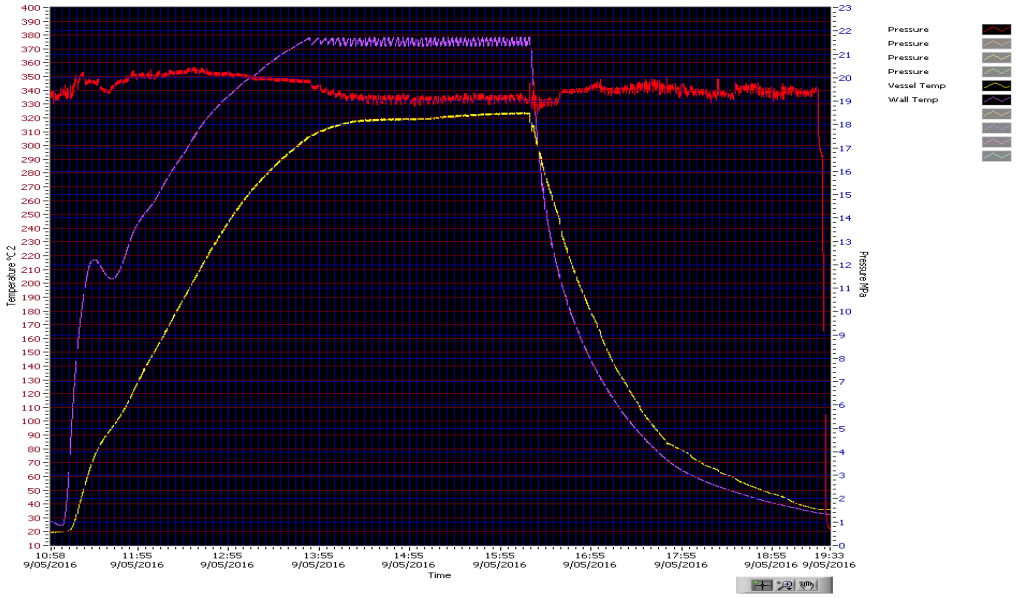

Figure 2.7: Representative heating and cooling profile for thermal cycle. The system is pressurised to 20 MPa. Heating via a ceramic heater on the exterior of the vessel wall commences, an average heating rate of 2°C/min used for all experiments. A lag between the temperature of the ceramic heater and the vessel results in target temperature being exceeded, before cooling to the target temperature. Once target temperature is met the vessel was left for 120 minutes to allow for thermal equilibration. At this point heating jacket is turned off and quenching cycle is initiated. We see an increase of system pressure due to the rapid pumping of fluids and also due to a rapid decrease of vessel temperature which results in a decrease of internal volume further raising pressure. Quenching continues until system reaches 20°C at which point the vessel undergoes gradual depressurisation and sample can be removed to measure changes that may have occurred.

Samples were placed in the reservoir, which is bolted closed and the system was flooded with experimental fluids. In this thesis, experimental fluids used were distilled deionized water H_2O and low-pressure geothermal brine from the Nga Awa Purua station. Once the system had flooded the micrometer valve was closed allowing the system to pressurise. Airlocks were bled from the system to ensure correct pressure readings and the heating cycle was initiated. The sample was heated to target temperature (eg. 240°C, 270°C, 325°C) at a rate of 2°C/min. Once the target temperature was obtained, the system was left to dwell for 120 minutes to allow thermal (and perhaps chemical) equilibrium to be reached. Cooling of the system was rapid. Cold fluid (20°C) was pumped through the system at the rate of 8.6 l/hr with discharge rate and reservoir pressure controlled by a pressure relief valve. Cooling continued until the reservoir returned to an ambient temperature of 20°C. Pressure was bled and the sample removed from the reservoir for further testing. Fluid discharged from the system was also tested for changes to monomeric silica concentrations.

For an in depth overview of the apparatus used and its individual components refer to Appendix C.

2.8 Spectrophotometric Determination of Dissolved Silica

Geothermal brines used in this thesis are reported by GNS (2015) as having 1147ppm of silica at the re-injection well-pad. Colloidal silica is likely to have developed upon cooling at the power station, and during transport to and storage at the University of Canterbury. To determine concentrations of monomeric silica and to determine whether digestion of colloids was occurring during thermal cycling, spectrophotometric testing was conducted.

Spectrophotometric methods and chemicals were supplied by Dr. Kevin Brown (2015) as a recommended method (Public Health Association et al. 1999) for determining monomeric SiO_2 concentrations. Discharged brine was collected downstream of the reservoir throughout the thermal cycling experiments and concentrations recorded in an effort to further understand the processes occurring within the reservoir.

This method is based on the formation of the yellow β – molybdosilicate anion and is suitable for analysing geothermal fluids containing no phosphate impurities or dissolved sulphides. High concentrations of iron, calcium and magnesium can interfere with results. The monomeric fraction of silica is stabilised upon collection by the addition of hydrochloric acid (HCl). Polymerization may still occur during transport from reservoir to analytical test.

2.8.1 Stock Solutions required

Four Stock solutions were required:
1. SiO_2 stock standard : 2140 ppm (1000 ppm Si)
2. Working SiO_2 standard : 400 mg aliquots
3. 1.5 N Sulphuric acid (H_2SO_4)
4. 100g/litre ammonium heptamolybdate $(NH_4)6Mo\ 7O_24\ 4H_2O$
& 47g/litre concentrated ammonium hydroxide $(28\%)NH_4OH$

The stock solutions are stable and can be stored over prolonged periods.

Reagent Solution

The molybdic acid reagent mixture was required to be made fresh each day. A minimum of 20ml reagent was required per sample. I found that to measure a thermal cycle around 400ml of reagent was required. The recipe is as follows:

To makes 400ml of reagent pH(1.2):
1. 250ml distilled H_2O
2. 50ml of molybdate stock solution
3. 100ml of 1.5 N concentration H_2SO_4

Calibration of Reagent

A calibration curve is required for each batch of reagent. To construct the calibration curve I added 20 ml of the reagent to 5 ml of SiO2 working standard at varied concentrations from 0.01 to 1.0 mg of SiO2 diluted with distilled water. Samples were shaken to ensure thorough mixing, left to stand for 10 minutes and then adsorbance of 420nm light was measured using an Orbeco-Hellige 975MP spectrophotometer. A blank sample is required for testing. Higher concentrations of SiO_2 resulted in the solution turning to bright yellow.

Adsorbance vs. known SiO_2 concentration was plotted, with a linear best fit line applied (Figure 2.8). Correct methodology typically produced a correlation of $R^2 = 0.99$

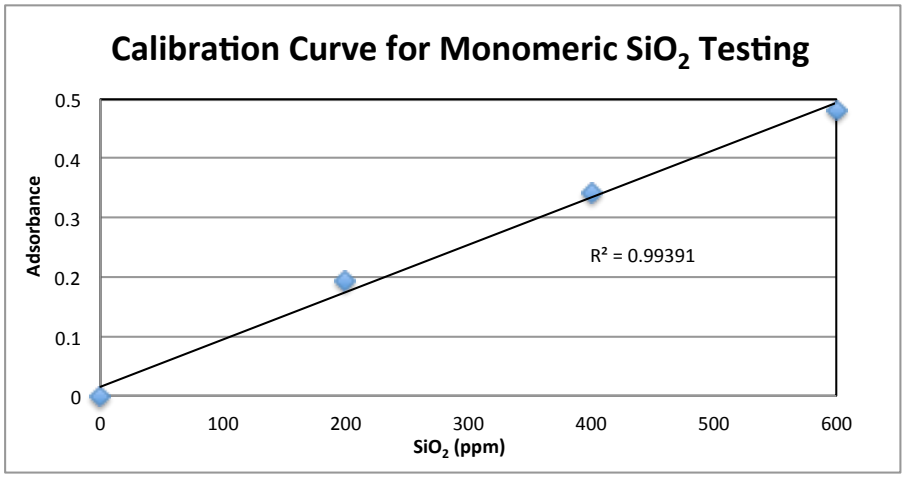

Figure 2.8: Example of monomeric SiO_2 calibration curve.

By comparing absorbance from known concentrations of silica to the adsorbance of geothermal brines, concentrations of monomeric silica within the fluid can be calculated.

2.8.2 Testing Geothermal Brines

To determine the amount of monomeric silica in the geothermal brine at various stages of thermal-cycling, fluid was collected at the pressure relief discharge. 10ml of discharged brine was collected in a glass container that had been rinsed with H_2O. One drop of 38% HCl was added to buffer the fluid and inhibit colloid formation during time delay from collection of fluids to spectrophotometric testing. The time and reservoir temperature when the fluid was collected was recorded. 800mg of brine was added to the 20ml of reagent. The mixture was topped up to 25ml with H_2O, mixed thoroughly and left to stand for 10 minutes. The testing container was rinsed twice, first with H_2O, and then with reagent mixture to ensure no cross-contamination between tests.

To force discharge of fluids, the pump rate was increased to 100 stroke/min. In response to increased pumping rates, reservoir temperature would drop as much as 20°C while fluids were being collected. Temperature used in the calculation of reservoir conditions uses the temperature recorded at the beginning of fluid extraction.

2.9 PHREEQC Modelling

A highly simplified PHREEQC (pH-redox-equilibrium-c) model was made for the reservoir using Ghibli granite, H_2O and NAP Brine. The model considered Ghibli granite as having plagioclase, K-feldspar, quartz and biotite. Relative abundances of minerals are converted to their respective molar masses with a total granite species' mass of 32 grams being considered. Reservoir volume was 1kg/l of H_2O or NAP Brine. For NAP Brine I have simplified the chemistry to Sodium (720mg/l), Chloride (1182ppm), and monomeric Silica (690ppm) which has been measured in PV reservoir at 240°C. The pH for each fluid at 25°C was: H_2O - pH5.6 and NAP Brine - pH4.31 (GNS 2015) respectively. Reservoir pressure is 197atm (20MPa) with reaction temperature set at 240°C or 270°C. The model is allowed to reach equilibrium.

There is significant assumptions, limitations and error associated with this model. The purpose was is not for quantitative analysis but to give indication of possible fluid conditions within a hypothetical reservoir that has been allowed to reach equilibrium conditions. The saturation index for various minerals at equilibrium give indication of A) the most likely species that are being altered B) minerals in solution that may be deposited during subsequent cooling of the reservoir. Reservoir pH when at equilibrium could also be estimated.

REACTION_TEMPERATURE 240 celsius REACTION_PRESSURE 197 atm (20MPa) EQUILIBRIUM_PHASES (molar) Albite 0 0.053 Anorthite 0 0.023 K-feldspar 0 0.029 Quartz 0 0.133 K-mica 0 0.0037 SOLUTION (H2O) temp 25 pH 5.6 pe 4 redox pe units mmol/kgw density 1 C(4) 1 mg/kgw -water 1 kg	REACTION_TEMPERATURE 240 Celsius REACTION_PRESSURE 197 atm (20MPa) EQUILIBRIUM_PHASES (molar) Albite 0 0.053 Anorthite 0 0.023 K-feldspar 0 0.029 Quartz 0 0.133 K-mica 0 0.0037 SOLUTION (NAP brine) temp 25 pH 4.31 pe 4 redox pe units mmol/kgw density 1.007 C(4) 1 mg/kgw Cl 1182 mg/kgw Na 720 mg/kgw Si 1142 mg/kgw -water 1 kg

Table 2.2: Summary table of PHREEQC model parameters. The left example is for H_2O, the right NAP brine.

Assumptions:

- Models assume that the reservoir has approached equilibrium. There is no time constraint.
- Assumed relative percentages of minerals in Ghibli granite and that all mass has surface area available for reaction.
- Simplified chemistry of the NAP Brine is the same as that reported by GNS (2015). Reinjected fluid chemistry varies depending on the current field-operation.
- Carbonates not considered, although were likely included to H_2O through mixing with air.
- Only monomeric silica is considered. Average measure concentration of SiO2 at 240°Cis 690ppm. GNS (2015) quotes 1142ppm total silica.

Chapter 3

Results

In the following chapter results from thermal-cycling experiments of Ghibli granite and Rotokawa andesite are presented. The properties observed and reported include: petrology, bulk density, connected porosity, permeability, ultrasonic wave velocities, and point load indicies. Monomeric silica concentrations within the reservoir were modelled and measured. Table (3.1) provides a summary of the thermal-cycling experiments conducted in this study and the samples used for each experiment

Experiment	Lithology	Reservoir Fluid	Temperature	Sample ID
1	Granite	H_2O NAP Brine	270°C	G5, G10, G11, G16 G1, G3, G7
2	Granite	H_2O NAP Brine	240°C	G13, G21 G8, G20
3	Andesite	H_2O NAP Brine	240°C	21.4_2 21.4_4
4	Andesite	NAP Brine	325°C	21.4_6

Table 3.1: Table of the experiments conducted and the associated sample ID's

3.1 Petrology

3.1.1 Optical thin section analysis

Polished thin-sections (30μm) were made from Ghibli granite and Rotokawa andesite before and after two thermal-cycles. Physical changes to the rock fabric and mineral assemblage are reported.

3.1.2 Ghibli Granite Petrology

The Ghibli granite is a medium grained (2-5mm crystal size) granite, comprising of 90% felsic minerals (plagioclase, k-feldspar, quartz) and 10% mafics (biotite, and minor traces of Fe/Ti oxides). Quartz and microcline crystals are anhedral, and plagioclase phenocrysts are subhedral and zoned. All show intergrown (consertal) crystal boundaries indicating fluctuating magma conditions during crystal growth. K-felspar displays perthitic texture. Ghibli granite shows evidence of fabric deformation: the alignment of mica minerals, undulatory extinction of quartz and the presence of clay-infilled, pervasive, intragranular micro-fracturing (Figure 3.1).

Thermal-cycling has resulted in the alteration of Ghibli granite with differences in alteration products between NAP brine and H_2O observed in thin-section. In H_2O at 240°C biotite is observed to have been completely replaced with needles of chlorite, whereas in NAP brine, chlorite alteration is to a lesser extent with some biotite remaining. K-feldspars have become dull in texture after reaction with both fluids, with an increase in perthitic texture, low relief white spots (albite?) were identified predominantly in samples from NAP brine. Quartz and Plagioclase feldspars appear unaltered. Micro-fractures do not appear significantly more prevalent, and the calcite infilling remains. Clay minerals, amorphous SiO_2 and salt, predicted alteration products, were not observed but may have been removed during thin-section preparation. The presence of biotite-chlorite alteration indicates that fracture networks are conductive pathways for fluid migration.

3.1.3 Rotokawa Andesite Petrology

The Rotokawa andesite (RKA) is a moderate to intense altered lava and breccia. The average phenocryst size is 0.5 to 1 mm with occasional plagioclase of 1.5 to 2 mm; amygdales also range from 1 to 1.5 mm in size. Both groundmass and phenocrysts show pervasive, propylitic hydrothermal alteration to the original mineral assemblages. Primary plagioclase feldspar assemblages have been altered to albite, adularia, occasional calcite, and rare pyrite. Ferromagnesian minerals have been replaced by chlorite, quartz, calcite. Occasional epidote have been predominantly replaced with calcite, chlorite, quartz and minor-to-common epidote or hematite, with minor-to-rare albite, adularia, titanium-oxide and pyrite. Fractures are common and are both intragranular and transgranular and infilled with quartz, calcite, anhydrite, and epidote. Amygdales within the sample are often filled with chlorite, calcite, hematite, pyrite, and chalcedony, often with quartz rims. Micro-fractured phenocrysts are abundant with many relict phenocrysts retaining their original texture but have been replaced by secondary mineralization. The presence of chlorite, adularization of plagioclase, calcite, and quartz rimming of fractured matrix indicates that fracture networks were conductive pathways for fluid migration (Wyering et al. 2014, Siratovich et al. 2014). (Figure 3.2).

The RKA contains a pervasive network of isotropic micro-fractures, is highly altered, micro-structurally complex and spatially variable. The isotropic distribution of micro-fractures is consistent with micro-fractures that result from thermal stressing (Siratovich et al. 2014). Thermal stressing of the Rotokawa Andesite is likely to have occurred during: the initial eruption, burial in a faulted graben, hydrothermal alteration, and the eventual exhumation during well drilling and core recovery (Rae 2007). The 3 samples of RKA used in this thesis (RK30-21.4) were produced by Tim Jones (2016). Core was retrieved during drilling of production well RK30 (Figure 1.9). The approximate depth of these 3 samples is 2140 meters below surface level. At this depth the reservoir temperature is approximately 325°C. The samples were produced in very close proximity to one another but heterogeneity is high. Variations in mineralogy and ground-mass percentages observed in thin-section, as well varied amounts of alteration between samples, makes the identification and interpretation of thermal-cycling derived alteration difficult.

Thermal cycling has resulted in no observable variation in alteration for the samples cycled at 240°C in NAP brine and H_2O. For NAP brine at 325°C significant amounts of oxidation can be observed in thin-section, and phenocrysts appear more fractured than those in 240°C experiments.

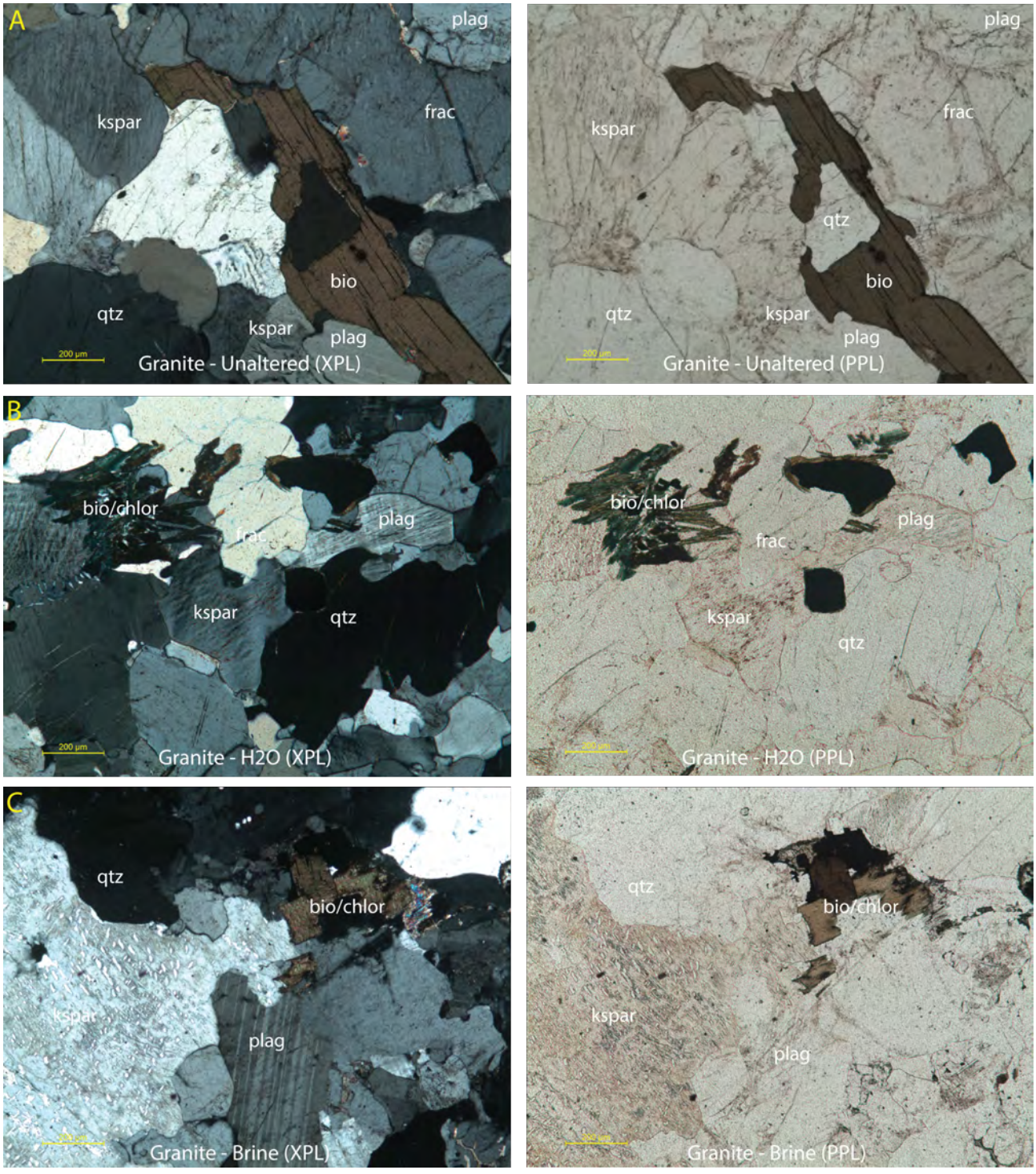

Figure 3.1: Photomicrography of 30µm thin-sections of Ghibli granite pre and post thermal cycling. Unaltered granite (A) displays 'clean' biotite and calcite infilled micro-fracturing. Sample B has been thermally cycled twice in H_20 at 240°C. Biotite displays alteration to chlorite, with mineral assemblage representing needles. Calcite appears to have been replaced (or altered) by a lower birefringence mineral. Sample C has been thermally cycled twice in NAP brine at 240°C. Biotite displays alteration to chlorite, with mineral assemblage representing square flakes. No other significant differences were identified in thin section.

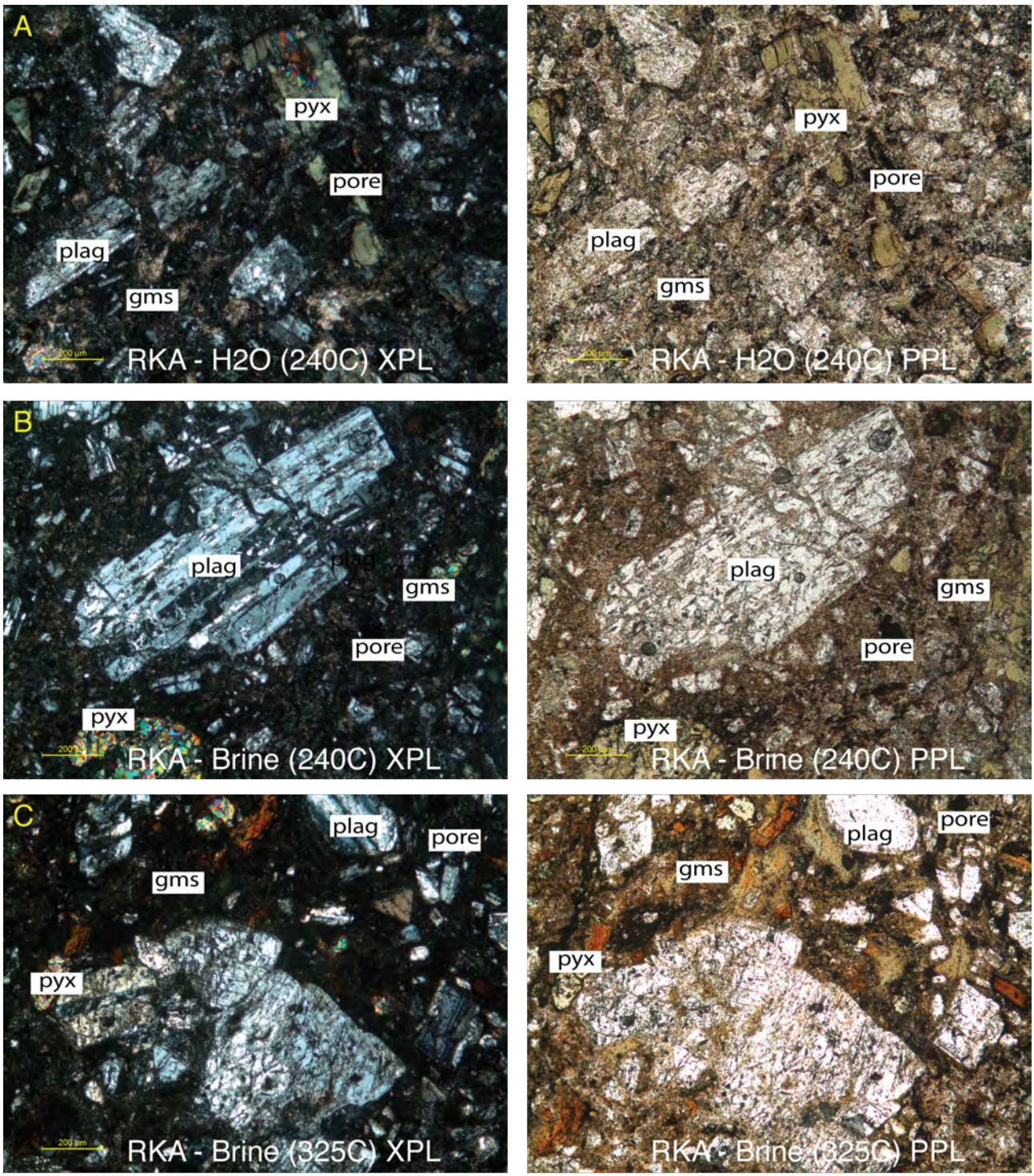

Figure 3.2: Photomicrography of 30μm thin-sections of Rotokawa andesite pre and post thermal cycling. No significant differences between Sample A and B can be identified in thin section. This may in part be due to rock heterogeneity. Sample C which was cycled twice at 325°C using NAP brine shows high amounts of oxidation to the ground mass.

3.2 Scanning Electron Microscopy

3.2.1 Chemical analysis of infilled fractures within granite

Chemical analysis of infilled fractures observed in Ghibli granite thin-sections was undertaken using Energy-Dispersive X-ray Spectroscopy (EDS) on a Scanning Electron Microscope (SEM) at the University of Canterbury. Chemical analysis suggests that the secondary mineralisation of fractures within the granite is predominantly silica and calcite. Analysis of fractures is provided in Figure 3.3. Carbon identified in results reflects carbon-dust that is applied to sample surface to improve conductivity. EDS analysis identifies the infilling material to be calcite.

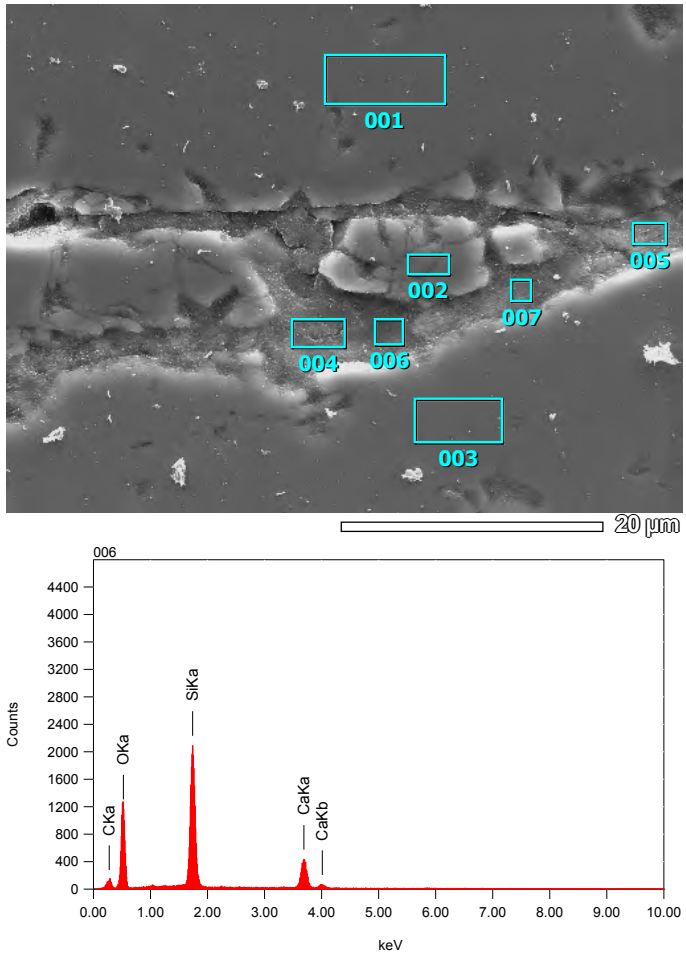

Figure 3.3: Scanning Electron Microscope image of Ghibli Granite showing Energy-dispersive X-ray spectroscopy (EDS) of pervasive intragranular micro-fracturing, infilled with high-birefringence calcite. Numbered boxes indicate the different analysis points, with number 006 being the location from which the results reported here were taken.

3.3 Physical properties of Ghibli granite and Rotokawa andesite

Lithology		Porosity (%)	Density (g/cm3)	VP (m/s)	VS (m/s)	Young's Modulus (Gpa)	Dynamic Poisson's Ratio
Granite	Mean	0.89	2.61	3615.5	2208.5	31.0	0.21
	Minimum	0.77	2.60	3465	2156.5	30.7	0.20
	Maximum	0.98	2.62	3696	2229	31.2	0.22
RK_30_21.4	Mean	6.93	2.57	3698.5	2408.5	33.8	0.13
	Minimum	6.49	2.54	3578	2332.5	31.2	0.13
	Maximum	7.24	2.59	3788.5	2459	35.6	0.14
RK_30 from Siratovich (2014)	Mean	6.61	2.55	4161	2573	40.4	0.17
	Minimum	5.3	2.53	4002	2495	36.9	0.15
	Maximum	7.51	2.57	4352	2659	43.2	0.2

Table 3.2: Table of measured physical properties of Ghibli granite and Rotokawa Andesite (RK30-21.4). Results from previous studies of RK_30 (Siratovich et al. 2014) have been included for comparison.

3.3.1 Porosity, Density and Permeablity

Connected porosity and bulk density results (Table 3.4). were obtained using the triple-weight method. Initial tests conclude that the Ghibli granite bulk-density ranges from 2.60 to 2.62 g/cm^3, with connected porosity ranging from 0.77% to 0.98%. For the Rotokawa andesite, the bulk-density ranges from 2.54 to 2.59 g/cm^3, and connected porosity ranges from 6.49% to 7.24%. The Ghibli granite is more dense, and displays significantly lower connected-porosity than the Rotokawa andesite. The corrected true permeability of the Ghibli granite ranges from 2.62E – 18 to 5.24E – 18m^2. Samples of Rotokawa andesite (RK30-21.4) range from 4.99E – 19 to 7.92E – 19m^2. The Ghibli granite is an order of magnitude more permeable that the Rotokawa andesite despite having a significantly lower connected-porosity.

3.3.2 Point Load Test

Point load testing of Ghibli granite core identified mechanical anisotropy between axial and diametral tensile strength for unaltered Ghilbi granite. In total 17 diametral, and 12 axial point-load tests were conducted. Samples that did not fail within the specified guidelines were discarded. Rejecting the lowest and highest results, mean diametric point-load index 4.12 MPa and a mean axial point-load index of 3.69 MPa were measured respectively. The lower point load indices reflects the biotite-mica fabric, with failure preferentially occurring along this axis. This may play a role in the development of micro-fractures that arise through thermo-mechanical stresses, impacting how permeability evolves in relation to porosity.

Point Load Index (MPa)		
	Axial	Diametral
Mean	3.69	4.12
Minimum	2.33	3.27
Maximum	4.84	5.16
	n=12	n=17

Table 3.3: Summary of axial and diametral point-load index for the Ghibli granite

3.4 Thermal Cycling Experiments

3.5 Triple weight

The triple-weight method has been used to make simple measurement of sample bulk-density, and connected porosity. By using this method before, and after thermal-cycling, I was able to readily identify changes that had occurred to these two physical characteristics. Variation in results between samples thermally-cycled using NAP Brine and H_2O have been observed. From triple-weight experimentation alone it can be concluded that fluid chemistry plays an important roll in thermal-cycling processes.

Sample ID	Bulk Density (g/cm3)			Permeability (m2)			Porosity (%)		
	Initial	Stim 1	Stim 2	Initial	Stim 1	Stim 2	Initial	Stim 1	Stim 2
G8	2.602	2.579	2.588	4.38E-18	1.29E-17	1.57E-17	0.879	1.140	1.272
G20	2.615	2.588	2.588	4.70E-18	1.27E-17	1.39E-17	0.838	1.066	1.242
G13	2.612	2.597	2.599	2.62E-18	1.14E-17	1.45E-17	0.888	1.030	1.178
G21	2.603	2.588	2.588	3.20E-18	1.16E-17	1.24E-17	0.913	1.068	1.171
G1	2.603	2.585	-	5.24E-18	1.80E-17	-	0.896	1.064	-
G3	2.609	2.606	-	4.05E-18	1.37E-17	-	0.775	1.078	-
G7	2.605	2.585	-	3.96E-18	1.25E-17	-	0.950	1.228	-
RK_30_21.4_2	2.591	2.586	2.586	5.47E-19	4.74E-19	6.70E-19	6.497	5.907	6.211
RK_30_21.4_4	2.574	2.590	2.569	4.99E-19	3.90E-19	4.25E-19	7.047	6.377	6.262
RK_30_21.4_6	2.556	2.540	2.532	7.92E-19	9.34E-19	1.15E-18	7.244	7.348	7.438

Table 3.4: Summary table of inital and measured changes to porosity, density and permeability as a result of thermal-cycling.

3.5.1 Porosity and Density

The thermal-cycling of Ghibli granite at 240°C or 270°C in either NAP brine or H_2O resulted in significant increases to sample connected porosity, and decreases in dry bulk density. Second thermal cycles were typically less effective in developing porosity than the first. Increases in dry density were identified on samples (G8, G20 : NAP brine) and (G21 : H_2O) as a result of a second thermal cycle.

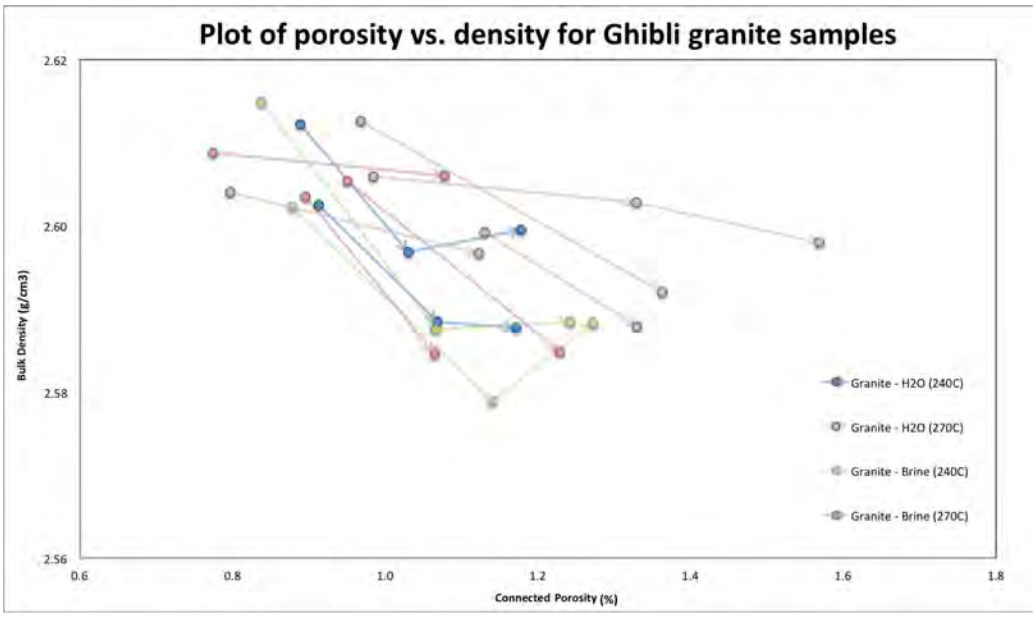

Figure 3.4: Plot of porosity vs density for themally cycled granites. Arrows indicate the direction of succesive thermal cycles.

Samples that were thermally cycled at 270°C developed more porosity than those thermally cycled at 240°C. Samples thermally cycled using NAP brine were observed to develop more porosity than those cycled in H_2O in both initial and second thermal cycles. In 270°C experiments H_2O is observed to develop more porosity than NAP brine. At 240°C NAP brine is observed to develop more porosity than H_2O (Figure 3.4).

Thermal-cycling of the Rotokawa andesite at 240°C resulted in a significant reduction in connected porosity when either NAP brine or H_2O was used as reservoir fluid. NAP brine resulted in an increase to bulk-density whereas H_2O saw reduction to bulk-density. For second thermal cycles using NAP brine further decreases in porosity, and bulk-density were measured. Second thermal cycle using H_2O resulted in an increase in porosity and little or no change to bulk-density. The thermal cycling of Rotokawa andesite at 325°C resulted in an increase in connected porosity, and a decreases in bulk-density (Figure 3.5).

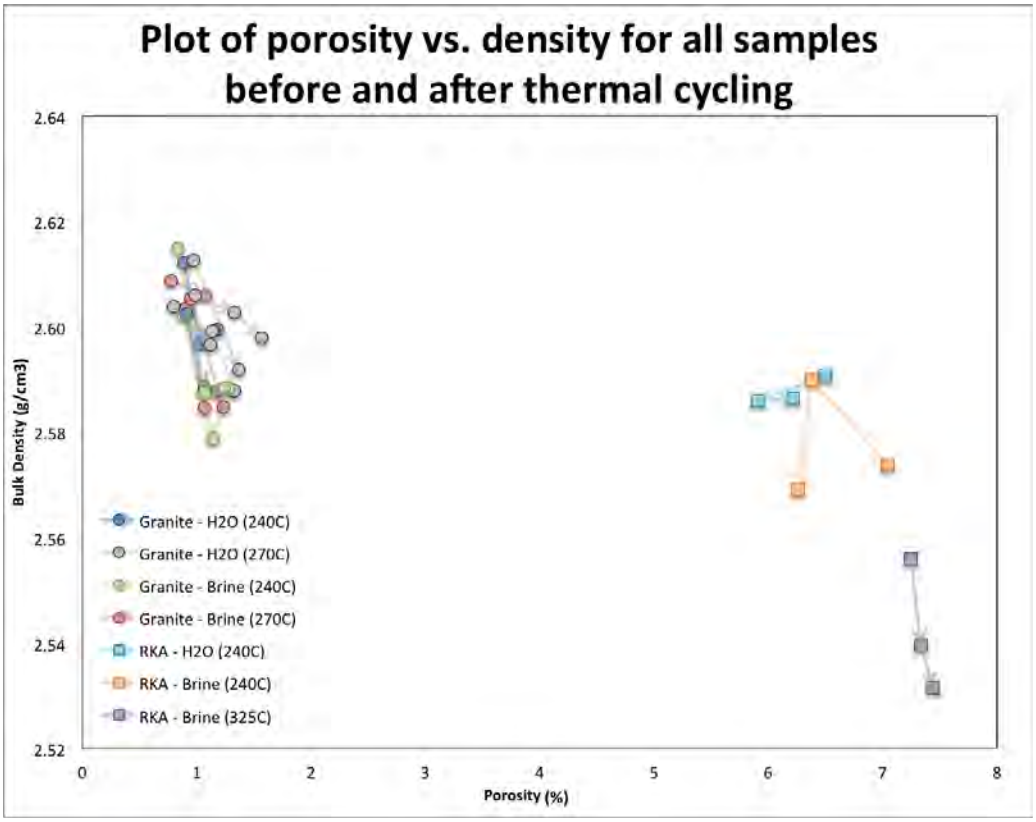

Figure 3.5: Plot of porosity vs density for all samples that were succesfully thermally cycled in this study. Arrows indicate the direction of succesive thermal cycles. All samples except for those that were thermally cycled at 270°C in the first cycle were subject to a second thermal cycles.

3.5.2 Porosity and Permeability

In all but one experiment, increases in sample permeability can be correlated to increases in sample porosity. Figure 3.6 illustrates typical permeability development from two thermal cycles using H_2O. The initial thermal cycle develops significantly more permeability than the second thermal cycle for all granite thermal-cycling experiments.

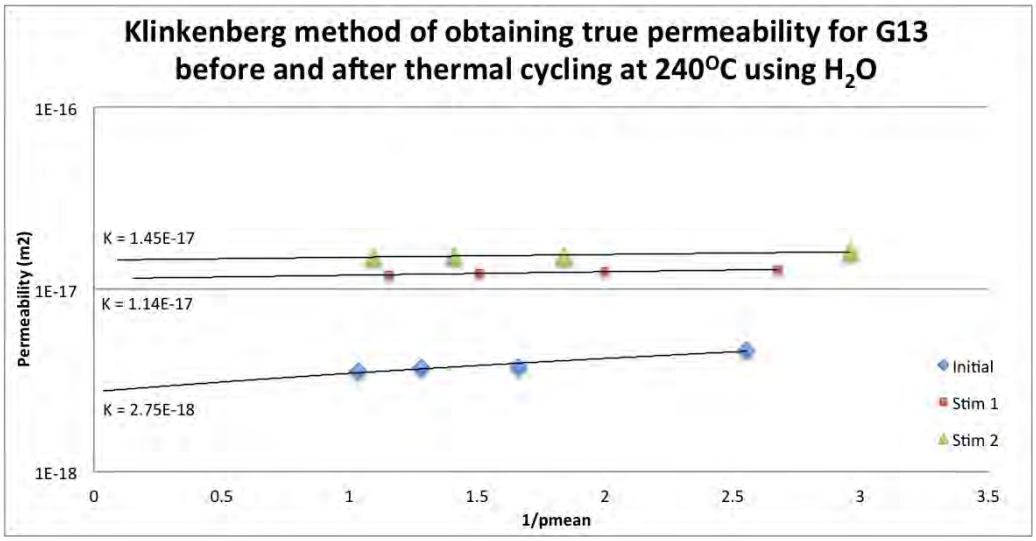

Figure 3.6: Plot of Klinkenberg correction for true permeabilty of sample G13 following successive thermal-cycling at 240°C using H_2O.

Figure 3.7 illustrates porosity and permeability development for samples of granite stimulated using either H_2O or NAP brine at temperatures of 240°C or 270°C. The permeability of granite samples thermally-cycled at 270°C in H_2O have not been presented in this chapter due to permeability measurements being outside of testing equipment range (see discussion regarding Forcheimmer flow).

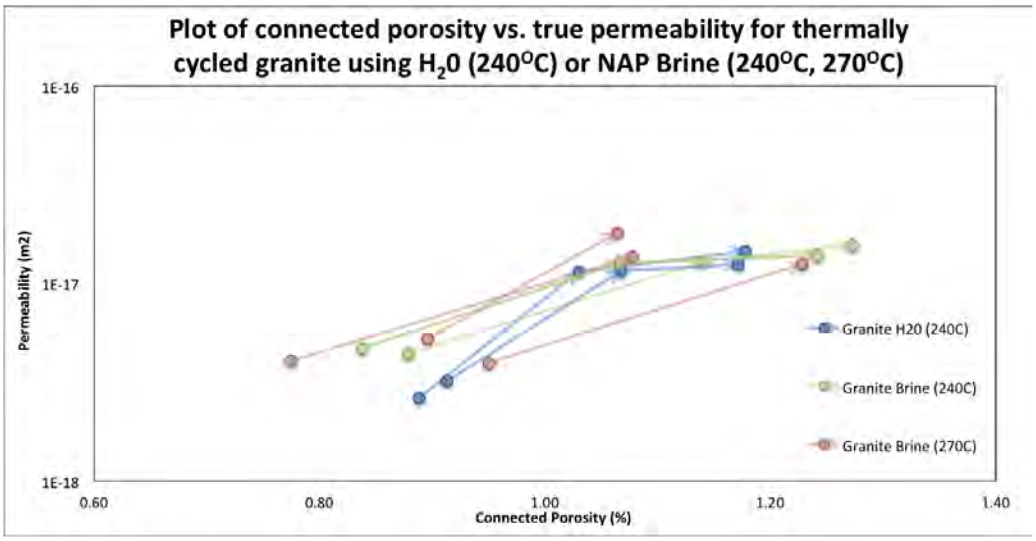

Figure 3.7: Plot of porosity and permeability for thermally-cycled granites. Samples stimulated in H_2O at 270°C have been omitted from this chart due to error in permeability measurements.

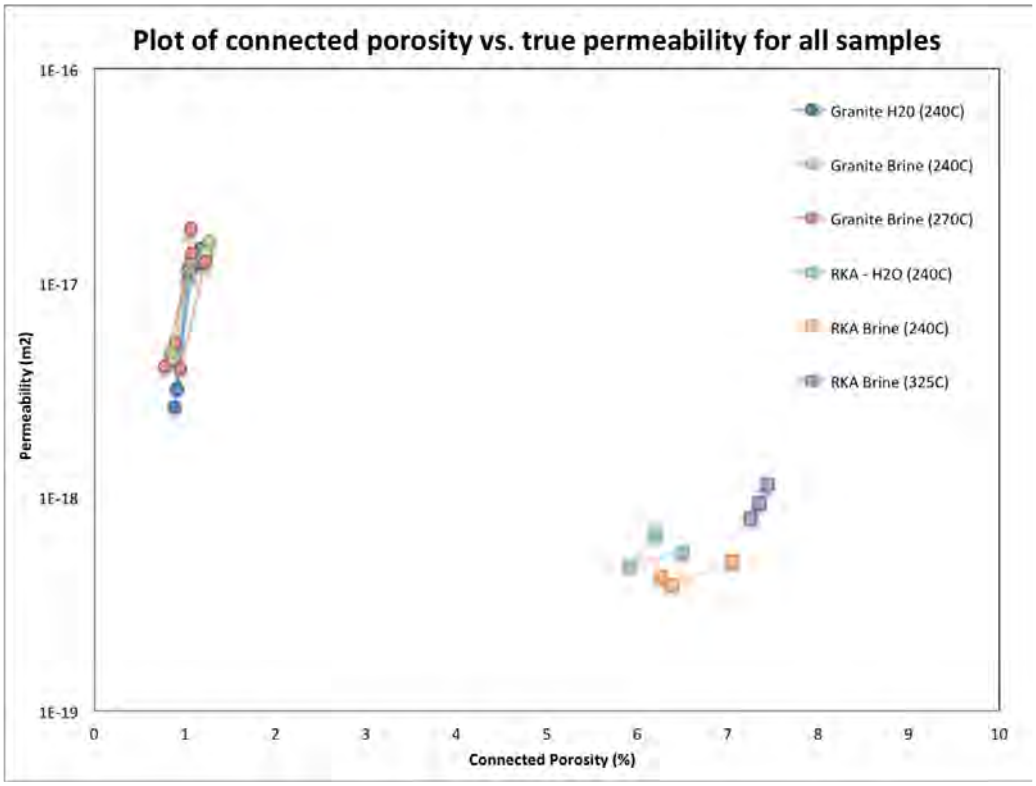

Figure 3.8: Plot of porosity vs permeability deveolpment for all samples. Arrows indicate direction of progressive thermal-cycles.

From three different experiments on 7 similar samples of Ghibli granite, H_2O at 240°C showed the greatest increase in permeability (Figure 3.7). When compared to NAP brine at the same temp, H_2O resulted in samples becoming on average 2.99 times more permeable. NAP brine was on average 1.82 times more permeable. For NAP brine, an increase in reservoir temperature to 270°C saw samples generate 0.5 times more permeability than at the lower temp of 240°C. For second thermal cycles at 240°C, there was little difference in the amount of permeability generated. This result agrees with porosity development, which for the second thermal cycles was in the same order of magnitude, but only half as much as in the first thermal-cycle.

For the three experiments conducted on Rotokawa andesite the resulting changes to permeability were significantly different than those of the granite. Initial thermal-cycling of RKA at 240°C using either NAP brine or H_2O resulted in a reduction in permeability and porosity. NAP brine resulted in twice as much permeability loss than H_2O. In the second thermal-cycles at 240°C, permeability was observed to increase in both samples. H_2O created four times as much permeability as the NAP brine. This second thermal-cycle using NAP brine is the only example of a sample decreasing in porosity but increasing in permeability.

3.5.3 Density and Permeability

The initial thermal-cycle of granites samples always resulted in a decrease in density and an increase in permeability (Figure 3.9). Samples that were thermally cycled in NAP brine had greater reductions in density but showed similar developments in permeability as H_2O treated samples did. For second thermal cycles at 240°C, both brine samples and one H_2O sample showed an increase in density and

increases in permeability.

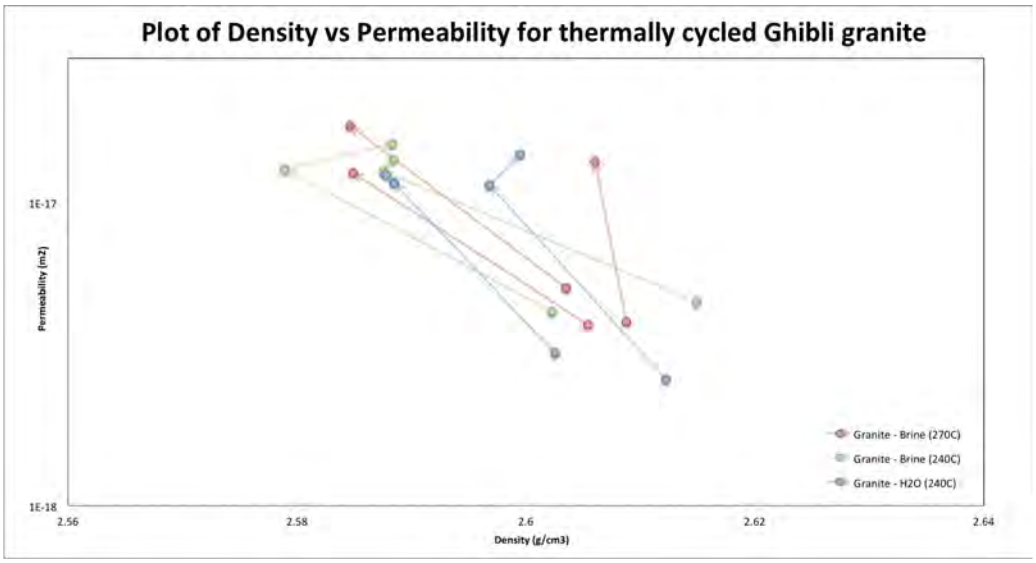

Figure 3.9: Plot of density vs permeability for thermally cycled Ghibli granite. Arrows indicate direction of progressive thermal-cycles.

Samples of Rotokawa andesite behaved differently to granite in respect of density and permeability changes (Figure 3.10). At 240°C: H_2O treatment resulted in decreased in density and permeability after initial thermal cycle and then increased in permeability but with no change to density in the second cycle. NAP brine treatment resulted in increased density, and decreased in permeability after the initial thermal-cycle, with a reduction in density and increase in permeability in the second. For experiments with NAP brine at 325°C, reduction in density and an increase in permeability were observed in both thermal-cycles.

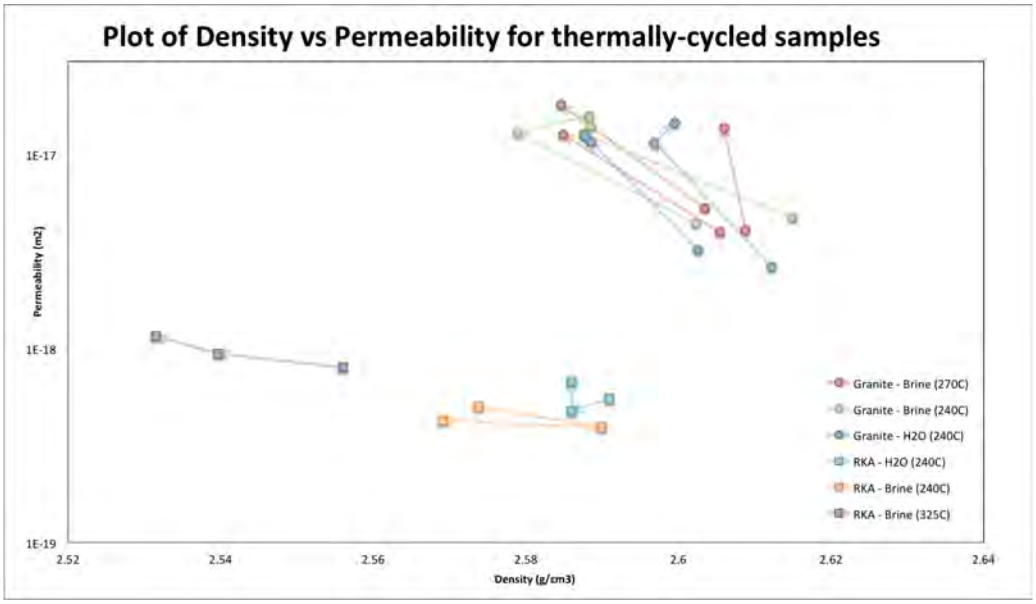

Figure 3.10: Plot of density vs permeability for thermally cycled Ghibli granite and Rotokawa andesite. Arrows indicate direction of progressive thermal-cycles.

3.6 Ultrasonic Velocity Testing

Ultrasonic wave velocity testing was carried out on dry and saturated samples before and after thermal stimulation. Samples were tested under both dry and saturated conditions. Samples were tested in both upward and downward directions with the averaged velocities reported.

For the granite samples, ultrasonic velocities agree with porosity development for all samples. Increases in porosity are attributed to decreases in ultrasonic P and S wave velocites. The same trend is observed in saturated and dry samples (Figure 3.11).

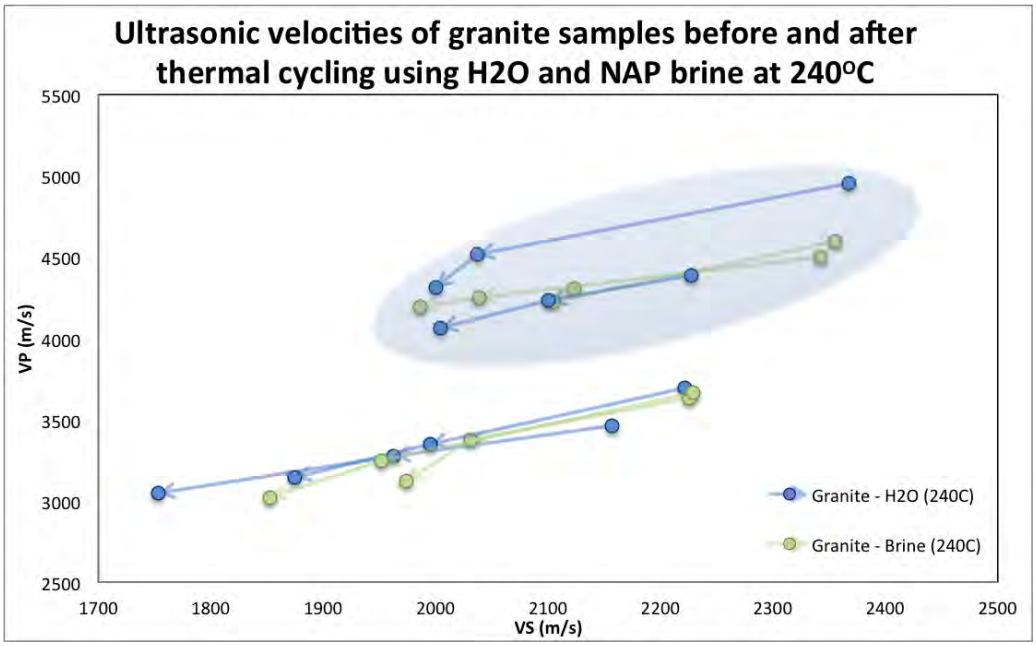

Figure 3.11: Ultrasonic velocities for granite samples before and after thermal cycling. Arrows point in the direction of progressive thermal cycles. Shaded area indicates saturated samples

For andesite experiments at 240°C, reductions in sample porosity were observed alongside initial increases to ultrasonic wave velocities. However, saturated ultrasonic tests indicate decreasing P-S wave velocities. For the second thermal-cycle, porosity was observed to increase, ultrasonic velocities are observed to decrease in both dry and saturated conditions. For 325°C experiments using NAP brine, we see increasing porosity and decreasing ultrasonic P and S wave velocities when tested in both saturated and dry conditions (Figure 3.12).

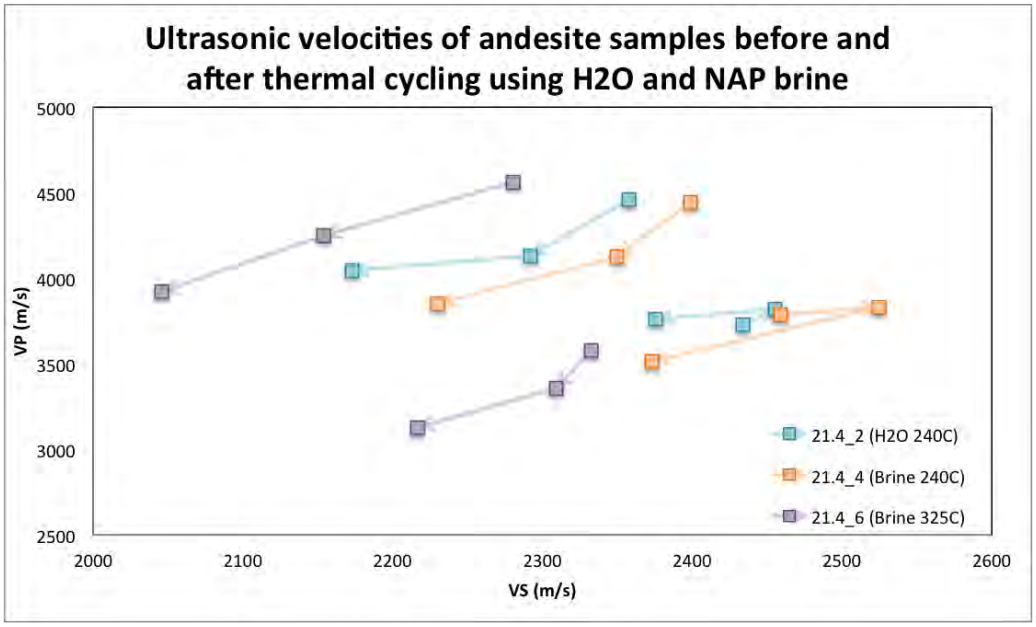

Figure 3.12: Ultrasonic velocities for Rotokawa andesite samples before and after thermal cycling. Arrows point in the direction of progressive thermal cycles. Shaded area indicates saturated samples.

Sample ID	INITIAL DRY		STIM1 DRY		STIM2 DRY		INITIAL SATURATED		STIM1 SATURATED		STIM2 SATURATED	
	VP	VS	VP	VS	VP	VS	VP	VS	VP	VS	VP	VS
G8	3634.5	2225.5	3374.5	2031.5	3122.5	1973.5	4598	2355.5	4226	2105	4308	2123.5
G20	3666.5	2229	3244.5	1951.5	3021.5	1852.5	4502.5	2342	4251.5	2039	4192.5	1986
G13	3696	2221.5	3350.5	1995	3143.5	1874.5	4952	2368	4517	2037	4314	2000
G21	3465	2156.5	3274.5	1962.5	3047.5	1753	4385	2227	4234	2100	4064	2004.5
RK_30_21.4_2	3729	2434	3820	2455.5	3760	2375.5	4459	2357.5	4132.5	2292	4043.5	2173
RK_30_21.4_4	3788.5	2459	3833	2524.5	3511	2373	4445	2399	4127.5	2349.5	3850	2230
RK_30_21.4_6	3578	2332.5	3360	2309.5	3128	2216.5	4563.5	2280.5	4249.5	2154	3921.5	2046

Table 3.5: Summary table of measured ultrasonic wave velocities for samples of granite and Rotokawa andesite before and after thermal cycling.

3.6.1 Young's Modulus and Poisson's Ratio

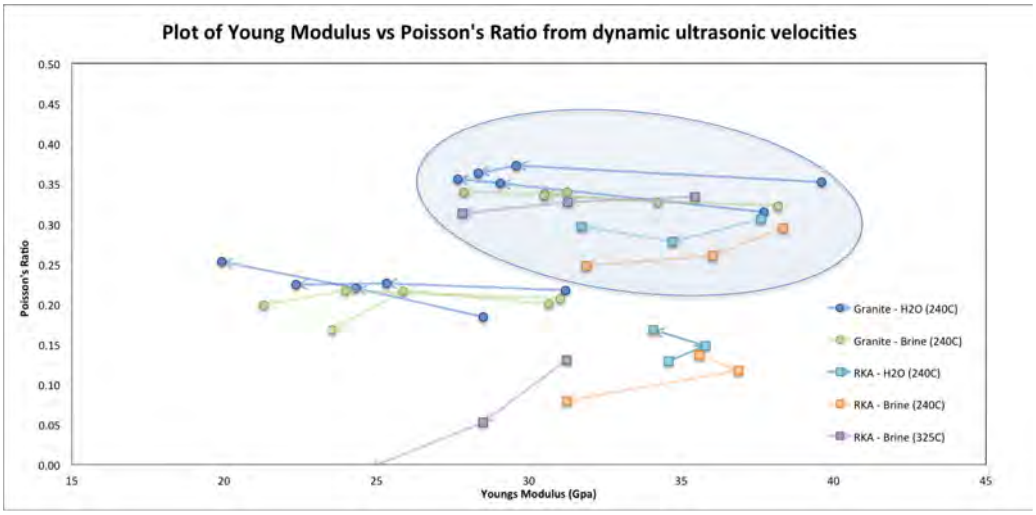

Figure 3.13: Plot of Young's Modulus and dynamic Poisson's Ratio for samples in both saturated, and dry conditions. Arrow points in direction of progressive thermal cycles. Shaded area indicates saturated samples.

Sample ID	Young's Modulus (Mpa)			Poisson's Ratio			Young's Modulus (Mpa) - Saturated			Dynamic Poisson's - Saturated		
	Initial	Stim 1	Stim 2	Initial	Stim 1	Stim 2	Initial	Stim 1	Stim 2	Initial	Stim 1	Stim 2
G8	30.7	25.9	23.5	0.20	0.22	0.17	38.2	30.5	31.3	0.32	0.34	0.34
G20	31.0	24.0	21.3	0.21	0.22	0.20	37.7	29.1	27.7	0.31	0.35	0.36
G13	31.2	25.3	22.4	0.22	0.23	0.22	39.6	29.6	28.3	0.35	0.37	0.36
G21	28.5	24.3	19.9	0.18	0.22	0.25	34.2	30.5	27.9	0.33	0.34	0.34
RK_30_21.4_2	34.6	35.8	34.1	0.13	0.15	0.17	37.6	34.7	31.7	0.31	0.28	0.30
RK_30_21.4_4	35.6	36.9	31.2	0.14	0.12	0.08	38.4	36.0	31.9	0.29	0.26	0.25
RK_30_21.4_6	31.2	28.5	24.8	0.13	0.05	0.00	35.5	31.3	27.8	0.33	0.33	0.31

Table 3.6: Young's Modulus and Poisson's Ratio before and after thermal cycling

3.7 XRD results

Limited XRD analysis was conducted on three samples of Ghibli granite (G0,G20,G21). Thermal-cycling has resulted in significant increases of plagioclase end-member albite and a reduction in quartz with the differences in results relating to the fluid that they were thermally-cycled in.

Sample ID	Lithology	Reservoir Fluid	Quartz	Albite	Biotite	Augite
G0	Granite	unaltered	55	45	trace	trace
G21	Granite	H_2O	45	55		
G20	Granite	NAP Brine	15	85	trace	

Table 3.7: Table of X-ray diffraction (XRD) results. All values are estimates and given as a percentage of the crystalline materials that is present within the air dried sample. The purity of albite was not specified.

3.8 Monomeric silica testing

Using spectrophotometric methods, the concentration of monomeric SiO_2 in the NAP brine at room temperature (20°C), averaged over 4 separate tests was 128ppm; the amorphous silica saturation curve predicts concentrations of 106ppm at this temperature. High concentrations of colloidal silica are obvious, with the brine displaying a milky texture indicating significant amounts of colloidal silica in suspension.

Measurement of monomeric silica was conducted during 3 thermal-cycling experiments: 2 at 240°C the other at 325°C. Monomeric silica concentrations increased with reservoir temperature in all tests. For tests conducted at 240°C reservoir conditions reached an average monomeric silica concentration of 691ppm for NAP brine and 120ppm for H_2O. When the reservoir temperature was heated to 325°C with NAP brine, the monomeric silica concentration averaged 1332ppm. The monomeric silica concentration measured at 325°C is similar to the total measured silica (GNS 2015) indicating that at this temperature colloidal silica has been fully de-polymerised. Figure 3.14 illustrates the evolution of the brine in respect to amorphous silica during two thermal cycling experiments. Monomeric silica is shown to increase during heating and thermal equilibration stages of the cycle indicating the de-polymerisation of colloidal silica into monomeric silica. During the cooling cycle, the reservoir is over-saturated with respect to amorphous silica, which would favour the polymerisation of silica monomers.

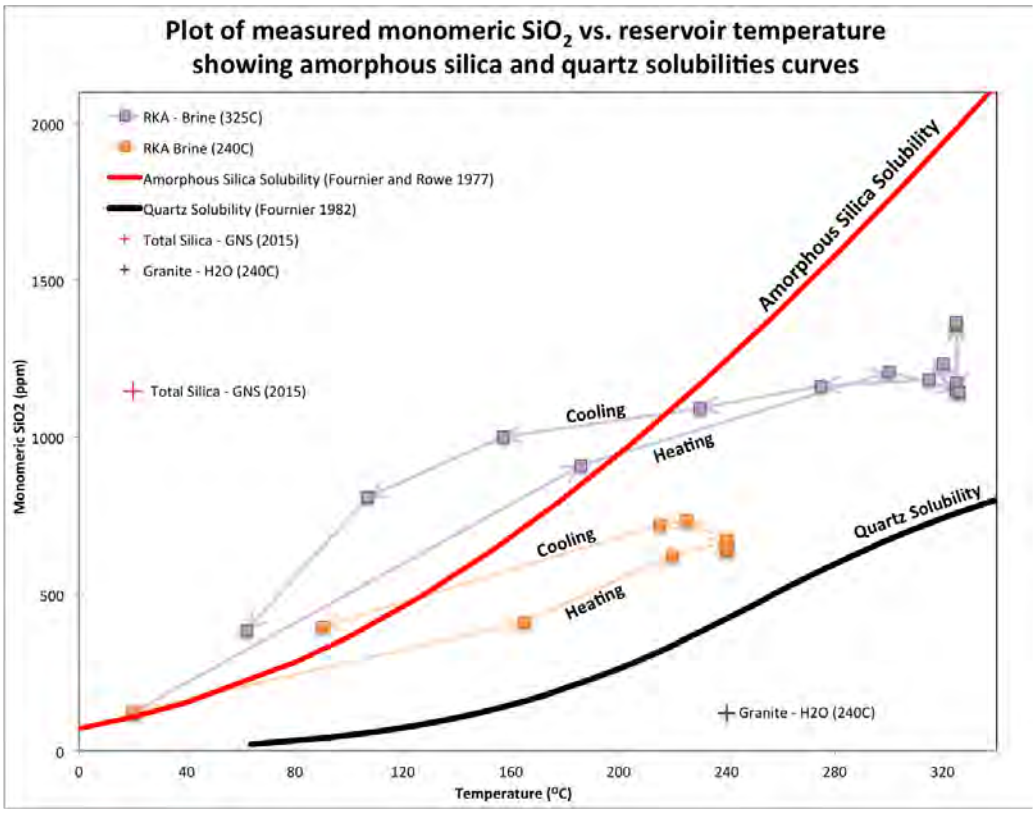

Figure 3.14: Measured monomeric SiO_2 plotted against reservoir temperature for thermal cycling experiments. Changes to concentrations during experimentation are indicated by arrows. The amorphous silica and quartz solubility curves are also plotted.

Temperature (celsius)	Monomeric Silica (ppm)	Elapsed Time (minutes)	Measured Adsorbance	Temperature (celsius)	Monomeric Silica (ppm)	Elapsed Time (minutes)	Measured Adsorbance
20	128	0	0.034	20	130	0	0.034
186	960	78	0.252	165	432	60	0.111
300	1275	168	0.334	220	660	93	0.170
325	1214	316	0.318	240	702	105	0.181
325	1239	317	0.325	240	677	139	0.174
325	1435	367	0.376	240	693	171	0.178
325	1445	367.5	0.379	240	679	199	0.175
326	1206	396	0.316	240	708	229	0.182
320	1303	396.3	0.342	225	776	230	0.200
315	1248	396.6	0.327	215	761	231	0.196
275	1227	399	0.322	90	416	247	0.107
230	1153	403	0.302				
157	1055	415	0.277				
107	855	428	0.224				
62	405	474	0.106				

Table 3.8: Table of monomeric silica testing results for NAP brine during 240°Cand 325°Cexperiments.

3.9 PHREEQC Modelling

PHREEQC modelling gave information on the predicted pH at equilibrium, as well as the saturation index of minerals in solution and likely reaction products. This model has been highly simplified and inherently has significant limitations.

Mineral Phase	Saturation Index			
	H2O 240	H2O 270	Brine 240	Brine 270C
Albite	-0.76	-0.75	-0.6	-0.6
Anorthite	0.02	0.14	0.01	0.12
Aragonite	-1.23	-1.02	-1.39	-1.16
Calcite	-1.18	-0.98	-1.34	-1.12
Chalcedony	-0.04	-0.01	-0.04	-0.01
Gibbsite	-2.97	-3.02	-2.95	-3
Halite	-	-	-4.67	-4.77
K-feldspar	-1.09	-1.14	-1.13	-1.18
K-mica	0	0	0	0
Kaolinite	-4.54	-4.61	-4.51	-4.58
Quartz	0	0	0	0
SiO2	-0.41	-0.35	-0.41	-0.35
Sylvite	-	-	-6.14	-6.21
CO2	-5.46	-5.01	-5.59	-5.12
O2	-7.27	-6.34	-11.52	-8.62
pH	9.26	9.182	9.24	9.151

Table 3.9: Model of reservoir saturation index using PHREEQC, considering reservoir conditions for Ghible granite in NAP brine or H_2O.

Chapter 4

Discussion

4.1 Introduction

The primary objective of this thesis was to apply thermal-cycling experimental methods developed by Siratovich et al. (2013, 2015a), and begin preliminary investigations into the use of geothermal fluids rather than distilled water. Samples of Ghibli granite were thermally-cycled in distilled H_2O to provide an experimental benchmark. Experiments were then repeated using low-pressure geothermal brine retrieved from Nga Awa Purua (NAP) station. Results obtained in this project clearly indicate that the different geochemistry of H_2O and NAP brine play significant roles in the alteration of Ghibli granite. Experiments were then translated to samples of Rotokawa andesite, with significant differences observed in how the two vastly different lithologies responded to the thermal cycling. Variability in the physical disturbance and chemical alteration of samples was observed through the measurement of: porosity, permeability, density, ultrasonic-wave velocity and limited XRD, SEM and study of thin-sections. When considering samples that were subject to the same reservoir temperatures, differences in porosity development relate directly towards mineral alteration processes and not micro-fracturing. Some of the mechanisms the are responsible for the alteration could be identified, others had to be assumed and reflect limitations in the methodology used. To comprehensively understand reservoir processes during thermal-cycling, in order to make predictions in reservoir operational management, significantly more experimentation and numerical modelling is required. In the section of further research I have identified key areas for the future development of both experimental equipment and methodology.

Figures 4.1 and 4.2 illustrate some of the key relationships observed as a result of thermal-cycling. These relationships were dependant on fluid-chemistry, reservoir temperature and lithology. The measured changes following successive thermal cycles are presented in Table 4.1.

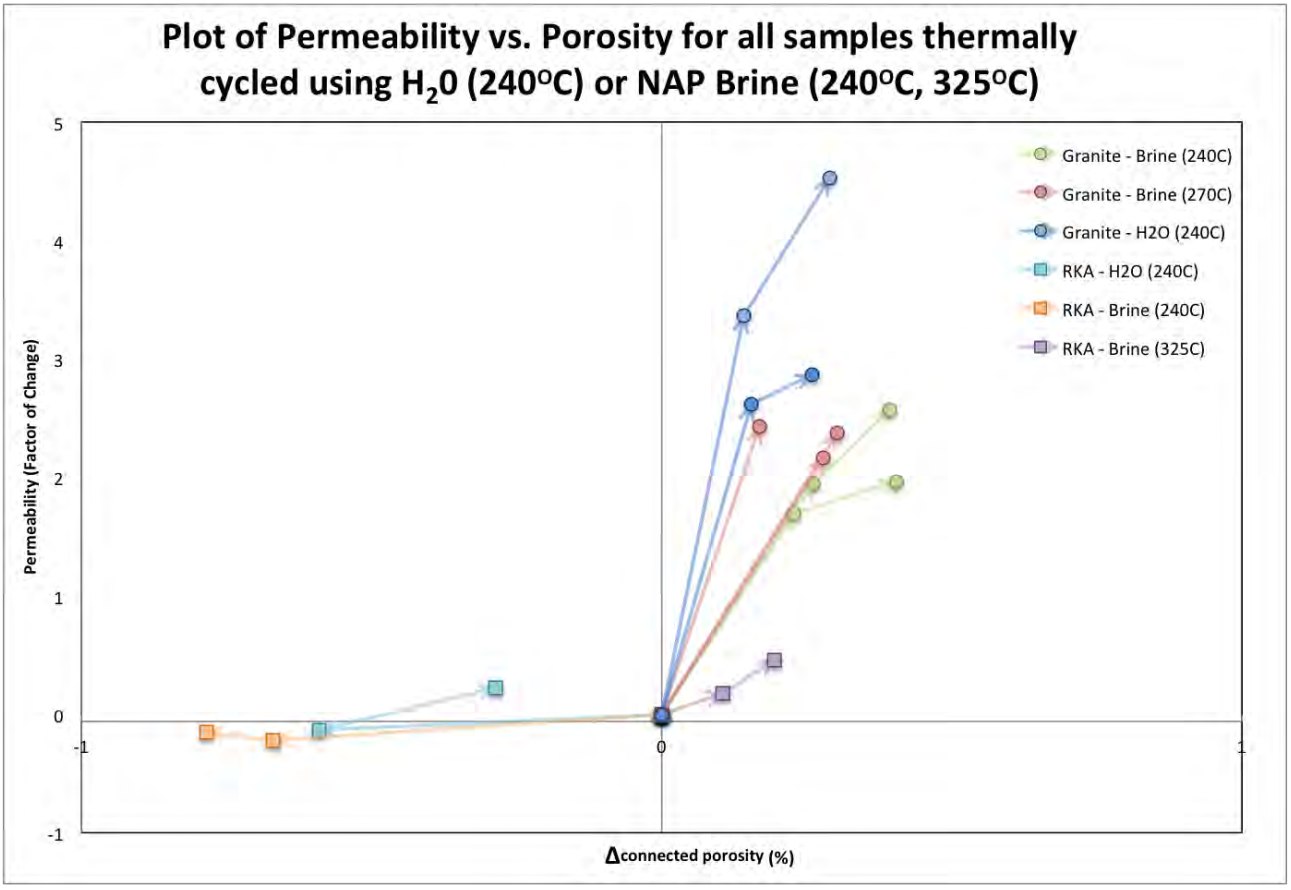

Figure 4.1: Plot of changes to permeability (Factor of Change) and porosity (% change of pore-space) as a result of thermal-cycling. Arrows indicate the direction of progressive thermal-cycles. There is clear distinction between Ghible granite and RKA samples.

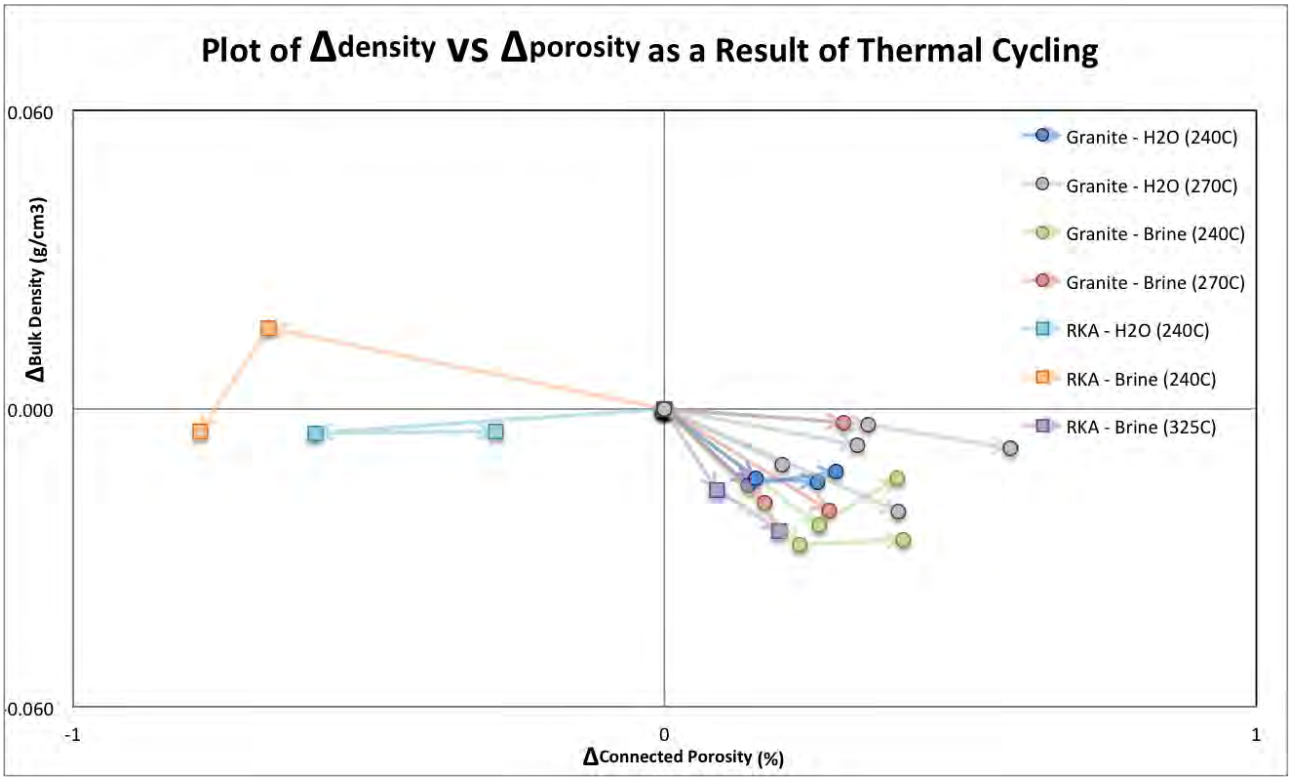

Figure 4.2: Plot of relative foctors of change to porosity and density as a result of thermal cycling. All points are assumed relative to samples initial porosity and density as measure by triple-weight method.

Sample ID	ΔBulk Density (g/cm3)		ΔPermeability (m2)		ΔPorosity (%)	
	Stim 1	Stim 2	Stim 1	Stim 2	Stim 1	Stim 2
G8	- 0.023	+ 0.009	+ 8.51E-18	+ 2.76E-18	+ 0.261	+ 0.132
G20	- 0.027	+ 0.001	+ 7.97E-18	+ 1.24E-18	+ 0.228	+ 0.175
G13	- 0.015	+ 0.003	+ 8.81E-18	+ 3.04E-18	+ 0.141	+ 0.148
G21	- 0.014	- 0.001	+ 8.37E-18	+ 8.16E-19	+ 0.155	+ 0.104
G1	- 0.019	-	+ 1.27E-17	-	+ 0.169	-
G3	- 0.003	-	+ 9.61E-18	-	+ 0.303	-
G7	- 0.021	-	+ 8.57E-18	-	+ 0.278	-
RK_30_21.4_2	- 0.005	+ 0.000	- 7.28E-20	+ 1.96E-19	- 0.590	+ 0.304
RK_30_21.4_4	+ 0.016	- 0.021	- 1.09E-19	+ 3.46E-20	- 0.670	- 0.115
RK_30_21.4_6	- 0.016	- 0.008	+ 1.42E-19	+ 2.17E-19	+ 0.104	+ 0.090

Table 4.1: Summary table of changes to porosity, density and permeability

4.2 Microfracturing

Previous experimentation by Siratovich et al. (2013) indicates that mechanical damage is likely to occur to samples as a result of thermal-cycling. Assuming that thermal-stresses are equal between the two different fluids used, micro-fracture porosity formation is unlikely to vary across homogenous samples, therefore observed changes in porosity relate to chemical processes and mineral alteration. Pre-existing intra-granular micro-fracturing is observed in unaltered Ghibli granite and accounts for the relatively high permeability. Rotokawa andesite displayed significant micro-fracturing of phenocrysts, but these fractures were not observed to continue through the matrix. Following thermal-cycling, granite thin-sections suggested that no significant increase to the density of micro-fractures had occurred. Thin-sections of Rotokawa andesite after thermal-cycling at 325°C, perhaps display slight evidence of new micro-fracture formation in phenocrysts although as the rock is so heterogenous it is hard to be certain.

4.3 Mineral Alteration

Mineral alteration is complex with no one model suitable to explain every system, although key relationships exist across all systems. The chemical alteration of a rock-mass occurs through ionic instability between the geothermal fluid and the mineral. Important characteristics that influence alteration include: fluid pH, concentration of salts, crystalline structure of minerals in the rock mass, conductivity of fractures and pore-space surface area (Henley et al. 1984). The degree or intensity of alteration will depend on the age of the system and the conductivity of heat and fluids over time.

4.3.1 Gradient Reactions

Reactions that occurs in experiments are likely to be highly variable and depend on: temperature, fluid pH and the location of the surface that is being altered. Greater rates of alteration can be expected to occur to the outside of samples than to the surface of pore-walls inside the sample ie, the ground-mass. The alteration of pore-space likely reflects the low-flow conditions. Flow-controlled reactions are common to geologic settings and are often referred to as gradient reactions. Gradient reactions occur simultaneously throughout the entire rock-matrix, or along pore-walls of fracture networks at rates proportional to flow-speed, temperature and pressure in the direction of flow (Phillips 1991). As the fluid moves through the rock, from one mineral assemblage to the next (at slow velocities, beyond equilibration length) it approaches equilibrium with the new assemblages for the ambient temperature

and pressure. The reaction fronts pass back and forward through the sample with diffusion being the dominant method of mass-transport. The rate of mineral dissolution will depend on the proportions of both the area available for reactions and the degree of disequilibrium between products and reactants. Patterns of dissolution, precipitation, and alteration depend on reaction kinetics. Reaction kinetics are influenced by temperature, pressure, pH, and in geologic settings, flow rates. Not all geochemical reactions are caused by interstitial fluids. In the case of mineral dehydration reactions, water produced by the reaction may subsequently move through the matrix.

4.3.2 Ghibli granite

Un-altered Ghibli granite provided a simple homogenous system to test physical changes that are occurring to the rock-mass with differing fluid chemistry. Although granites are not common hosts to high-enthalpy geothermal reservoirs, significant studies (Zoback and Byerlee 1975, Darot et al. 1992, David et al. 1998, Nara et al. 2011, Siratovich et al. 2015a) on the thermal cycling and mineral alteration of granite have been conducted with mechanisms responsible for change being relatively well understood.

The major mineral components of Ghibli granite are plagioclase feldspar, K-feldspar and quartz. XRD analysis of crushed whole-rock granite samples pre and post thermal-cycling (Table 3.7) measured an increase in the relative crystalline abundance of the plagioclase end-member species albite. Thermal-cycling using NAP brine had resulted in 30% more albite and 30% less quartz than when H_2O was used.

In hand-samples of thermally-cycled Ghibli granite surface texture was coarse and dusty with the original pink lustre now a dull grey. In thin-section alteration to the mineral assemblages was observed. Biotite-mica had been altered to chlorite, with the extent of alteration depending on the fluid used. With H_2O, the initially 'clean' crystals of biotite were now dominantly chlorite. With NAP brine the biotite alteration was as observed brown-green square flakes, suggesting only partial chlorite alteration had occurred. The XRD results agree with this observation in that while 'trace' amounts of biotite were found in NAP brine samples, only chlorite was observed in H_2O samples. K-feldspar minerals appear dusty and display increased development of a pre-existing perthitic texture with occasional low-relief, white spots (albite?) noted, particularly in NAP brine samples. Quartz and plagioclase appeared unaltered in thin-section, with calcite infilled fractures still existing through-out.

The intensity and method of alteration to the Ghibli granite is likely to have been governed by the pH of the reservoir fluid. At 25°C the NAP brine pH is 4.31 and H_2O 5.6. At reservoir temps of 240°C a highly simplified PHREEQC (pH-redox-equilibrium-c) model indicates that equilibrium pH of NAP brine is 9.26 and H_2O 9.24 respectively. The fluid transitions from acidic to basic as the reservoir temperature increases. This is an important factor when considering alteration processes. The PHREEQC model does not consider the likely progressive change in pH during of reservoir during heating which would likely see alteration process and product vary with time.

Biotite-chlorite

The hydrothermal alteration of biotite-mica to chlorite results in two layers of biotite becoming one layer of chlorite. Cation K^+ is removed from the system with Al, Mg and Fe typically retained as alteration processes strip biotite layers off at random with clay minerals and SiO_2 being produced as a result of the alteration. Although there is up to 35% reduction in mineral volume associated with biotite-chlorite alteration, much of the created void space is filled with clay-minerals, reaction products and amorphous SiO_2 on cooling. Net porosity gain for the individual mineral may be as little as 5% (Eggleton and Banfield 1985). Although biotite is of relatively low abundance ($\leq$ 5% in the Ghibli granite), the alteration of biotite to chlorite is likely to have been a significant factor in the porosity development observed between the two fluids. When we consider the pre-existing mica-fabric, which is also observed by an axially varied point load index, the development in porosity may have had significant impact on sample permeability. Biotite dissolves in both acid and alkaline aqueous solutions, with higher dissolution rates occurring in lower pH fluids. PHREEQC modelling of the reservoir indicates that the alteration of biotite to chlorite occurs predominantly at lower temperatures, with rates slowing with the increasing temperature. During cooling of reservoir, pH returns to acidic conditions and the rate of chlorite alteration accelerates.

K-feldspar

Perthitic texture observed in thin-sections suggest subsolidus un-mixing (a cation exchange process between feldspar species) of K-feldspar is occurring in the reservoir. Sub-solidus un-mixing (spinodal decomposition) is often referred to as albitization, in that near-pure plagioclase end-member species albite is being produced from both plagioclase and/or K-feldspar (Wyart and Sabatier 1965, Beaty and Albee 1980). The Al, Si high-ordering in K-feldspar is thought to be reversible down to temperatures as low as 200°C (Brown and Parsons 1989). In hydrothermal systems the albitization of K-feldspar is most likely at temperatures of 120-150 degrees, and is shown to decrease with increasing temperature, a function of pH (Ben Baccar et al. 1993). Albite is well known to be synthesised hydrothermally (Bowen and Tuttle 1950). Aluminosilicate layers that build K-feldspar are electronically neutral, with bonding occurring through weak van de Waals bonds with the included cation. The removal of K^+ by fluids, and the exchange with the smaller Na^+ cation results in crystal restructuring and pore-space development.

XRD and thin-section observations in this study indicate that NAP brine played a significant role in albitization with brine samples being significantly more altered in respect to albite than H_2O samples. A sodium-rich fluid (such as NAP brine) can induce albitization by transforming any alibite-orthoclase-anorthite solid solution into nearly pure albite, along with the formation of new Si-rich phases and recrystallization of new quartz (Kaur et al. 2012). During albitization the original textures of the granitoid rocks may remain well preserved, even after complete alteration of the primary mineralogy (Nijland and Touret 2001). Albitization is commonly accompanied by quartz dissolution (episyenitization), despite some secondary silicification. Kinetic modelling of the albitization reaction predicts instability, with quartz generally considered a K-feldspar albitization product (Boulvais et al. 2007). The measured monomeric SiO_2 for samples thermally cycled in H_2O (120ppm) is likely to have been contributed to by both the albitization of K-felspar and the dissolution of quartz.

Electron microprobe analysis of crystals is likely to identify and zone this exchange, allowing for further quantitative and spatial analysis of this process occurring. Changes to bulk-chemical composition of the rock can be measured through ICP-MS analysis, with the removed K^+ & Ca^+ cations also likely observed in ICP-OS analysis of reservoir fluid.

Plagioclase feldspar

Plagioclase feldspar has excess silica (Weill et al. 1970) with excess silica typically increasing monotonically from core to rim of the plagioclase (Beaty and Albee 1980). The two mechanisms that may result in excess silica being discarded are exsolution and diffusion. Calcite is produced through the alteration of plagioclase in a CO_2 rich system, is described by the following equation:

Plagioclase + CO_2 = clay + calcite

However, there was limited (or no) evidence that the alteration of plagioclase feldspar was occurring as a result of thermal-cycling.

Calcite

Calcite was identified in fractures both pre and post thermal-cycling, making it unclear as to whether calcite is being produced through the breakdown of plagioclase feldspar. However, the likely presence of CO_2 in both NAP brine and H_2O, through contamination with atmospheric gases, suggests that plagioclase alteration is likely to have occurred. Calcite undergoes retrograde solubility and with increasing temperature, solubility is reduced. The dissolution of calcite may have occurred during low temperature experiments such as porosity measurement via triple-weight methods, and then have re-deposited as a result of the alteration of plagioclase at higher temperatures.

Quartz

Quartz did not show alteration as a result of thermal-cycling and there was no visible increase in the density of pre-existing micro-fractures. Based on the fluid chemistry and modelling of the quartz and amorphous silica solubilities (Figure 3.14), the dissolution of quartz in H_2O can be expected to occur. At 240°Cthe spectrophotometric measurement of monomeric SiO_2 in H_2O indicated concentrations of 120ppm SiO_2 in the reservoir, agreeing with the model. Quartz is not expected to be dissolved in the NAP brine due to the brine already being super-saturated in respect to amorphous silica.

Clay Minerals

The alteration of feldspars results in the formation of clay minerals. For plagioclase feldspar the alteration product its commonly kaolinite and for K-feldspar, prophylitte or illite. For clay minerals to form, bulk cation such as Na^+, K^+, Ca^{2+}, Mg^{2+}, and Fe^{3+} must first be leached by an alteration process, with leaching increasing in acidic conditions (low pH). As the reservoir temperature increases,

so does the pH and therefore the production of clay minerals is likely to decrease.

The distribution of clay minerals reflect reservoir temperature and pH, they are therefore used as indicators of reservoir conditions at the time that the secondary minerals were being formed (Browne and Ellis 1970). Kaolinite is the most common in the kaolin group of clays, other kaolins with similar structures include: anauxite, dickite, and nacrite. Kaolinite is formed by weathering or hydrothermal alteration of aluminosilicate minerals. Granititc rocks are rich in feldspar and commonly change to kaolinite. Argillic alteration is characterised by the formation of clay minerals such as smectite, smectite-illite, illite. These clay minerals replace primary plagioclase, and mafic silicates like pyroxenes, amphiboles and biotite (Pirajno 2009). Reservoir temperatures below 140°C are typically indicated by the presence of smectite. With increasing depth and temperature (up to 210°C), smectite becomes inter-stratified with illite forming an inter-layered smectiteillite clay. The presence of illite plus chlorite is generally indicative of temperatures above 210°C. The presence of kaolin group minerals points to reservoir temperatures of less than 200°C (Simmons and Browne 2000).

The direct measurement of reservoir pH is difficult, with the modelling of reservoir geochemistry and intensity of alteration often required to make predictions. PHREEQC modelling suggests that reservoir pH is 9.2 when NAP brine reached equilibrium at 240°C. At lower reservoir temperatures, pH is acidic with argillic or propylitic alteration predicted. At higher reservoir temperatures chlorite alteration was predicted and observed. The formation of kaolinite is also possibile. It is likely that all of these clay minerals have formed at different stages in the reservoir due to the high range in operating temperatures. The formation of clay minerals accounts for significant porosity development to the rock mass, with there subsequent transport and location of deposition playing a critical roll in rock-mass permeability.

Porespace surface area

Knowledge of fracture geometry, density and development will allow for the further constraint of available reaction surfaces in numerical modelling. The area of outer surfaces of sample G8 is around 31.3cm^2. The initial measured void volume is 0.11cm^3 which if assumed to take the shape of a unit sphere (smallest possible surface area for volume), the minimum surface-area available for reactions to occur within the pore spaces is 1.11cm^2. After two thermal-cycles internal surface area had increased by a minimum of 28%. This new surface area is available for reactions to occur. In addition, the increase in pore-volume and permeability allows for more fluid to pass through the system resulting in an increase in localised alteration. Non-soluble reaction products such as clay minerals accumulate in pore-spaces and migrate slowly through the system as a result of molecular diffusion processes (due to clay minerals binding with free cations resulting in particles having an charge). Over time clay minerals may accumulate in pore-throat apertures, constricting flow and resulting in a significant reduction to localised permeability, slowing the reaction speed down as locally stagnant solution begins to approach equilibrium. Micro-fracturing may lead to new reaction pathways being established and and enhanced permeability.

4.4 Monomeric Silica

In the natural-state reservoir dissolved silica is in equilibrium with quartz, but due to the high enthalpy resulting in a high steam-fraction, enrichment of SiO_2 occurs in the triple-flashed NAP brine. The high silica concentrations of NAP brine used in this investigation can be attributed to natural reservoir variation such as multiple fluid sources, boiling zones and fluid pH. Field operation methods may also have a significant impact on the enrichment of reservoir SiO_2 (Lovelock 1995). GNS (2015) report low pressure NAP brine as having SiO_2 concentrations of 1147ppm where the production reservoir has an estimated 950ppm SiO_2.

The spectrophotometric measurement of monomeric SiO_2 has been measured in three different experiments in this investigation. Monomeric SiO_2 in the NAP brine was measured throughout a complete thermal cycle at both 240°C and 325°C. A comparative measurement was taken from an experiment using H_2O at 240°C. For the NAP brine experiments, the stabilisation of monomeric silica concentration indicates that no further de-polymerisation of colloidal silica to monomeric SiO_2 is occurring. Reservoir temperature appeared to be a limiting factor in the formation of monomeric SiO_2 in 240°C experiments. Higher concentrations of monomeric silica were predicted, however results indicate that not all colloidal silica had been de-polymerised. This is likely to be the influence of temperature on reaction kinetics. When these results were plotted against quartz and amorphous silica solubility curves (Figure 3.14), the reservoir fluid was shown to be under-saturated with respect to amorphous silica, but with significantly higher concentrations than the quartz solubility curve. During cooling of the reservoir, monomeric silica is measured to be above the amorphous silica saturation curves. These conditions are favourable for the polymerisation and the precipitation of amorphous silica.

For NAP experiments the injection of colloidal rich NAP brine (120 ppm monomeric) during cooling stage of thermal-cycling will result in dilution and the under-estimation of reservoir monomeric SiO_2. During the transport of NAP brine from the header tank to the reinjection point, heating of the fluid occur. The colloidal rich brine will begin depolymerisation. Simultaneously amorphous SiO_2 in solution will begin to approach saturation at which point the deposition of amorphous silica is able to occur on surfaces.

Monomeric silica concentrations in the H_2O reservoir at 240°C were measured as 119ppm. This silica concentration is likely to have been from the dissolution and the alteration of quartz, mica and feldspars. Given sufficient time, reservoir quartz should approach the quartz equilibrium curve. As this is a simple, closed system, the reservoir cannot become over-saturated with respect to quartz unless boiling is allowed to occur. For NAP brine experiments, the further dissolution of quartz is unlikely due to the reservoir fluid already being over-saturated with respect to quartz. At 240°C the solubility of quartz in H_2O is 420ppm and at 270°C is 560ppm (Fournier and Potter 1982). The measurement of SiO_2 in distilled water after thermal-cycling results show that dissolution is occurring in the reservoir, that it is temperature dependant, and that reservoir rocks in these experiments may not have yet reached a state of thermo-chemical equilibrium. The rate of dissolution is not likely to be linear with time, but dependant on the available surface area for reactions to occur. Rock heterogeneity may result in highly-varied rates of dissolution. To give further information on the relative contributions that weathered silicates have made to the total reservoir SiO_2, measurement of bulk cations would be necessary.

4.5 Comparison of Ghibli granite to Rotokawa andesite

In this investigation the limited experimentation on the Rotokawa Andesite has resulted in no definable trends or repeated results. It is therefore difficult to draw conclusion as to the effects of thermal cycling on the RotoKawa Andesite. Significant variations exist in the measured matrix permeability, porosity, mineral composition and intensity of alteration in the andesite, with poor correlations between most parameters (Siratovich et al. 2015a, Mielke et al. 2015). The centre of andesite lava flows have very different properties to the brecciated margins. RKA also has an order-of-magnitude lower permeability than the granite resulting in low-flow conditions within the rock-mass during experimentation and a reduced rate of alteration.

Changes to density, porosity and permeability have been measured, but the mechanisms responsible were not able to be identified in hand-sample or thin-section. Distinguishing differences in the alteration of samples cycled in NAP brine or H_2O at 240°C was inconclusive. Heterogeneity resulting in high variations of phenocrysts and ground-mass percentages made observing change between samples challenging. For the sample thermally-cycled at 325°C in NAP brine, oxidation of the ground-mass (hematite?) was prevalent throughout thin-section. Greater density of micro-fractures within phenocrysts were also observed.

It can be concluded that, when considering the thermal-cycling of Rotokawa andesite at low temperatures, less then desirable effects (in terms of reduction to permeability and porosity) have been observed. At 325°C using NAP brine for two successive thermal cycles, the changes to porosity permeability and density were linear. A distilled water control for this experiment would be likely to provide further information.

4.6 Further Research

This investigation has shown that both mineralogy and fluid chemistry play significant roles in thermal cycling processes. The scope for development of these methods to further understand alteration processes is extensive. Through refined and extensive experimentation and more precise analytical methods, results collected will allow us to further constrain geochemical models, enhancing the understanding of geothermal systems.

Direct comparisons between the response of Ghibli granite and Rotokawa andesite to thermal-cycling using H_2O and NAP brine requires more experimentation. Heterogeneity of the Rotokawa andesite makes identifying processes and extrapolating them across the reservoir difficult with the development of further methodology required. Future research would benefit from a more comparable control sample, such as the well-preserved, un-altered andesite forming Mt. Ruapehu which occupies the southern extent of the TVZ. Observing the evolution of the andesite through thermal-cycling induced alteration, insight may be provided to the processes occurring in the Rotokawa reservoir. Samples should be collected from numerous locations of an andesitic flow and include both breccias and lavas.

In future experiments with the Rotokawa andesite, the matching of experiment conditions to those predicted in the reservoir would be beneficial. For example, applying reservoir specific confining pressures to samples when measuring permeability. Other iterations could include confining the sample during thermal stimulation which is technically complex.

Specific focus should be directed towards the fluid chemistry and how it evolves through time. Changes to mineral assemblages, as observed in thin-section suggest that fluid composition has changed to reflect new equilibrium conditions. These changes might include: dissolved ionic species, pH, mineral solubility and reaction products. In future experiments, ICP-OS analysis of fluids should be undertaken both up and downstream in the system. Measured variations to chemistry will directly reflect the alteration processes occurring in the reservoir. Simple measurements like fluid pH and conductivity will also enable the further refinement and proofing of the geochemical model. ICP-OS would provide very specific information on mineral concentrations and how they fluctuate through time. Measuring soluble gas species such as CO_2 would provide invaluable information to pH modelling.

Further research could also see the development of methodologies such that clay-minerals could be both collected and measured using XRF for bulk composition or more specifically XRD. PHREEAC modelling predicts some of these clay species but the collection of them is challenging due to the very low amounts of clay being produced. Alternatively, electron microprobe analysis of clays or salts that have been identified on pore walls may be able to provide this information. Electron microprobe and EDS analysis would also be used to map albite alteration of plagioclase species.

The data from this study indicates that thermal cycling results in reductions to rock-mass Young's Modulus and Poisson's Ratio's, agreeing with previous studies by Siratovich et al. (2015a). Increased thermo-mechanical damage will likely lead to weakening of microstructures and eventually the collapse of pore-structures resulting in irreversible damage to permeability. Determining the relationships between thermal-cycling and rock strength degradation, important modelling parameters could be defined. This may include information on safe reservoir operating pressures and minimise the risk of pore-collapse occurring. Obtaining ultrasonic velocities for samples under triaxial confinement would provide significantly more accurate results.

At Rotokawa field brines are also re-injected into deep-reservoir greywacke. To date no thermal-cycling experiments have been conducted on rocks of this nature. Greywacke is likely to be strongly influenced by fracture permeability and it is unknown how samples of intact rock would respond to thermally-induced stresses or chemical alteration, this is an area for further investigation.

Chapter 5

Conclusions

The objective of this thesis was to develop methods required for the determination of physical, mechanical and chemical changes occurring to the rock-mass during thermal-cycling using geothermal brine. The following are some of the key conclusions:

Fluid composition plays an important role in the development of porosity and permeability when thermal-cycling Ghibli granite and Rotokawa andesite. Results do not correlate well with increasing temperature, suggesting fluid pH is playing a significant role. Significant differences exist between the lithology, structure and pre-existing alteration of the samples tested. With such limited sample sizes, direct translation of results between two different lithologies is not yet feasible, with significant future work required.

In geologically short periods of time, thermal-cycling has resulted in measurable amounts of mineral alteration to samples with alteration products observable in thin-section.

Ghibli granite samples thermally-cycled in NAP brine were observed as having significantly more albitization than those cycled in H_2O. Albitization and associated process are thought to be responsible for the measured differences in porosity development, with NAP brine samples on average developing more porosity than H_2O samples.

Ghibli granite samples that were thermally-cycled in H_2O developed more permeability than those cycled in NAP brine, despite developing less porosity. This is associated with the alteration of biotite to chlorite, which was more dominant in H_2O experiments. It is thought that the chlorite assemblage has allowed for the linking of flow paths, reducing tortuosity and enhancing permeability.

Deposition of amorphous silica was not observed despite modelling indicating that reservoir conditions were favourable to this process occurring. It is possible that deposited minerals were not well preserved, with products removed during further experimentation and the preparation of thin sections. Another explanation is that the NAP brine used was acid-dosed and therefore the polymerization of amorphous SiO_2 has been significantly delayed.

References

Addison, S. J., Brown, K. L., Hirtz, P. H. V., Gallup, D. L., Winick, J. A., Siega, F. L., and Gresham, T. J. (2015). Brine Silica Management at Mighty River Power , New Zealand. In *Proceedings World Geothermal Congress*, number April, Melbourne, Australia.

Angcoy, E. C. and Arnórsson, S. (2010). An Experiment on Monomeric and Polymeric Silica Precipitation Rates from Supersaturated Solutions. *World Geothermal Congress*, (April):25–29.

Ashby, M. and Sammis, C. (1990). The damage mechanics of brittle solids in compression. *Pure and Applied Geophysics*, 133(3):489–521.

Axelsson, G. and Thorhallsson, S. (2009). Review of Well stimulation Operations in Iceland. *Geothermal Resource Council TRANSACTIONS*, 33:795–800.

Barton, C., Zoback, M., and Moos, D. (1995). Fluid flow along potentially active faults in crystalline rock. *Geology*, 23(8):683– 686.

Beaty, D. W. and Albee, A. L. (1980). Silica solid solution and zoning in natural plagioclase. *American Mineralogist*, 65:63.

Bégué, F., Deering, C. D., Gravley, D. M., Kennedy, B. M., Chambefort, I., Gualda, G. a. R., and Bachmann, O. (2014). Extraction, storage and eruption of multiple isolated magma batches in the paired Mamaku and Ohakuri eruption,Taupo volcanic zone, New Zealand. *Journal of Petrology*, 55(8):1653–1684.

Ben Baccar, M., Fritz, B., and Made, B. (1993). Diagenetic albitization of K-feldspar and plagioclase in sandstone reservoirs; thermodynamic and kinetic modeling. *Journal of Sedimentary Research*, 63(6):1100–1109.

Bibby, H., Caldwell, T., Davey, F., and Webb, T. (1995). Geophysical evidence on the structure of the Taupo Volcanic Zone and its hydrothermal circulation. *Journal of Volcanology and Geothermal Research*, 68(1-3):29–58.

Bibby, H. M. (1988). Electrical resistivity mapping in the central volcanic region of New Zealand. *New Zealand Journal of Geology and Geophysics*, 31(3):259–274.

Bibby, H. M. and Hohmann, G. W. (1993). Three-dimensional interpretation of multiple-source bipole-dipole resistivity data using the apparent resistivity tensor. *Geophysical prospecting*, 41(6):697–723.

Björke, J. K., Mountain, B. W., and Seward, T. M. (2012). The Solubility of Amorphous Aluminous Silica : Implications for Scaling in Geothermal Power Stations. In *New Zealand Geothermal Workshop*, number November, Auckland, New Zealand.

Boulvais, P., Ruffet, G., Cornichet, J., and Mermet, M. (2007). Cretaceous albitization and dequartzification of Hercynian peraluminous granite in the Salvezines Massif (French Pyrenees). *Lithos*, 93(1-2):89–106.

Bourbie, T. and Zinszner, B. (1985). Hydraulic and acoustic properties as a function of porosity in Fontainebleau Sandstone. *Journal of Geophysical Research*, 90(B13):11524.

Bowen, N. L. and Tuttle, O. (1950). The System NaAlSi_{3}O_{8}-KAlSi_ {3}O_{8}-H_{2}O. *Journal of Geology*, 58:489–511.

Bowyer, D., Bignall, G., and Hunt, T. (2008). Formation and Neutralisation of Corrosive Fluids in the Shallow Injection Aquifer, Rotokawa Geothermal Field, New Zealand. *GRC Transactions*, 32.

Brace, W. (1980). Permeability of crystalline and argillaceous rocks. *International Journal of Rock Mechanics and Mining Sciences & Geomechanics Abstracts*, 17(5):241–251.

Britannica (2015). Geothermal energy uses. Retrieved from http://www.britannica.com/science/geothermal-energy.

Brown, W. L. and Parsons, I. (1989). Alkali Feldspars: Ordering Rates, Phase Transformations and Behaviour Diagrams for Igneous Rocks. *Mineralogical Magazine*, 53(369):25–42.

Browne, P. R. L. and Ellis, A. J. (1970). The Ohaki-Broadlands Hydrothermal Area, New Zealand: Mineralogy and Related Geochemistry. *American Journal of Science*, 269:97–131.

Browne, P. R. L. and Lawless, J. V. (2001). Characteristics of hydrothermal eruptions, with examples from New Zealand and elsewhere. *Earth-Science Reviews*, 52(4):299–331.

Burton, E., Bourcier, W., Wallace, A., Bruton, C., and Leif, R. (2003). Silica scale management : lowering operating costs through improved scale control, and adding value by extracting marketable by-products. *Geothermal Resource Council Transactions*, pages 519–522.

Buscarlet, E., Hernandez, D., and Power (2014). Geochemical modelling of an injection well. In *36th New Zealand Geothermal Workshop*, number November, Auckland.

Cant, J. L. (2015). *Matrix Permeability of Reservoir Rocks , Ngatamariki Geothermal Field, Taupo Volcanic Zone , New Zealand*. Master's thesis, University of Canterbury.

Chaki, S., Takarli, M., and Agbodjan, W. (2008). Influence of thermal damage on physical properties of granite rock: Porosity, permeability and ultrasonic wave evolutions. *Construction and Building Materials*, 22(7):1456–1461.

Clearwater, J., Azwar, L., Barnes, M., Wallis, I., and Holt, R. (2015). Changes in Injection Well Capacity During Testing and Plant Start-Up at Ngatamariki. In *World Geothermal Congress*, pages 19–25, Melbourne, Australia.

Cole, J. (1990). Structural control and origin of volcanism in the Taupo volcanic zone, New Zealand. *Bulletin of volcanology*, pages 445–459.

Collar, R. J. (1985). *Hydrothermal eruptions in the Rotokawa geothermal system, Taupo Volcanic Zone, New Zealand*. Geothermal Institute, University of Auckland.

Collar, R. J. and Browne, P. R. L. (1985). Hydrothermal eruptions at the Rotokawa geothermal field, Taupo volcanic zone, New Zealand. In *Proc. 7th NZ Geotherm. Workshop*, pages 171–175.

Darcy, H. P. G. (1856). *Dètermination des lois d'ècoulement de l'eau à travers le sable.*

Darot, M., Guegue, Y., and Baratin, M. (1992). Permeability of Thermally Cracked Granite. *Geophysical Research Letters*, 19(9):869–872.

David, C., Menendez, B., and Darot, M. (1998). Influence of stress-induced thermal cracking on physical properties and microstructure of La Peyratte granite. *International Journal of Rock Mechanics and Mining Sciences*, 36(4):433–488.

David, C., Menendez, B., and Darot, M. (1999). Influence of stress-induced and thermal cracking on physical properties and microstructure of La Peyratte granite. *International Journal of Rock Mechanics and Mining Sciences*, 36(4):433–448.

DeMets, C., Gordon, R. G., Argus, D. F., and Stein, S. (1994). Effect of recent revisions to the geomagnetic reversal time scale on estimates of current plate motions. *Geophysical research letters*, 21(20):2191–2194.

Dobroskok, A., Ghassemi, A., and Linkov, A. (2005). Numerical simulation of crack propagation influenced by thermal and porous liquid stresses. *International Journal of Fracture*, 134(2):29–34.

Dove, P. and Crerar, D. (1990). Kinetics of quartz dissolution in electrolyte solutions using a hydrothermal mixed flow reactor. *Geochimica et Cosmochimica Acta*, 54(11):955–969.

Eggleton, R. A. and Banfield, J. F. (1985). The alteration of granitic biotite to chlorite. *American Mineralogist*, 70(9-10):902–910.

Faoro, I., Vinciguerra, S., Marone, C., Elsworth, D., and Schubnel, a. (2013). Linking permeability to crack density evolution in thermally stressed rocks under cyclic loading. *Geophysical Research Letters*, 40(11):2590–2595.

Fortin, J., Stanchits, S., Vinciguerra, S., and Guéguen, Y. (2011). Influence of thermal and mechanical cracks on permeability and elastic wave velocities in a basalt from Mt. Etna volcano subjected to elevated pressure. *Tectonophysics*, 503(1-2):60–74.

Fournier, R. and Rowe, J. (1977a). The Solubility of Amorphous and High Pressures Silica in Water at High Temperatures. *American Mineralogist*, 62:1052–1056.

Fournier, R. and Rowe, J. (1977b). The solubility of amorphous and high pressures silica in water at high temperatures. *American Mineralogist*, 62:1052–1056.

Fournier, R. O. (1977). Chemical geothermometers and mixing models for geothermal systems. *Geothermics*, 5(1):41–50.

Fournier, R. O. and Potter, R. W. (1982). Revised and expanded silica (quartz) geothermometer. *Bull., Geotherm. Resour. Counc.(Davis, Calif.);(United States)*, 11(10).

Fournier, R. O. and Rowe, J. J. (1966). Estimation of underground temperatures from the silica content of water from hot springs and wet-steam wells. *American Journal of Science*, 264(9):685–697.

Fredrich, J. T. and Wong, T.-f. (1986). Micromechanics of thermally induced cracking in three crustal rocks. *Journal of Geophysical Research*, 91:743–764.

Giggenbach, W. F. (1995). Variations in the Chemical and Isotopic Composition of Fluids Discharged from the Taupo Volcanic Zone, New-Zealand. *Journal of Volcanology and Geothermal Research*, 68(95):89–116.

Gilluly, J. (1937). The water content of magmas. *American Journal of Science*, S5-33(198):430–441.

GNS (2015). NAP Station Chemistry. Technical Report May.

Gowd, T. and Rummel, F. (1980). Effect of confining pressure on the fracture behaviour of a porous rock. *International Journal of Rock Mechanics and Mining Sciences & Geomechanics Abstracts*, 17(4):225–229.

Graham, I., Cole, J., Briggs, R., Gamble, J., and Smith, I. (1995). Petrology and petrogenesis of volcanic rocks from the Taupo Volcanic Zone: a review. *Journal of Volcanology and Geothermal Research*, 68(1-3):59–87.

Grant, M. A. and Bixley, P. F. (2011). *Geothermal Reservoir Engineering*.

Gravley, D. M., Wilson, C. J. N., Leonard, G. S., and Cole, J. W. (2007). Double trouble: Paired ignimbrite eruptions and collateral subsidence in the Taupo Volcanic Zone, New Zealand. *Bulletin of the Geological Society of America*, 119(1-2):18–30.

Grindley, G. (1960). Sheet 8 Taupo; Geological Map of New Zealand 1:250,000.

Guéguen, Y. and Palciauskas, V. (1994). *Introduction to the Physics of Rocks*. Princeton University Press, Princeton, New Jersey.

Guerra, C. E., Jacobo, P. E., and Lageo, S. (2012). pH modifications for silica control in geothermal fluids.

Gunnarsson, I. and Arnórsson, S. (2005). Impact of silica scaling on the efficiency of heat extraction from high-temperature geothermal fluids. *Geothermics*, 34(3):320–329.

Gunnarsson, I., Ívarsson, G., Sigfússon, B., Thrastarson, E. Ö., Gíslason, G., and Station, N. P. (2010). Reducing Silica Deposition Potential in Waste Waters from Nesjavellir and Hellisheii Power Plants , Iceland. (April):25–29.

Healy, J., Schofield, J., and Thompson, B. (1964). Sheet 5 Rotorua (1st Ed.). Geological Map of New Zealand 1:250,000.

Heap, M. J., Mollo, S., Vinciguerra, S., Lavallée, Y., Hess, K.-U., Dingwell, D. B., Baud, P., and Iezzi, G. (2013). Thermal weakening of the carbonate basement under Mt. Etna volcano (Italy): implications for volcano instability. *Journal of Volcanology and Geothermal Research*, 250:42–60.

Heap, M. J., Xu, T., and Chen, C.-f. (2014). The influence of porosity and vesicle size on the brittle strength of volcanic rocks and magma. *Bulletin of Volcanology*, 76(9):856.

Heard, H. C. and Page, L. (1982). Elastic moduli, thermal expansion, and inferred permeability of two granites to 350C and 55 megapascals. *Journal of Geophysical Research*, 87(B11):9340.

Heise, W., Caldwell, T. G., Bibby, H. M., and Bannister, S. C. (2008). Three-dimensional modelling of magnetotelluric data from the Rotokawa geothermal field, Taupo Volcanic Zone, New Zealand. *Geophysical Journal International*, 173(2):740–750.

Henley, R. W., Truesdell, A. H., Barton, P. B., and Whitney, J. A. (1984). *Fluid-mineral equilibria in hydrothermal systems*, volume 1. Society of economic geologists El Paso, TX.

Horie, T. (2008). Kawerau and Nga Awa Purua Geothermal Power Station Projects , New Zealand. *Fuji Electric Review*, 55(3):80–87.

Horie, T. and Muto, T. (2010). The World's Largest Single Cylinder Geothermal Power Generation Unit - Nga Awa Purua Geothermal Power Station, New Zealand. *GRC Transactions*, 34:1039–1044.

Iler, R. K. (1979). *The chemistry of silica: solubility, polymerization, colloid and surface properties, and biochemistry*. Wiley.

Jones, T. (2016). *Physical and mechanical controls of matrix permeability on rocks from Rotokawa Geothermal Field, Taupo Volcanic Zone, New Zealand*. Msc thesis, University of Canterbury.

Kaur, P., Chaudhri, N., Hofmann, A. W., Raczek, I., Okrusch, M., Skora, S., and Baumgartner, L. P. (2012). Two-stage, extreme albitization of A-type granites from Rajasthan, NW India. *Journal of Petrology*, 53(5):919–948.

Kaya, E., Zarrouk, S. J., and O'Sullivan, M. J. (2011). Reinjection in geothermal fields: A review of worldwide experience. *Renewable and Sustainable Energy Reviews*, 15(1):47–68.

Kissling, W. M. and Weir, G. J. (2005). The spatial distribution of the geothermal fields in the Taupo Volcanic Zone, New Zealand. *Journal of Volcanology and Geothermal Research*, 145(1-2):136–150.

Kitao, K., Ariki, K., Hatakeyama, K., and Wakita, K. (1990). Well stimulation using cold-water injection experiments in the Sumikawa geothermal field, Akita prefecture, Japan. *Geothermal Resource Council Transactions*, 14(Part II):1219–1224.

Klinkenberg, L. (1941). The permeability of porous media to liquids and gases. Technical report, American Petroleum Institute, New York.

Krupp, R. and Seward, T. (1987). The Rotokawa geothermal system, New Zealand; an active epithermal gold-depositing environment. *Economic Geology*, 82(5):1109–1129.

Leonard, G., Begg, J., and Wilson, C. (2010). Geology of the Rotorua area: scale 1:250,000. Institute of Geological & Nuclear Sciences geological map 5.

Lovelock, B. (1995). Deviations in Silica Geothermometry at Wairakei. *World Geothermal Congress*, (1 966):983–988.

Mahon, W. A. J. (1966). Silica in hot water discharged from drillholes at Wairakei, New Zealand. *NZJ Sci.*, 9:135–144.

Manville, V., Segschneider, B., Newton, E., White, J. D. L., Houghton, B. F., and Wilson, C. J. N. (2009). Environmental impact of the 1.8 ka Taupo eruption, New Zealand: Landscape responses to a large-scale explosive rhyolite eruption. *Sedimentary Geology*, 220(3-4):318–336.

Massiot, C., McNamara, D., Nicol, A., and Townend, J. (2015). Fracture Width and Spacing Distributions from Borehole Televiewer Logs and Cores in the Rotokawa Geothermal Field, New Zealand. In *World Geothermal Congress*, Melbourne, Australia.

McDowell, A., Zarrouk, S. J., and Clarke, R. (2015). Modelling Viscous Fingering during Reinjection in Geothermal Reservoirs. In *Proceedings World Geothermal Congress*, number April, pages 19–25, Melbourne, Australia.

McNamara, D. D., Sewell, S., Buscarlet, E., and Wallis, I. C. (2015). A review of the Rotokawa Geothermal Field, New Zealand. *Geothermics*, (2).

M.E.D (2011). New Zealand's Energy Outlook 2011 — Reference Scenario and Sensitivity Analysis. Technical report, Ministry of Economic Development.

Mielke, P., Nehler, M., Bignall, G., and Sass, I. (2015). Thermo-physical rock properties and the impact of advancing hydrothermal alteration - A case study from the Tauhara geothermal field, New Zealand. *Journal of Volcanology and Geothermal Research*, 301:14–28.

Mountain, B. W. and Sonney, R. (2011). Experimental simulation of fluid-mineral interaction using a continuous flow hydrothermal apparatus. *33rd New Zealand Geothermal Workshop*, (November):21–24.

Mroczek, E., Graham, D., Siega, C., Nicholson, S., and Urgel, A. (2013). Silica Scaling Trial and Injection of Cold Separated Geothermal Water At Wairakei , New Zealand. In *35th New Zealand Geothermal Workshop*, number November, pages 2–4, Rotorua, New Zealand.

Nairn, I. a., Wood, C. P., and Bailey, R. a. (1994). The Reporoa Caldera, Taupo Volcanic Zone: source of the Kaingaroa Ignimbrites. *Bulletin of Volcanology*, 56(6-7):529–537.

Nara, Y., Meredith, P. G., Yoneda, T., and Kaneko, K. (2011). Influence of macro-fractures and micro-fractures on permeability and elastic wave velocities in basalt at elevated pressure. *Tectonophysics*, 503(1-2):52–59.

Nijland, T. G. and Touret, J. L. R. (2001). Replacement of graphic pegmatite by graphic albite-actinolite-clinopyroxene intergrowths (Mjåvatn, southern Norway). *European Journal of Mineralogy*, 13(1):41–50.

Nolan-Hoeksema, R. (2014). Flow through pores. *Oilfield Review*, 26(3):63–64.

NZGA (2013). Geothermal Energy & Electricity Generation.

Olalla, C., Hernandez, L., Rodriguez-Losada, J., Perucho, Á., and González-Gallego, J., editors (2010). *Volcanic Rock Mechanics: Rock Mechanics and Geo-engineering in Volcanic Environments*. Taylor & Francis Group, CRC Press, London.

Parson, L. and Wright, I. (1996). The Lau-Havre-Taupo back-arc basin: A southward-propagating, multi-stage evolution from rifting to spreading. *Tectonophysics*, 263(1-4):1–22.

Phillips, O. M. (1991). *Flow and reactions in permeable rocks*. University of Cambridge.

Pirajno, F. (2009). Hydrothermal processes and mineral systems. *Hydrothermal Processes and Mineral Systems*, pages 1–1250.

Plummer, M., Huang, H., Podgorney, R., Bradford, J., and Moore, J. (2015). Reservoir Response to Thermal and High-Pressure Well Stimulation Efforts at Raft River , Idaho. In *Fourtieth Workshop on Geothermal Reservoir Engineering*, pages 1–9, Stanford, California.

Pochee, A. (2010). Mass transfer and hydrothermal alteration in the Rotokawa Andesite, Rotokawa geothermal field, New Zealand.

Powell, T. (2011). Natural subsidence at the Rotokawa Geothermal Field and implications for permeability development. In *New Zealand Geothermal Workshop*, number November, Auckland, New Zealand.

Public Health Association, A., Water Works Association, A., and Water Environment, F. (1999). Standard Methods for the Examination of Water and Wastewater. *Standard Methods*, page 541.

Rae, A. (2007). Rotokawa geology and geophysics. *GNS Science consultancy report*, (May).

Rae, A. J., McCoy-West, A., Ramirez, L. E., and McNamara, D. (2010). Geology of Production Wells RK30L1 and RK30L2 Rotokawa Geothermal Field. *GNS Science Consultancy Report 2010/02*, (January):41.

Rimstidt, J. D. (1997). Quartz solubility at low temperatures. *Geochimica et Cosmochimica Acta*, 61(13):2553–2558.

Risk, G. F. (2000). Electrical resistivity surveys of the Rotokawa Geothermal Field, New Zealand. *Proceedings of the 22nd New Zealand Geothermal Workshop.*, pages 121–126.

Rosenberg, M. D., Kilgour, G. N., and Fraser, H. L. (2005). Geology of wells RK16, RK17 and RK18 at Rotokawa geothermal field. *IGNS Client Report*, 144.

Rowland, J. V. and Simmons, S. F. (2012). Hydrologic, magmatic, and tectonic controls on hydrothermal flow, Taupo Volcanic Zone, New Zealand: Implications for the formation of epithermal vein deposits. *Economic Geology*, 107(3):427–457.

Rust, A. C. and Cashman, K. V. (2004). Permeability of vesicular silicic magma: inertial and hysteresis effects. *Earth and Planetary Science Letters*, 228(1):93–107.

Sammis, C. and Ashby, M. (1986). The failure of brittle porous solids under compressive stress states.

Seebeck, H., Nicol, a., Giba, M., Pettinga, J., and Walsh, J. (2013). Geometry of the subducting Pacific plate since 20 Ma, Hikurangi margin, New Zealand. *Journal of the Geological Society*, 171(1):131–143.

Sewell, S., Cumming, W., Bardsley, C., Winick, J., Quinao, J., Wallis, I., Sherburn, S., Bourguignon, S., and Bannister, S. (2013). Interpretation of Microseismicity at the Rotokawa Geothermal Field, 2008 to 2012. In *35th New Zealand Geothermal Workshop*, pages 17–20.

Sewell, S., Cumming, W., Bardsley, C., Winick, J., Quinao, J., Wallis, I., Sherburn, S., Bourguignon, S., and Bannister, S. (2015). Interpretation of Microseismicity at the Rotokawa Geothermal Field, 2008 to 2012. In *World Geothermal Congress*, number April, pages 19–25, Melbourne, Australia.

Sewell, S. M., Cumming, W. B., Azwar, L., and Bardsley, C. (2012). Integrated MT and Natural State Temperature Interpretation for a Conceptual Model Supporting Reservoir Numerical Modelling and Well Targeting at the Rotokawa Geothermal Field, New Zealand. *Proceedings: Thirty-Seventh Workshop on Geothermal Reservoir Engineering*, page 8.

Shook, G. M. (2001). Predicting thermal breakthrough in heterogeneous media from tracer tests. *Geothermics*, 30(6):573–589.

Sigurdsson, H., Houghton, B., McNutt, S., Rymer, H., and Stix, J., editors (2015). *The Encyclopedia of Volcanoes*. Academic Press, Elsevier, London, 2nd edition.

Simmons, G. and Cooper, H. (1977). The effect of cracks on the thermal expansion of rocks. *Earth and Planetary Science Letters*, 36:404–412.

Simmons, S. F. and Browne, P. R. L. (2000). Hydrothermal minerals and precious metals in the Broadlands-Ohaaki geothermal system: Implications for understanding low-sulfidation epithermal environments. *Economic Geology*, 95(5):971–999.

Siratovich, P., Davidson, J., Villeneuve, M., Gravley, D., Kennedy, B., Cole, J., Wyering, L., and Price, L. (2012). Physical and Mechanical Properties of the Rotokawa Andesite from Production Wells RK 27_L2, RK 28 and RK 30. In *New Zealand Geothermal Workshop*, Auckland, New Zealand.

Siratovich, P., Heap, M. J., Villeneuve, M., Cole, J., and Reuschlé, T. (2014). Physical property relationships of the Rotokawa Andesite, a significant geothermal reservoir rock in the Taupo Volcanic Zone, New Zealand. *Geothermal Energy*, 2(1):10.

Siratovich, P., Sass, I., Homuth, S., and Bjornsson, A. (2011). Thermal Stimulation of Geothermal Reservoirs and Laboratory Investigation of Thermally Induced Fractures An Overview of Thermal Stimulation. *GRC Transactions*, 35:1529–1535.

Siratovich, P., Villeneuve, M., Cole, J., Kennedy, B., and Begue, F. (2015a). Saturated heating and quenching of three crustal rocks and implications for thermal stimulation of permeability in geothermal reservoirs. *International Journal of Rock Mechanics and Mining Sciences*, 80:265–280.

Siratovich, P., Villeneuve, M., Kennedy, B., Gravley, D., Cole, J., and Davidson, J. (2013). The Geothermal Stimulator: A High-Temperature, High-Pressure Device For Inducing Thermal Fracture In Rocks. In *35th New Zealand Geothermal Workshop*.

Siratovich, P., von Aulock, F., Lavallée, Y., Cole, J., Kennedy, B., and Villeneuve, M. (2015b). Thermoelastic properties of the Rotokawa Andesite: A geothermal reservoir constraint. *Journal of Volcanology and Geothermal Research*, 301:1–13.

Snelling, A. and Woodmorappe, J. (1998). The Cooling of Thick Igneous Bodies on a Young Earth. *Proceedings of the Fourth International Conference on Creationism*, pages 527–545.

Spinks, K. D., Acocella, V., Cole, J. W., and Bassett, K. N. (2005). Structural control of volcanism and caldera development in the transtensional Taupo Volcanic Zone, New Zealand. *Journal of Volcanology and Geothermal Research*, 144(1-4 SPEC. ISS.):7–22.

Stimac, J. A., Powell, T. S., and Golla, G. U. (2004). Porosity and permeability of the Tiwi geothermal field, Philippines, based on continuous and spot core measurements. *Geothermics*, 33(1):87–107.

Truesdell, A. H. and Fournier, R. O. (1977). Procedure for estimating the temperature of a hot-water component in a mixed water by using a plot of dissolved silica versus enthalpy. *J. Res. US Geol. Surv.;(United States)*, 5(1).

Ulusay, R. and Hudson, J. (2007). *The complete ISRM suggested methods for rock characterization, testing and monitoring: 1974-2006*. Ankara, Turkey.

Verma, M. P. (1997). Thermodynamic classification of vapor and liquid dominated reservoir and fluid geochemical parameter calculations. *Geofisica International Mexico*, 36:181–190.

Verma, M. P. and Electricas, I. D. I. (2000). Revised Quartz Solubility Temperature Dependence Equation Along the Water-Vapor Saturation Curve. *World Geothermal Conference*, (1997):1927–1932.

Villamor, P. and Berryman, K. (2001). A late Quaternary extension rate in the Taupo Volcanic Zone, New Zealand, derived from fault slip data. *New Zealand Journal of Geology and Geophysics*, 44(2):243–269.

Villamor, P. and Berryman, K. R. (2006). Late Quaternary geometry and kinematics of faults at the southern termination of the Taupo Volcanic Zone, New Zealand. *New Zealand Journal of Geology and Geophysics*, 49(1):1–21.

Wallace, L., Beavan, J., McCaffrey, R., and Desmond, D. (2004). Subduction zone coupling and tectonic block rotations in the North Island, New Zealand. *Journal of Geophysical Research*, 109(B12):B12406.

Wallis, I., Bardsley, C., Powell, T., Rowland, J., and O'Brien, J. (2013). A structural model for the Rotokawa geothermal field, New Zealand. In *35th New Zealand Geothermal Workshop*, Rotorua, New Zealand.

Weill, D. F., McCallum, I. S., Bottinga, Y., Drake, M. J., and McKay, G. A. (1970). Mineralogy and petrology of some Apollo 11 igneous rocks. *Geochimica et Cosmochimica Acta Supplement*, 1:937.

White, D. E., Brannock, W. W., and Murata, K. J. (1956). Silica in hot-spring waters. *Geochimica et Cosmochimica Acta*, 10(1):27–59.

Williams, H., Turner, F., Francis, J., and Gilbert, C. M. (1982). *Petrography: an introduction to the study of rocks in thin section*. W. H. Freeman Company, San Francisco, 2nd edition.

Wilson, C. J. and Rowland, J. V. (2015). The volcanic, magmatic and tectonic setting of the Taupo Volcanic Zone, New Zealand, reviewed from a geothermal perspective. *Geothermics*.

Wilson, C. J. N., Houghton, B. F., McWilliams, M. O., Lanphere, M. A., Weaver, S. D., and Briggs, R. M. (1995). Volcanic and structural evolution of Taupo Volcanic Zone, New Zealand: a review. *Journal of Volcanology and Geothermal Research*, 68:1–28.

Winick, J., Powell, T., and Mroczek, E. (2009). The Natural-State Geochemistry of the Rotokawa Reservoir. *New Zealand Geothermal Workshop Proceedings*.

Winick, J., Siega, F., Addison, S., Richardson, I., Mountain, B., and Barry, B. (2015). Coupled Iodine-125 and 2NSA Reservoir Tracer Testing at the Rotokawa Geothermal Field , New Zealand. In *World Geothermal Congress*, Melbourne, Australia.

Wyart, J. and Sabatier, G. (1965). Reactions of alkalic feldspars with hydrothermal CaCl solutions. *C. R. Academic Science*, 260:1681–1685.

Wyering, L., Villeneuve, M., and Wallis, I. (2012). The effects of hydrothermal alteration on mechanical rock properties of the Andesite Breccia and Tahorakuri Formation from the Ngatamariki geothermal field, New Zealand and empirical relations between rock strength and pyhsical properties. In *New Zealand Geothermal Workshop Proceedings*, Auckland.

Wyering, L., Villeneuve, M., Wallis, I., Siratovich, P., Kennedy, B., Gravley, D., and Cant, J. (2014). Mechanical and physical properties of hydrothermally altered rocks, Taupo Volcanic Zone, New Zealand. *Journal of Volcanology and Geothermal Research*, 288:76–93.

Zarrouk, S. J., Woodhurst, B. C., and Morris, C. (2014). Silica scaling in geothermal heat exchangers and its impact on pressure drop and performance: Wairakei binary plant, New Zealand. *Geothermics*, 51:445–459.

Zoback, M. D. and Byerlee, J. D. (1975). The effect of microcrack dilatancy on the permeability of westerly granite. *Journal of Geophysical Research*, 80(5):752.

Appendices

A Nga Awa Purua geothermal power station

The power plant at NAP is designed to handle 3 process interfaces; incoming two-phase fluid, and outgoing hot brine and cold condensate. The triple-flash design means that two-phase production steam undergoes 3 stages of separation; high-pressure (HP), intermediate-pressure (IP) and low-pressure (LP). This process is dictated by temperature of the fluid at the cyclone separator and the pressure. By using a triple-flash system an additional 6MW of energy is generated from the high enthalpy (1,560 kJ/kg) two-phase fluid.

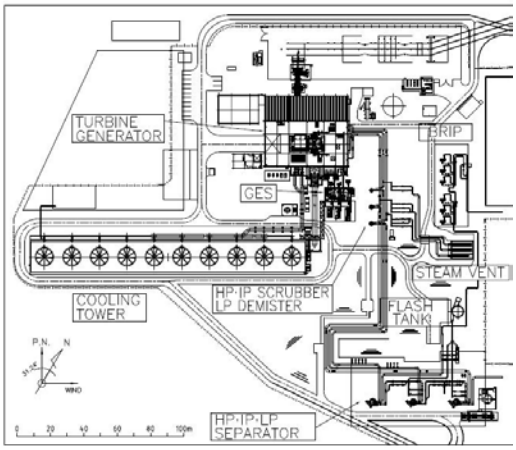

Figure 1: Plan view of the Nga Awa Purua Power Genaration Facility. From (Horie and Muto 2010).

The NAP plant utilises an 8.7m long, 62 tonnes single-shaft geothermal turbine which is the largest in the world. The generator is a totally enclosed water to air-cooled (TEWAC) type with a brushless exciter. The turbine has a triple pressure inlet, single casing and shaft, a bottom exhaust, and a double-flow high and low-pressure sections. Steam is fed into the turbines via inlet pipes. The small blades at the centre of the turbine are designed for high-pressure steam and the 800mm long last-stage blades on the sides are for the low-pressure steam. The turbine turns at 3,000rpm. Production pipelines supply the station with 45,000t a day of two-phase fluids from 2,000m-2,500m deep production wells. Pipelines are approximately 9km long, 1m above the ground and covered with 50mm of thermal insulation. Water for cooling is sourced from the Waikato River which is situated 1km away from the plant site. NAP is connected to the existing 220kV transmission lines of Rotokawa I (RGEN) which run directly above the field (Horie and Muto 2010).

A.1 Steam Separation System

To minimise scaling, erosion and/or corrosion issues of the NAP steam turbine, steam is separated and purified before reaching the turbine inlet. The steam separation system (SSS) receives two-phase fluid delivered from the production wells. Vertical Webre type cyclones separate the steam from the brine and impurities in 3 stages. Impurities are collected at condensate drain pots and through scrubbing processes before delivery to the turbine.

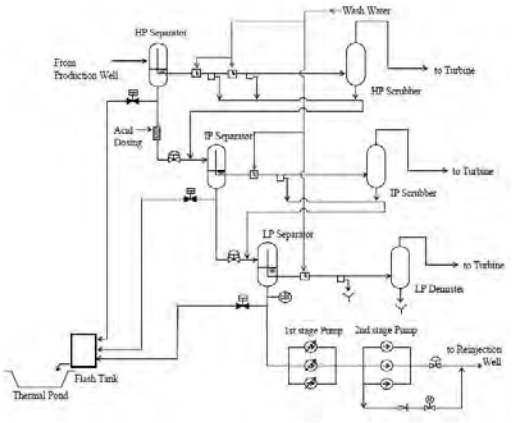

Figure 2: Overview of the Nga Awa Purua steam separation system (Horie and Muto 2010)

High-pressure separated steam carries minor quantities of impurities, including brine and volatile silica. To capture the impurities, wash water is injected downstream of the separator. Moisture binds to the impurities, and falls to the bottom of piping where it is collected in condensate pots. To enhance the scrubbing effect, plant design called for a minimum 200m length of piping between the separators and steam-turbine, with steam velocity in pipes to be no more than 20 m/s. Downstream of the HP-separator, brine becomes two-phase IP fluid at approximately 8.8 bar abs. Drains from condensate pots and the HP scrubber are also directed towards the intermediate-pressure (IP) separator to further utilise available energy and to minimise discharge into surface drains. The purity of IP steam is achieved in similar manner as HP steam. This process then repeats, with IP brine becoming two-phase low-pressure (LP) fluid at approximately 2.5 bar abs. The LP separator fluid levels are controlled by 2 stages of variable speed brine reinjection pumps. In the event of pressure surges steam is vented through a rock muffler. Brine is discharged into a thermal pond through emergency dump valves on the brine lines, downstream of separators. Dumping to the thermal pond also occurs when the separator level is extremely high, the LP brine pH is out of specified range and/or the brine reinjection pumps stop (Horie and Muto 2010).

Flash	Separation stage	Abbreviation	Flash pressure
1	High-pressure	HP	24.3 bar
2	Intermediate-pressure	IP	8.8 bar
3	Low-pressure	LP	2.5 bar

Table 1: NAP steam flash pressures

B Fluid Chemistry

B.1 NAP brine

NEW ZEALAND GEOTHERMAL ANALYTICAL LABORATORY
Private Bag 2000, Taupo
Phone: (07) 374 8211
Fax: (07) 374 8199
Email: w.labmanager@gns.cri.nz

CERTIFICATE OF ANALYSIS
NAP STATION CHEMISTRY (& Hg) - MAY 2015
Report No: 2015050502
Customer Ref:RK15/15

Dave Anderson
Century Drilling & Energy Services (NZ) Ltd
PO Box 341
Taupo

GNS Lot No: 2015050502

GNS Sample No. Collection Date. Site ID: Field ID		2015002556 4/05/2015 NAP HP STEAM #1	2015002557 4/05/2015 NAP HP BRINE	2015002558 4/05/2015 NAP IP BRINE	2015002559 4/05/2015 NAP LP BRINE
pH		5.07	6.78	4.29	4.31
pH Analysis Temperature	°C	19	-	-	-
pH Date Analysed		05/05/2015	-	-	-
Total Inorg.C as HCO_3	mg/l	338	71	<20	<20
H_2CO_3 (calc)	mg/l	326	17.6	-	-
HCO_3 (calc)	mg/l	17.4	54	-	-
CO_3 (calc)	mg/l	-	-	-	-
HCO_3 Analysis Temperature	°C	-	21	21	21
HCO_3 Date Analysed		6/05/2015	6/05/2015	6/05/2015	6/05/2015
Aluminium	mg/l	-	0.72	0.81	0.92
Ammonia	mg/l	-	5.1	5.4	5.8
Antimony (Screen level)[1]	mg/l	-	0.24	0.95	0.29
Arsenic	mg/l	0.02	-	-	-
Arsenic (Screen level)[1]	mg/l	-	2.4	2.6	2.9
Boron	mg/l	0.88	27	29	32
Calcium	mg/l	0.03	1.9	2.2	2.5
Chloride	mg/l	<0.01	1027	1044	1182
Conductivity	µS/cm	186	3777	4120	4541
Fluoride	mg/l	0.02	3.1	3.4	3.7
Iron	mg/l	0.03	0.02	0.29	1.6
Lithium	mg/l	-	7.8	8.5	9.5
Magnesium	mg/l	-	<0.01	<0.01	<0.01
Potassium	mg/l	<0.11	165	181	200
Rubidium	mg/l	-	1.3	1.4	1.5
Silica (as SiO_2)	mg/l	0.17	945	1037	1142
Sodium	mg/l	0.02	590	643	720
Sulphate	mg/l	2.4	7.3	84	95

IANZ ACCREDITED LABORATORY 758
Tests marked with a † are not accredited and are outside the scope of the laboratory's accreditation.

GNS Lot No: 2015050502

		2015002556 4/05/2015 NAP HP STEAM #1	2015002557 4/05/2015 NAP HP BRINE	2015002558 4/05/2015 NAP IP BRINE	2015002559 4/05/2015 NAP LP BRINE
Sulphide (total as H_2S)	mg/l	137	11.7	0.09	<0.01
H_2S Date Analysed		5/05/2015	5/05/2015	5/05/2015	5/05/2015
Total Dissolved Solids[2]	g/m³	3.6	-	-	-
Total Suspended Solids	g/m³	<0.3	7.6	0.4	0.3

B.2 Permeameter pore-fluid

Carbon Dioxide	<1ppm
Carbon Monoxide	<1ppm
Ethane	<1ppm
Methane	<1ppm
Nitrogen	>99.99%
Oxygen	<10ppm
Water	<10ppm

Table 2: Chemical composition of pore fluid (BOC laboratory report)

C Autoclave Apparatus Overview

The key elements of the thermal cycling apparatus are: a bolted closure reactor vessel, ceramic heating jacket, pressurising system, fluid cooling system and an electronic controller.

Samples are placed inside the vessel on a hardened stainless steel (316SS) platen. Notches in the platen allow fluid to pass beneath the sample, penetrating from all angles. The reactor vessel is then bolted shut with the specimen inside (bolts tightened to 90 foot/pounds). The system is flooded with testing fluid (DIH_2O or brine) and airlocks are removed from the system and piping.

The confining fluid (or reservoir fluid) within the vessel is supplied via a Williams CP500-V300 pump fed by an air supply $\leq$ 10bar(g). Rates of discharge range from 0.1-8.6 l/hr by adjusting a stroke timer. The ceramic heater shrouding the vessel provides thermal input, heating both the reservoir fluids and the sample. Rate of heating was maintained at 2.0°C/min across all tests.

C.1 Data Collection

Monitoring of stimulation process was predominantly by the visual observation of pressure and temperature gauges. Data is collected by two thermocouples which feed into a LabView dataDAQ. These thermocouples monitor the temperature of the heater at the vessel wall and also the fluid temperature inside the vessel. Pressure is monitored by a 100 MPa pressure transducer, accurate to 0.001MPa.

C.2 Pressure Vessel Specifications

The pressure vessel (PV) is a Bolted Closure Reactor (model BCH-2) provided by High Pressure Equipment Ltd. The vessel is machined from 316 stainless steel, with an internal capacity of 1000ml. The interior diameter is 76.2 mm and the internal depth is 228.6mm. The maximum allowable pressure within the vessel is 34.4MPa at 343°C. The bolted closure top is fitted with for pressure tolerant ports: injection, ejection, thermocouple, and pressure gauge which also has a burst disk fitted that acts as a pressure release safety feature.

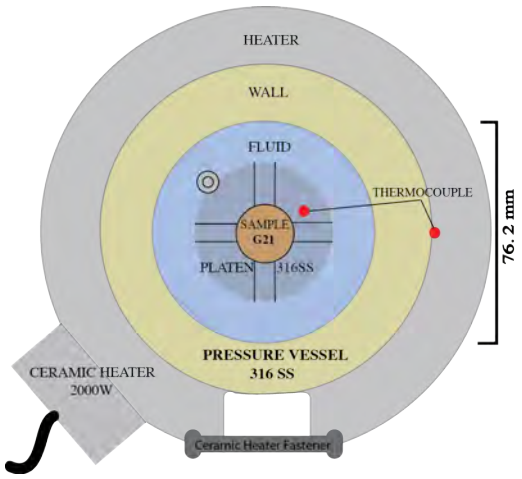

Figure 4: Plan view of the Pressure vessel used in this thesis, showing sample positioning

C.3 Heating System

The ceramic jacket heating system provided by High-Pressure Equipment Ltd. has a 2000W max output. The rate of reservoir heating is controlled by Eurotherm 3208i and 3208 proportional power controllers. Two thermocouples monitor temperature. One thermocouple goes through the top of the PV and is placed next to the sample; this thermocouple is used to monitor the sample temperature and controls the heating cycle of the system. The second thermocouple is located on the outside of the PV between the vessel wall and the ceramic heater jacket. This thermocouple is slaved to the heating system and is used to monitor the external temperature and controls heat input to the system. The heater controls allow a heating rate of 0.1 to 10 C/min. For this thesis a constant heating rate of 2°C/min was used.

C.4 Pressurising system

The pressure regimes in a geothermal system, are typically near or slightly under-pressured with respect to hydrostatic pressure in liquid dominated, two phase systems. Pressuring the vessel was required to recreate these conditions but also to prevent a steam cap building up within the reservoir, potentially hindering quenching of the system. The Williams CPV500-V300 pneumatic plunger pump delivers 8.6 l/hr at 3.2 ml/stroke. The maximum discharge pressure this pump can operate at is 22.4 Mpa. The Williams pump is driven by compressed air supply (1-2MPa). The discharge and pressure regulation is controlled with a Swagelok proportional relief valve (R4). When the system is heating (2°C/min) the expansion of water creates pressure on the relief valve which is set to 20 MPa. The valve opens periodically to relieve excess pressure (safety feature). To replace discharged fluid, ensuring system is kept free of air, the pump cycles a 3.2cm^3 pulse of water int the system every 2 minutes. The system operates under isobaric conditions. Given the relatively simple testing equipment, this allows for rapid temperature change to the reservoir. However, internal vessel pressure can range from 0.1-24 MPa.

D Complications with Experimental Equipment

D.1 Permeameter

Fans - fans that regulate the cabinet temperature went through progressive breakdown lead to results becoming inaccurate due to significant temperature fluctuation within the cabinet.

Pneumatic Valve Failure - valve failure led to the air compressor running overtime to restore system pressure. resulted in the air compressor overheating with oil being forced down the pneumatic control lines and then sprayed inside the housing.

PDP software - not responding - This is a frequently occurring and incredibly annoying. Computer is required to be restarted and USB ports need to be unplugged in order for the programme to start responding again. Each time this happens it requires a new file to be created along with the manual input of all required parameters. When test is restarted, it often applies an unexpected pulse of gas pressure to the sample. requiring a new equilibrium time to be waited for (1-2hours). Days and days of time was lost to this flaw.

D.2 Forchheimer Flow

Ghibli granite samples that were thermally cycled at 270°C(G1,3,10,11) showed good response, with significant increases in both porosity and permeability observed. However, as the permeability increased the relationship between pore-pressure and permeability became non-linear and slopes went from positive to negative. With increasing pore pressure we saw increasing permeability. This is indicative of Forchheimer-Darcy flow, in which flow velocities are significantly high that gas molecule inertia begins to play an important role. Forchheimer flow indicates high levels of mechanical degradation has occurred to the samples. To obtain true permeability for samples displaying Forchheimer flow, the calculation of a secondary permeability is required. To calculate secondary permeability, volume of gas passing through the sample is required. This allows for calculation of gas velocity and inertial energy. The permeameter used in this thesis is not equipped to determine gas volumes, or velocity and therefore further permeability measurements for these samples could not be conducted.

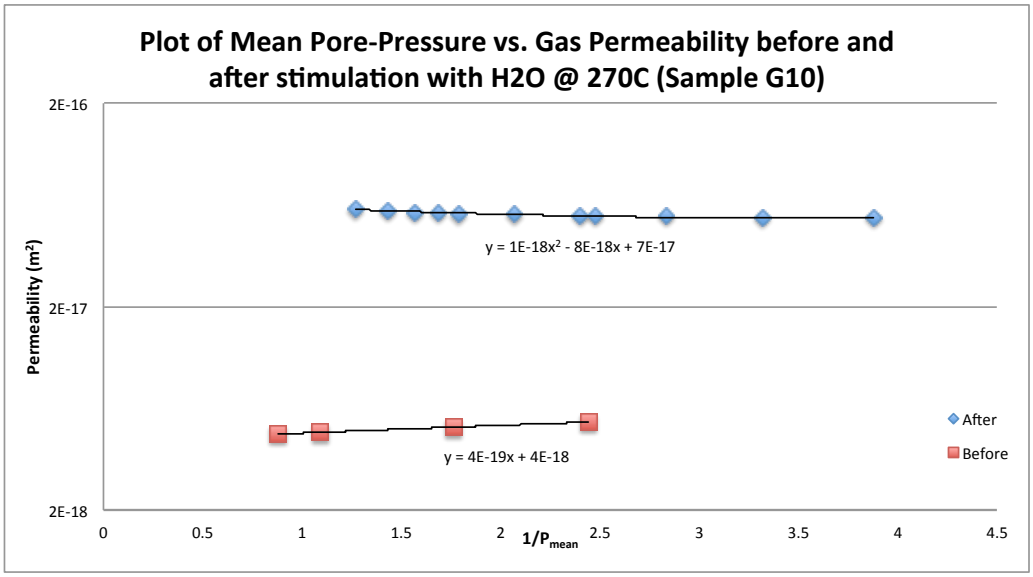

Figure 5: Non-linear relationship indicitave of non-darcian Forchheimer Flow

Unsuccessful attempts were made to eliminate Forchheimer flow by altering the permeameter methods for these samples. This included using very-low pore pressures (20-50psi) and allowing 24 hours of soaking time prior to commencing pulse-decay test. Quantitative changes to sample true permeability cannot be quoted due to not meeting fundamental assumptions of klinkenberg correction. However given the significant measured increase in porosity, and gas permeability we can conclude that significant thermally induced damage has occurred to these samples as a result of thermal cycling. To mitigate this undesired result a lower reservoir temperature of 240°Cwas required. This reduction in temperature was sufficient in that at least two thermal-cycles could be conducted without Forchheimer effects being observed.

H_2O and NAP brine were used for thermal-cycling at both temperatures, samples stimulated in NAP brine at 270°C did not display Forchheimmer-style flow and have been included. However, due to not having a comparative experiment using DI H_2O, no further thermal-cycles were conducted on these three samples. The lower reservoir temperature of 240°C was implemented to avoid having to deal with these effects.

D.3 Autoclave 2.0

Cyclic high-pressure, high-temperature conditions make the Autoclave used for thermal cycling more susceptible to mechanical breakdown. This is likely exacerbated by the introduction of corrosive fluids such as NAP brine. NAP brine contains high concentrations of sodium chloride which is well known to cause corrosion of stainless steel via pitting.

During this thesis several components of the autoclave perished and required replacement. These were:

The teflon-composite seal in the Williams Pump required replacement. As the deterioration of the seal was over a sustained period of time, gradual losses in pump of performance were not easily identified. I recommend doing frequent pump flow-rate tests to monitor performance. Once seal had perished, pump was unable to maintain 10MPa pressure during quenching. Fluid that was meant to be injected

began to leak from a inspection port screw on the pumps wall. As I was experimenting with NAP brine at the time of failure, leaking fluid left behind a silica-gel like residue.

Thermocouples that monitor PV wall temperature and internal fluid temp failed on two occasions. Repeated heating to high temperatures and being required to unplug the thermostat to open the reservoir lead to the eventual breakdown of the thermocouple where it meets the plug. The thermocouple that monitors PV fluid temperature failed during testing at 240°C. This lead to a rapid spike in ceramic heater output. Upon inspection the thermocouple was discovered to have completely ruptured, filling the vessel with a white, chalky substance. Corrosion of the thermocouples thin stainless-steal wall was likely accelerated due to Cl^- species in the NAP brine.

Thermocouples are easily replaced providing the parts are available. There is a small swage fitting that slides onto the thermocouple ensuring a good pressure seal.

Prolonged and unexpected power-cuts occurred on three occasions. All three samples had to be discarded due to this introduced error.